The copyright of this thesis vests in the author. No quotation from it or information derived from it is to be published without full acknowledgement of the source. The thesis is to be used for private study or non-commercial research purposes only.

Published by the University of Cape Town (UCT) in terms of the non-exclusive license granted to UCT by the author.

University of Cape Town

SYNTHESIS AND BIOLOGICAL ACTIVITY OF AJOENES WITH INCREASED AQUEOUS SOLUBILITY

BY

Mandla Mabunda

Thesis Presented for the **Degree of Master of Science in Chemistry**

Faculty of Science

UNIVERSITY OF CAPE TOWN

Supervisor: Professor Roger Hunter

April 2013

Declaration

I declare that the thesis is my own work. Where collaboration with others took place, or the material generated by other researchers is included, the parties and materials are indicated in the acknowledgements and/ or are explicitly stated with references as appropriate.

The work is being submitted for the Master of Science in Chemistry at the University of Cape Town. It has not been submitted to any other university for any degree or examination.

Mandla Mabunda

Date: 23th April 2013

University of Cape Town

Abstract

The synthesis of four new ajoene analogues is presented in this thesis. The key to the synthesis was gaining access to a phenol derivative containing the ajoene core structure (sulfoxide / vinyl disulfide) that could be functionalised with various substituents. Evaluation of biological activity returned excellent *in vitro* activity against a WHCO1 oesophageal cell-line, in which a derivative with a methoxycarbonylmethylene substituent (PMB-ester) was shown to be the most active analogue that was fifteen times more active than *Z*-ajoene with an IC_{50} of 1.7 μM. An aqueous solubility assay reveals that aqueous solubility increased with subsituition and the analogues with amido or acetate substituents were the most soluble ones. The analogues were also shown to enhance the apoptotic effects of two chemotherapeutic drugs Doxorubicin and Vincristine via chemosensitization. This effect was attributed to the presence of at least one *p*-methoxybenzyl substituent in the structure.

University of Cape Town

Acknowledgements

Firstly I thank the Almighty for blessing me with the gift of life and all the doors that have been open for me throughout my life, for also granting me the mind that has been able to absorb everything that I have been exposed. All the work that I have taken part in has been worship to the Almighty.

I would like to show my gratitude to the following people for their help and support during this thesis:

Professor Roger Hunter for his enthusiasm, encouragement, patience, passion to see me succeed in all I did and constantly ensuring I gave everything my best at all times during the two and a half years that he has supervised me.

A special thanks to my friends Thobela Bixa and Allistair Mokoena for being the two of three pillars that made the tripod stand firm, for all their prayers at all times and for the company we provided throughout the projects that we each took on.

I wish to thank Dr Catherine Kaschula, Professor Alessandra Pani, Dr Molahlehi Sonopo, Dr Jan Rijn Zeervaart and the IDMM lab for their contributions to the project.

For all the colleagues in the Department of Chemistry past and present, especially my group members Dr Sophie Rees-Jones, Rudy Cozett, Cathryn Driver, Kathryn Wicht, Wade Petersen, Greg Bowden, Ana Andrijevic, Thobela Bixa, Athi Msutu, James Biwi, John Woodland and Mpho Mafata thanks guys.

Mr Noel Hendricks, Mr Pete Roberts and the University of Stellenbosch CAF for their analytical services.

The National Research Foundation and the Nuclear Energy Council of South Africa for their financial support.

Nsovo Maceve thanks for standing by me each step of the way.

My family and friends, thank you all for all of your support, I really appreciate it.

To my grandpa and grandma I wish you had both lived to see me get where I am now. I dedicate this thesis to my family.

University of Cape Town

Abbreviations

A375	Human malignant melanoma epithelial cell-line
ACCN	1,1' –Azobis(cyclohexane-1-carbonitrile)
ADP	Adenosine diphosphate
AML	Acute myeloid leukemia
ATM	Ataxia-telangiectasia mutated
BCC	Basal cell carcinoma
BF_3: Et_2O	Boron trifluoride etherate
BHK21	Baby hamster kidney cells
BJA-B	Burkitt lymphoid cells
brs	broad singlet
Ca^{2+}	Calcium
CDK	Cyclin dependant kinase
d	doublet
dd	doublet of doublets
ddd	doublet of doublet of doublets
dt	doublet of triplets
DATS	Diallyl trisulfide
DCM	Dichloromethane
DMAP	Dimethylaminopyridine
DMEM	Dulbecco's modified Eagle Medium
DMF	Dimethyl formamide
DMSO	Dimethyl sulfoxide
DNA	Deoxyribonucleic acid
DOXO	Doxoburubicin

University of Cape Town

ER	Endoplasmic reticulum
ERK	Extra-cellular signal related kinases
Et	Etoposide
EtOAc	Ethyl acetate
FasL	Fas-lagand
FBS	Fetal bovine serum
FS4	Human fibroblast cells
GR	Glutathione reductase
HCl	Hydrochloric acid
HL60	Human leukemic cells
HRMS	High resolution mass spectroscopy
HSAB	Hard-soft acid-base theory
HSQC	Heteronuclear Single Quantum Coherence
Hz	Hertz
IIDMM	Institute of Infectious Diseases and Molecular Medicine
i.p.	Intraperitoneal injection
JNK	Jun N-terminal kinases
KB	Nasopharyngeal carcinoma
KIP1	Kinase inhibitor protein 1
LAH	Lithium Aluminium hydride
m-CPBA	meta-Chloroperbenzoic acid
MMP	Mitochondrial membrane permeabilization
Mp	Melting point
MTT	3-(4,5-Dimethylthiazol-2-yl)-2,5-diphenyltetrazolium bromide
NAC	*N*-acetylcysteine
NaH	Sodium hydride

University of Cape Town

NMR	Nuclear Magnetic Resonance
NECSA	South African Nuclear Energy Corporation
NEt_3	Triethylamine
OCS's	Organosulfur compounds
PARP	Poly (ADP-ribose)
PBMC	Peripheral blood mononuclear cells
PBS	Phosphate-buffered saline
PEG400	Polyethylene glycol 400
PET	Positron emission tomography
PT	Proton transfer
PtK2	Marsupial kidney cell
pRb	Retinoblastoma protein
s	singlet
SAR	Structure-activity relationship
RBC	Red blood cells
R_f	Retention factor
ROS	Reactive oxygenated species
t	triplet
TBDPS	*tert*-Butyldiphenylsilyl ether
THF	Tetrahydrofuran
THP	Tetrahydropyranyl
TLC	Thin later chromatography
TNF	Tumor necrosis factor
TR	*Trypanosoma cruzi* trypanothione reductase
UCT	University of Cape Town
UPR	Unfolded protein response

University of Cape Town

WHCO1	Oesophageal epithelial cancer cell-line
VCR	Vincristine

University of Cape Town

Table of Contents

University of Cape Town

University of Cape Town

Chapter 1: Review of Biological and Synthetic aspects of Ajoene

1.1 Introduction

This thesis describes the synthesis of several novel ajoene analogues designed for elucidating the biological mechanism of ajoene-induced anti-cancer activity. The project spans across a few disciplines, thus this chapter will offer an overview of the fundamental concepts and background information relevant to the project.

1.2 Overview of Garlic

The current human civilization has benefited tremendously from ancient ones who showed the importance of using plants to combat various infections and inflammations.[1,2] Plants such as Garlic or *Allium sativum* (thought to be of Central Asian origin) have been documented since around 2600-2100 BC to possess therapeutic benefits, although at that stage the exact cause of the benefits weren't known.[3, 7] The therapeutic benefits were later attributed to potent organosulfur compounds(OCS's), which are notably three times higher in garlic than in any other species of the same class .[4]

1.2.1 Organosulfur Compounds Found in Garlic

The two types of OCS's that are predominately located in whole garlic cloves are γ-glutamylcysteines and cysteine sulfoxide,[5, 6] Allylcysteine sulfoxide (alliin) is a major constituent, which upon maceration of the full clove is converted by its enzyme allinase (stored in a separate mesophyll vacuole) into 2-propenesulfenic acid (see Scheme 1, (i)). The sulfenic acid is unstable and spontaneously condenses to form the thiosulfinate Allicin together with other OCS's (see Scheme 1, step 2).[5] Allicin has been shown to possess an array of medical benefits, and can be synthesized from diallyl disulfide and peracetic acid, the latter from a mixture of hydrogen peroxide and acetic acid (see Scheme 1, (ii)). Allicin is also unstable and rearranges to more stable products.[4, 5] Some of the main products found in crushed and aged garlic are shown in Figure 1.

University of Cape Town

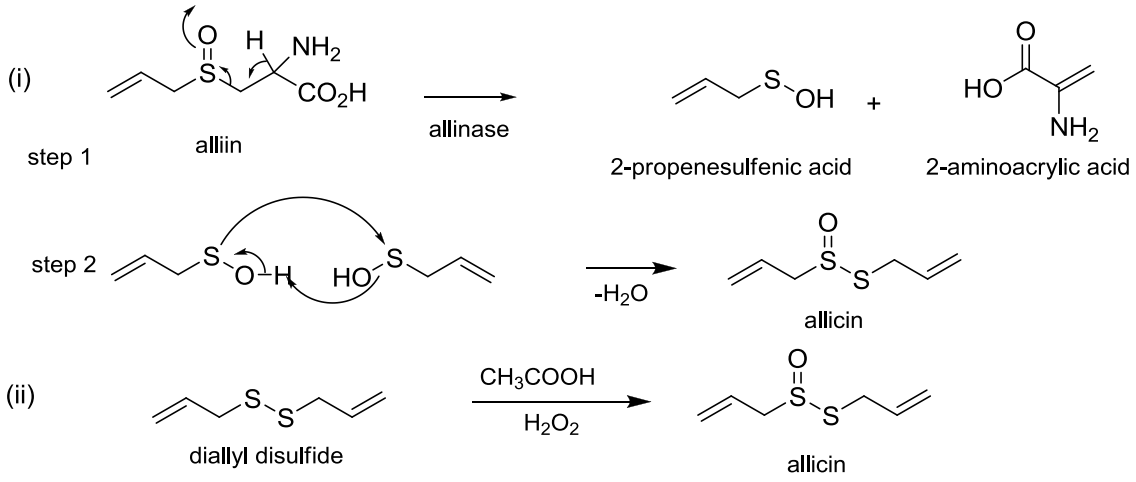

Scheme 1: (i) step 1: Conversion of alliin to 2-propenesulfenic acid and 2-aminoacrylic acid, step 2: self-condensation of 2-propenesulfenic acid into Allicin, (ii) The synthetic route to allicin from diallyl disulfide.

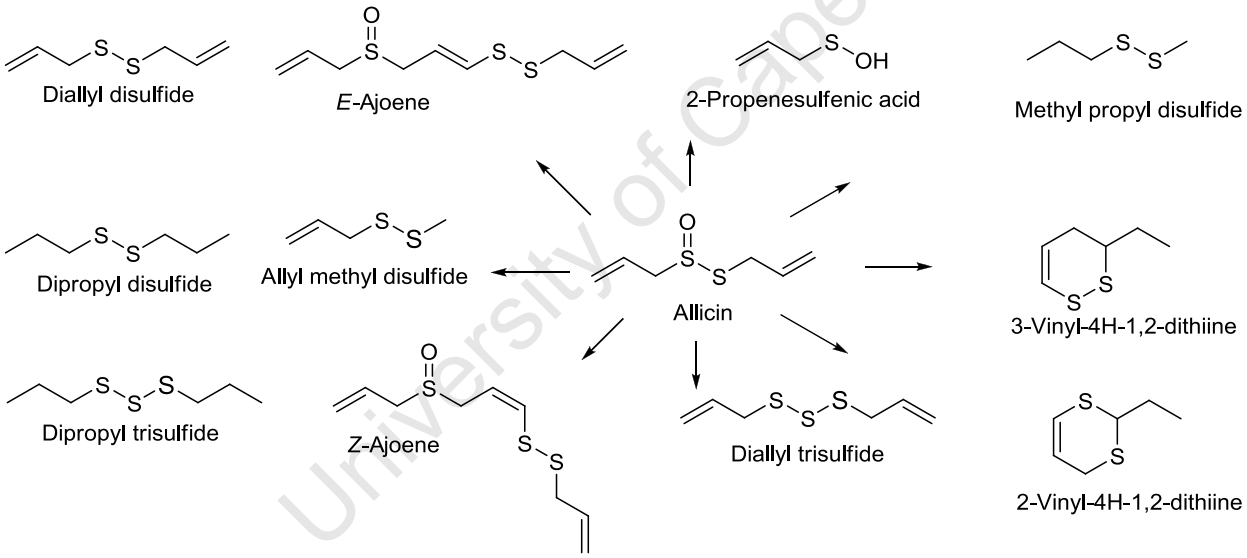

University of Cape Town

Figure 1: Examples of OSC's found in garlic.

1.3 Ajoene

Ajoene *(E/Z*-4,5,9-trithiadodeca-1,6,11-triene-9-oxide) was first characterized by Block and Apitz-Castro in the 1980s as a stable product of allicin self-condensation. They postulated that two allicin molecules combine via S-thioallylation to form a sulfonium ion, followed by a Cope-type elimination to give a

vinylthionium ion. Lastly, the 2-propenesulfenic acid adds via a Michael-type addition (to the vinylthionium) resulting in the (*E*/*Z*)-ajoene (see Scheme 2).[8]

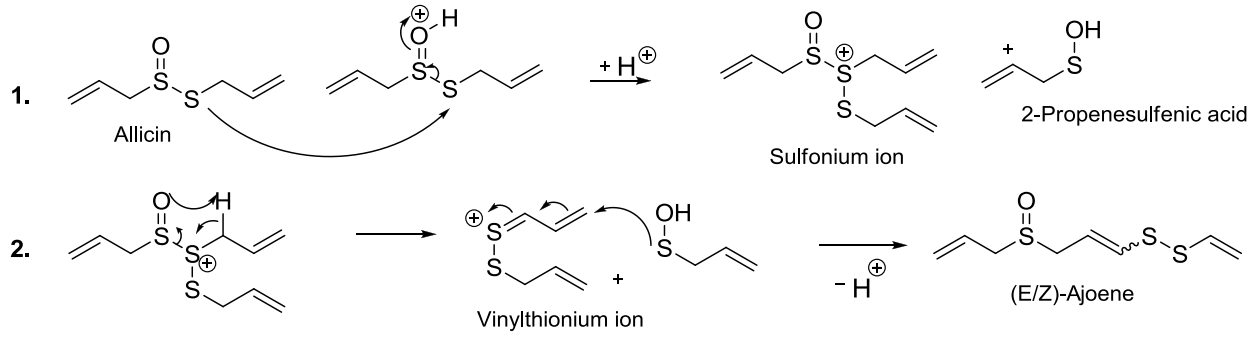

Scheme 2: Rearrangement of allicin to (*E*/*Z*)-ajoene.

The allicin rearrangement products shown in Figure 1 above share common structural functionality such as disulfide and in some examples trisulfides, in which the disulfide is thought to be the pharmacophore responsible for the various biological activities. Ajoene is noticeably different from the other molecules as it has a vinyl disulfide group, which is thought to increase the reactivity of the disulfide bond, thus making it more active than any of the related compounds. Since its discovery, anti-thrombotic activity, [8] as well as other biological activities ranging from anti-microbial[9], anti-obesity[10], anti-fungal[11] and also anti-cancer[12] have been identified, the latter being the most relevant to the current study.

1.4 Cancer

Cancer is described as a class of disease that is characterised by the uncontrolled growth of abnormal cells that are capable of spreading to other cells in the vicinity and organs (via metastasis). The survival of abnormal cells is governed by their ability to elude apoptosis. Cancer is a global burden that accounted for 8 million deaths in 2008. Furthermore, 70% of deaths occur in low- and medium-income parts of the world.[13]

1.4.1 Treatment of cancer

Since cancerous cells survive by avoiding apoptosis, most of the therapeutic drugs available have been designed to restrict the rapidly-growing cells by inducing programmed cell-death. Chemotherapeutic drugs that are toxic to other healthy cells are referred to as *cytotoxic*, and a number of chemotherapeutic drug classes are available on the market grouped by their mode of action as indicated in the following.

University of Cape Town

Chemotherapeutic drug groups:[14]

1. Alkylating agents: they have the ability to impair cell functionality by forming covalent bonds with nucleophilic groups such as carbonyl, sulfhydryl, amino and phosphate found in the cancer cells. DNA, RNA and proteins are targets for alkylating agents such as platinum complexes.

2. Anti-metabolites: they mimic the naturally occurring building blocks of DNA and RNA synthesis, where they will compete with the natural substrate for synthesis thus halting normal processes. Fludarabine is one such example of the purine analogue.

3. Natural products: Vinca alkaloids are derived from the periwinkle plant *Vinca rosea*, are able to bind to tubilin and prevent polymerization of microtubules that are required during cell division. Taxanes that are derived from yew plant extracts promote and stabilise the assembly of microtubules, blocking the cell-cycle at mitosis. Docetaxal and Paclitaxel are good promoters of microtubule assembly and apoptosis.

4. Anthracyclines: they are products originating from the fungus *Streptomyces percetus* var *caesius*, and intercalate between DNA bases as well as inhibit DNA topoisomerases I and II. Doxorubicin is one such example from *Streptomyces*.

There are many side-effects associated with the above drugs such as nausea, diarrhea, bone marrow depression and also skin changes. Over time the cancer cells develop resistance to the drugs, and such challenges have led to development of better chemotherapeutic agents with fewer side-effects.

1.4.2 The Eukaryotic cell-cycle

There is always a need for continuous cell proliferation in eukaryotes. In mammals, such processes are required for both the maintenance of tissues and the organs that are needed to sustain life. The cell-cycle is a highly regulated sequence of events leading to cell division and multiplication.[15, 16] All the classes of anti-cancer drugs described target various sites within the cycle, and with this knowledge of the cell-cycle designing more robust drugs can be achieved.

The cell-cycle (see Figure 2) comprises 5 phases:

i) A large proportion of cells in human bodies are in out-of-cycle state quiescent (G_0).

ii) Protein synthesis and initial cell growth occurs at G_1.

iii) Deoxyribonucleic acid (DNA) replication takes place in the S phase.

University of Cape Town

iv) Secondary growth and microtubule formation occurs at the G_2 phase.

v) Mitosis cell-division into identical daughter cells, (M) phase.

Cell proliferation is promoted by cyclin dependant kinase (CDK) family of serine/threonine kinase in complexation with their regulatory cyclin partners.[15]

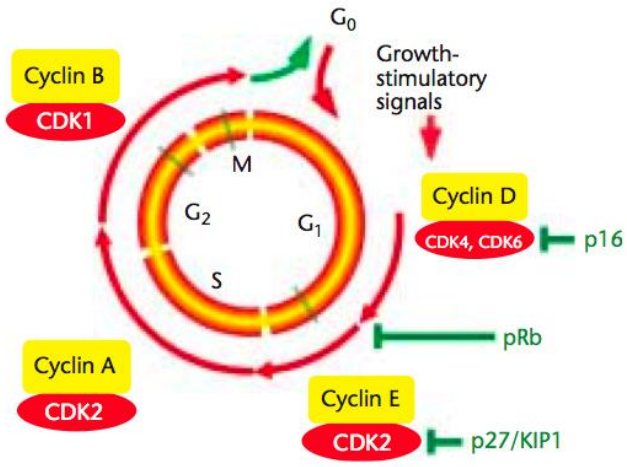

Figure 2: Cell-cycle portraying the critical regulators and checkpoints. The cycle comprise of G_1, S, G_2 and M as indicated with checkpoints in G_1, G_2, and M phases as shown by horizontal green T-bars. Sequential activation of the Cyclin-CDK complexes drives the cell cycle (red arrows). The cell-cycle progression can be blocked by negative regulators such as p16, (retinoblastoma protein) pRb, P27/ KIP1 (kinase inhibitor protein 1) or by exit from the cell cycle into G_0 phase. Growth-stimulatory signals can lead to re-entry into the cell cycle.[16]

Cyclin D-CDK4/6 is required for initiation of the cell-cycle from the G_0 state and it acts on pRb by causing hypophosporylation, which in its active state halts cell-cycle by binding and repressing transcription factor E2F. Whereupon, dissociation of pRb from E2F leads to transcription of genes required to proceed to the S phase. The cyclin E-CDK2 active complex drives progression to the S phase through the restriction point, the S phase being the most important as DNA synthesis is initiated by cyclin A-CDK2. Upon completion of DNA synthesis, cyclin B-CDK1 is activated which leads to entry into the M phase at which two new daughter cells are formed by mitosis. At this point the cell newly formed cells may re-enter into another cycle or go in out-of-cycle state.[15-17] Progression through the various cell cycle phases and transitions is strictly monitored by sensor mechanisms, called checkpoints (restriction points), which maintain order of events. Any defect detected will trigger reversible cell cycle arrest until the problem is resolved.[15]

1.4.3 Apoptosis

As cells are continuously proliferating to maintain a balance in the mammalian development, apoptosis has been adopted to be the mode by which cell density is kept in check. This occurs as a normal physiological response to the various imbalances experienced, which may include irreparable DNA damage. Apoptosis is a process by which old, damaged or dangerous cells are disposed off efficiently. It is also described as an active, energy-demanding, genetically determined process, proceeding without resulting in any inflammation as opposed to necrosis. Necrosis is an involuntary, energy-independent cell death that affects a group of cells resulting in inflammation.[16]

Apoptosis is tightly regulated by several molecular pathways, some of which have been well-defined. Damage sensors such as ATM ("*ataxia-telangiectasia mutated*") located in the nucleus or on death receptors on the cell membrane, are capable of initiating signalling cascades that lead to an 'execution machinery' resulting in cell death. Two prime pathways utilized are mitochondrial (intrinsic) and death receptor-mediated (extrinsic) apoptosis. The two pathways are intimately linked by a series of caspases such as cysteine proteases (see Figure 3). [16, 18]

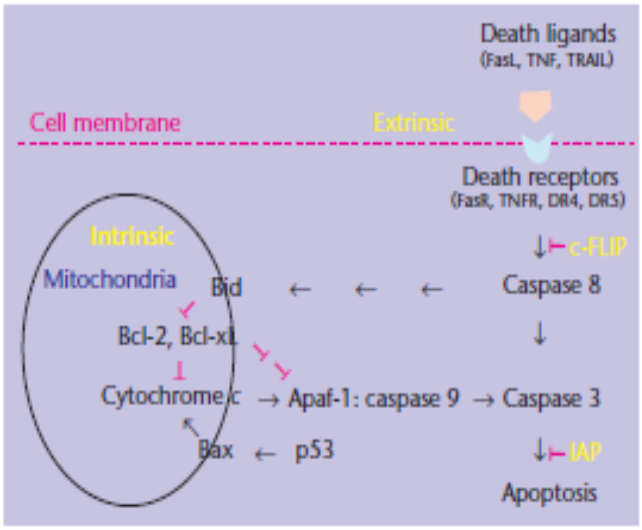

Figure 3: Cellular apoptosis pathways. The two pathways converge into a single point at caspase 3 irrespective of the stimuli initiating either pathway.

The extrinsic pathway is governed by an exterior stimulus, such as growth factor withdrawal matrix detachment and cytokine-mediated killing. The pathway is initiated when an appropriate death ligand such as tumor necrosis factor (TNF) and Fas-lagand (FasL) interact with its matching receptor (TNF and Fas receptor) respectively. These interactions lead to the activation of the caspase cascade, finally resulting in cell death by degradation of proteins that are required for cell viability. [16, 18]

The intrinsic pathway is initiated by intracellular stimuli such as DNA damage and cellular stress. The Bcl-2 family of proteins are responsible for mediating the pathway, and they exist in two opposing states, namely: anti- and pro-apoptotic forms. As a response to apoptotic signals such as anti-cancer drugs the pro-apoptotic Bcl-2 family of proteins such as BaX translocate to and alter the mitochondrial membrane permeability that leads to cytochrome c release and inevitable activation of caspase cascade. Anti-apoptotic Bcl-2 family members such as Bcl-2 and Bcl-xL can counter the effects caused by the stimuli. [16, 18]

1.4.4 Other Causes of Apoptosis

The endoplasmic reticulum (ER) plays a major role in the proliferation of eukaryotic cells as it provides the environment for proper protein folding and modification. [19] The lumen of the ER is a cellular storage compartment for calcium (Ca^{2+}) and is also a redox active site required for protein folding. Disruptions such as protein unfolding will lead to an unfolded protein response (UPR), if the cell is incapable of restoring normal ER function in which case apoptotic signals such as NF-κB are activated and subsequently the dysfunctional cell will be destroyed.

There are various proposed mechanisms to link how ER stress links to the activation of apoptosis but none of them have been clearly described to date. The process may proceed via: activation of proteases, transcription factors and Bcl-2- family proteins. Release of Ca^{2+} from the ER lumen has been shown to activate caspase 12 as well as further downstream caspase activation. [19, 20]

1.5 Anti-cancer Activity of Ajoene

1.5.1 Anti-mutagenic

The first aspect of ajoene's anti-cancer properties concerns prevention as opposed to treatment. Experimental and epidemiological studies conducted have shown that the consumption of garlic has a positive impact on people as it lowers risks associated with cancer and other diseases.[21, 22] These benefits may be attributed to OCS's found in garlic.

Ajoene, is more distinctive than the others in that it has been shown to have the ability to inhibit the activation of known carcinogenic agents such as 12-*O*-tetradecanoylphorbol-13-acetate, benzo[a] pyrene and 4-nitro-1, 2-phenylenediamine in *Salmonella Typhimurium in vitro.* [23] The exact mechanism that is employed to eliminate the carcinogen is not clearly understood, but it is proposed that it may be via the inhibition of cytochrome p450-dependent monooxygenases which are responsible for

University of Cape Town

bioactivation of carcinogens, and also by detoxification via phase II enzymes such as glutathione peroxidases.[21]

1.5.2 Anti-tumour

Ajoene's anti-tumour ability has been documented since the early 1990's, where it was shown to inhibit tumor cell proliferation in a number of cell lines with IC_{50}'s that range from 5-40 μM.[24-27] This is both *in vivo* and *in vitro* as described later.

Ajoene's ability to inhibit proliferation was first shown by Schrafenberg and co-workers in a letter published in 1990. They found that ajoene, *in vitro*, was cytotoxic towards tumourogenic Burkitt lymphoid (BJA-B) cells and caused apoptosis, although the exact mode as to how the apoptotic response is activated wasn't clear at the time. Conversely, the non-tumorgenic cells that are derived from baby hamster kidney (BHK21) and human fibroblasts (FS4) cells were not susceptible towards ajoene's cytotoxicity.[24]

Over the years there have been a number of reports on the anti-tumour effects of ajoene that support the observation by Scharfenberg. A comprehensive study conducted by Dirsch and co-workers showed that ajoene is indeed selective towards tumouorgenic cells as opposed to normal cells. Ajoene induced apoptosis in human leukemic (HL60) cells but not in peripheral blood mononuclear cells (PBMC) that were isolated from healthy donors.[27] Dirsch's findings were corroborated by Li and co-workers, which showed ajoene's specificity towards tumourogenic cells and not healthy cells. In their study, HL60 cells, nasopharyngeal carcinoma (KB) and one normal marsupial kidney cell line (PtK2) were each subjected to an increasing concentration of Z-ajoene (1-20 μM) and the survival of cells monitored after 48 hours. Their results showed what Dirsch and Scharfenberg had proposed about ajoene's specificity (see Figure 4). The HL60 cells were more sensitive to the varying concentration of ajoene in which only 10 % of cells survived exposure. Nasopharyngeal carcinoma was less sensitive towards ajoene with 30 % of cells surviving. Contrary to the two cancer cell lines 75 % of cells in the normal marsupial cells survived.[25] These results clearly demonstrate ajoene's specificity towards tumourogenic cells.

University of Cape Town

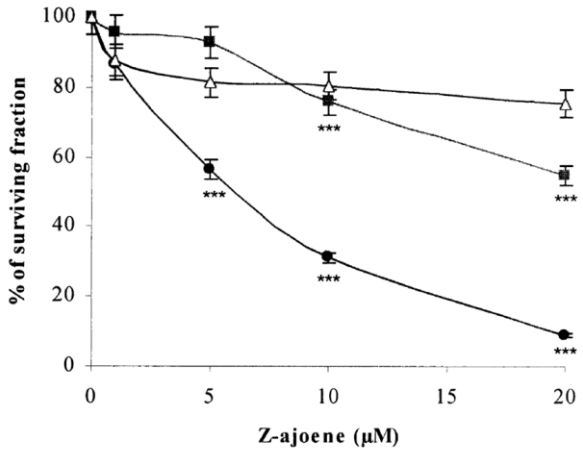

Figure 4: The effects of Z-ajoene on cell line cytotoxicity: HL60-●-, KB -■-, and PtK2-Δ-, were exposed to increasing concentrations of Z-ajoene (1-20 μM) for 48 hours.

In vivo, ajoene has been shown to inhibit tumourogenic growth in both humans with basal cell carcinoma (BCC), a skin cancer type that is prevalent amongst adults that have suppressed immune systems, as well as mouse model (xenografts).[25, 26, 28, 29] In a study conducted by Tilli and co-workers, 25 test subjects were each treated with a 4 % ajoene cream onto the tumours. After 6 months of treatment 23 of the test subjects displayed a positive response to the treatment, where tumour sizes were reduced by about 80 %. Three subjects displayed a negative response as tumours increased and 1 subject showed no change after treatment, (see Figure 5).

rsity of Cape Town

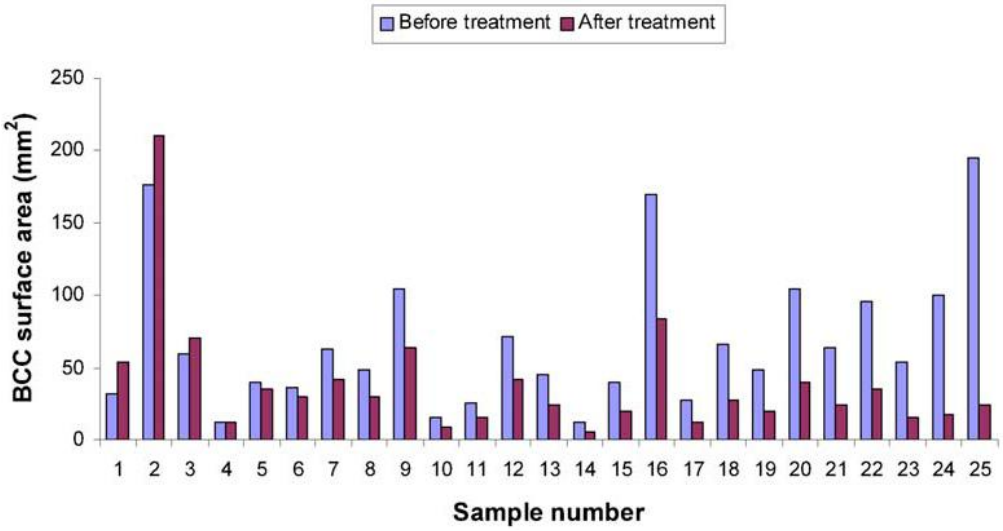

Figure 5: Effects of ajoene topic application on tumor size of individuals with BCC.

In a mouse model, the mice were innoculated with various tumours at the start of the study and then subjected to varying concentrations of ajoene (2, 4 and 8 mg/kg) via intraperitoneal (i.p.) injection every day for 4 weeks. After this period it was clear that the administration of ajoene had retarded tumour growth in rodents and it was also noted that ajoene inhibits tumor growth by 2-3 fold compared to the control cells, (see Figure 6).[25, 26]

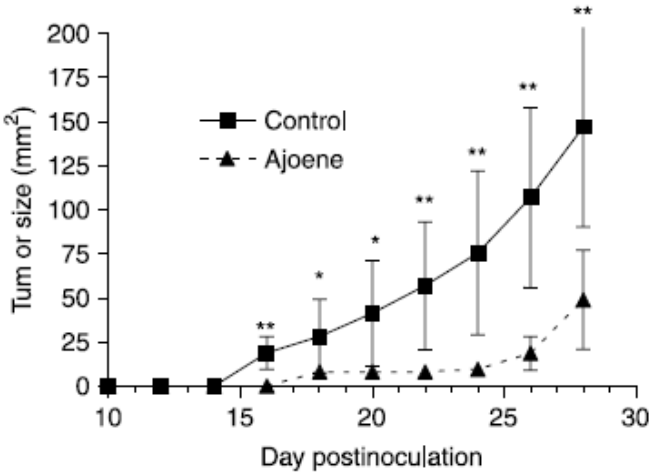

Figure 6: Effects of ajoene administered by i.p. injection on the growth of primary subcutaneous B16/BL6 tumor cells over 4 weeks.

1.5.3 Chemosensitization

Chemosensitization is a strategy to counteract the resistance of tumour cells towards anticancer agents. A chemosensitizing agent should have the ability to reinduce the sensitivity of tumours towards chemotherapeutic agents by reversing strategies employed by tumours such as detoxification, and also overexpression of pumps that efflux the chemotherapeutic drugs.[30]

Ajoene has been shown by Hassan to possess the ability to reinduce sensitivity of drug-resistant acute myeloid leukemia (AML) cells towards fludarabine and cytarabine.[12b] It was shown that ajoene inhibits the activation of anti-apoptotic Bcl-2 proteins which activate caspase-3 resulting in an apoptotic response.[27] A combination of the two drugs and ajoene displays a decrease in bcl-2 expression and an increase in caspase-3 activation, while ajoene did not cause any apoptotic response on its own against the AML cells. Thus it can be said that it was indeed a chemosensitization effect that was displayed by the combination of both fludarabine and cytarabine.[12b]

University of Ca

1.6 Signaling pathways

As mentioned previously there are two pathways to induce apoptosis in cells either via the mitochondria and caspase cascade or via surface death receptors.[16] Dirsch showed that treatment of HL-60 with increasing concentrations of ajoene caused a dose-dependent and time-dependent release of reactive oxygenated species (ROS), which was predominately composed of hydrogen peroxide. The production of ROS leads to the activation of transcription factor NF-κB, which is also known to be activated upon oxidative stress with the net result being apoptosis of the cell.[27, 31] To prove their hypothesis that ROS acts as the signal for apoptosis they incubated an antioxidant *N*-acetylcysteine (NAC) with ajoene in the HL-60 cells and found that it reduced the release of ROS, as well as both apoptotic activity and the activation of the NF-κB. Upon activation of NF-κB, it is thought that other pathways are activated which lead to apoptosis where the caspase cascade is not involved, and thus ROS is upstream of the mitochondrial-dependent activation.[27]

Ajoene-induced cell death is a time-dependent process in which activities was observed as early as 5 hours of incubating the HL-60 cells with ajoene. An experiment was set up to test whether caspase activation occurred upon ajoene treatment by utilizing a fluorometric DEVD-cleavage assay. It was noted that caspase-3 like activity was detected at about 4 hours and that increased extensively after 8 hours of the experiment. This result was confirmed by the cleavage of PARP [poly (ADP-ribose) polymerase – a 116-kDa nuclear protein involved in DNA repair] into a fragment which is 85-kDa in a time-dependent manner (see Figure 7a). Interestingly, it was also shown that CD95 death receptors were not activated upon ajoene treatment, which is evidence that apoptosis proceeds without their involvement. Moreover, cells that were treated with the caspase inhibitor zVAD-fmk and ajoene, showed no fragmentation of the DNA material implying that caspase activation is indeed responsible for cell death (see Figure 7b).[27]

University of Cape Town

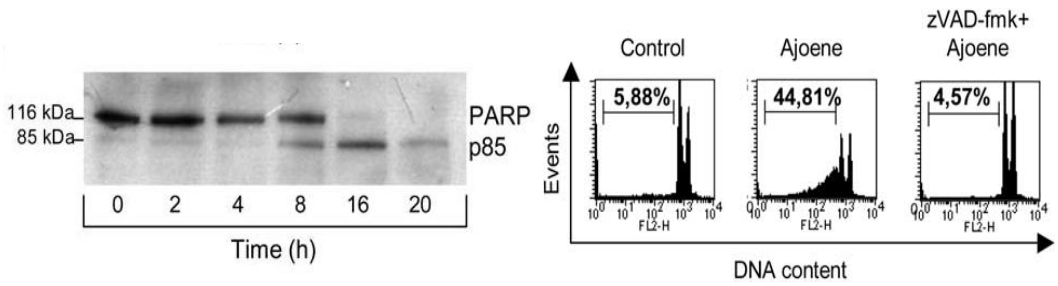

(a) (b)

Figure 7: (a) Time-dependent cleavage of PARP upon caspase-3 activation, (b) DNA content treated with zVAD-fmk and ajoene to display caspase activation.

Another important signaling pathway was also proposed by Dirsch, in which ajoene promoted mitochondrial membrane permeabilization (MMP). This is known to be a vital component in cell death (see Figure 8a). The activation of caspase-3 is linked to the release of cytochrome c into the cytosol in HL-60 cells. Significant cytochrome c was detected within the cytosol after 4 hours of the cells being exposed to ajoene (20 μM), which again also displayed the time-dependency of ajoene exposure to cell-death response and that release of cytochrome c precedes caspase activation. Cytochrome c binds to the cytoplasmic protein Apaf-1 initiating the caspase cascade, which results in a loss of transmembrane potential ($\Delta\Psi_m$) that was confirmed by confocal microscopy (see Figure 8b). The mechanism mentioned here does not require JNK (Jun N-terminal Kinases), but is amplified by the inhibition of ERK (extra-cellular signal related kinases). [16, 27, 32]

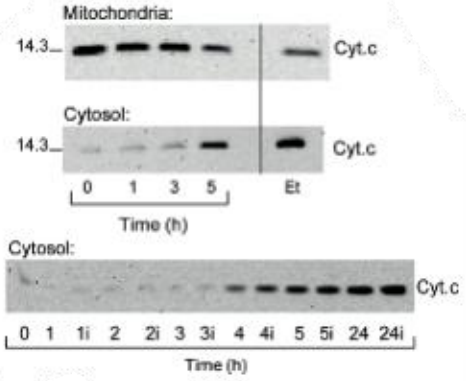

Figure 8(a): The upper panel represents a time-course of ajoene-mediated cytochrome c release into the cytosol as treated with ajoene (20 μM), as positive control with etoposide (Et,17μM) for 5h. The lower panel reflects a time-course of cytochrome c accumulation for the indicated time. In parallel, at each time-point, cells were preincubated for 1 h with the caspase inhibitor zVAD-fmk (100μM) and then treated with ajoene (20 μM).

University of Cape Town

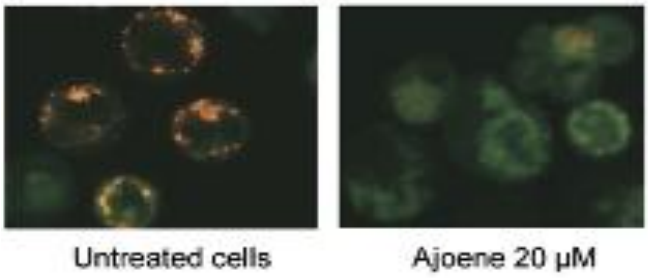

Figure 8(b): Dissipation of MMP in cells treated with ajoene (20 μM for 8h), stained with the fluorochrome JC-1 and analyzed by fluorescence microscopy. The red fluorescence reflects the multimer form of JC-1 localized in mitochondria under control (untreated) conditions. The green fluorescence corresponds to monomer JC-1 after ajoene-induced dissipation of MMP.[27]

As mentioned previously the Bcl-2 family of proteins are able to inhibit apoptosis by preventing the release of cytochrome c out of the mitochondria.[16] Incubation of HL-60 with *Z*-ajoene resulted in the induction of cleavage of Bcl-2, a 26-kDa protein, into a 23-KDa fragment, which was characteristic as it had been previously been obtained upon treatment of HL-60 cells with etoposide (see Figure 9).[33] From this result it was clear that Bcl-2 was only cleaved upon the activation of caspase-3, as treatment with zVAD-fmk didn't show any cleavage of Bcl-2 and PARP implying that Bcl-2 is a downstream substrate for caspase-3.

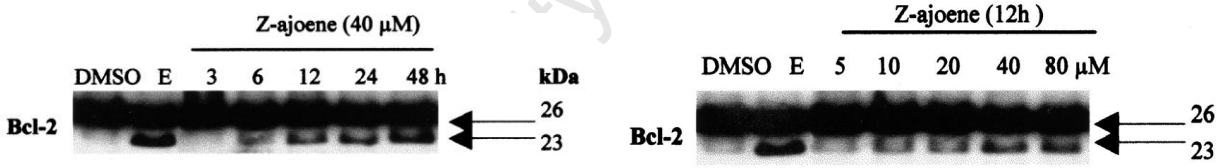

Figure 9: Z-ajoene induced Bcl-2 cleavage in HL-60 cells. Cells were treated with Z-ajoene 40 μM at various times. Etoposide (E) was used as a positive control in the experiment.[33]

1.7 Mode of Action of Ajoene

Ajoene and diallyl trisulfide (DATS) have been shown to exhibit their anti-cancer properties by associating with the mitochondrial-mediated apoptotic pathways, which results in G_2/M cell-cycle arrest. However a comprehensive account of this has not yet been formulated, but a few examples have been proposed.[34, 35] It has been well established that disulfide bonds in OCS's have the ability to act as thiol oxidizing agents, modifying enzymes and proteins via thiolation of exposed cysteine residues located on them. Modifications such as these may eventually result in cell death if not dealt with accordingly.[34]

University of Cape Town

1.7.1 Modification of Microtubule Formation and Cell-Cycle Arrest

It was proven by Hosono that apoptosis occurs as a result of oxidative modification of tubulin by thiolation on cys-12 and cys-354 to result in S-allylmercaptocysteine on each subunit.[38] Upon such modifications tubulin polymerization and microtubule formation are inhibited. As mentioned earlier that microtubule assembly is essential for mitosis, it will clearly be inhibited at this point and thus lead to cell-cycle arrest at G_2/M phase.[16, 25, 38] Other sites in the cells are implicated by induction of cell-cycle arrest by OCS's that leads to an apoptotic response via the mitochondrial-mediated pathways as mentioned earlier (see Figure 10).

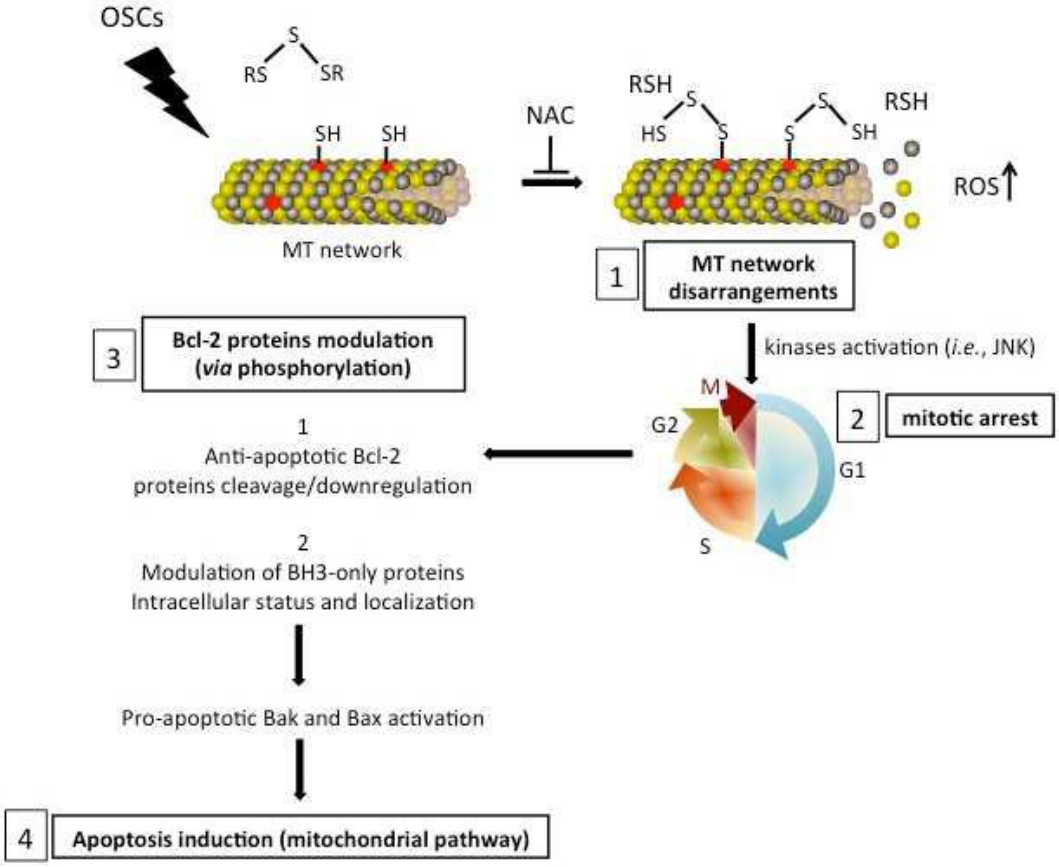

Figure 10: Modifications by organosulfur compounds on microtubule leads to apoptosis via a series of ordered events.

1.7.2 Modification of Enzymes

Gallwitz and co-workers have demonstrated that ajoene is a covalent inhibitor of human glutathione reductase (GR) and *Trypanosoma cruzi* trypanothione reductase (TR), in which both enzymes have been shown to react in a time and temperature-dependent manner towards their substrates and also inhibitors. Interestingly, both enzymes react exclusively in their 2 electron reduced state (EH_2) where

two cysteine residues may react with ajoene to form mixed disulfides. Evidence of such an inhibition of the enzymes was extrapolated from X-ray crystallography which showed an oxidative modification of cysteine-58 on GR, to form a CH_2=CH-CH_2-SO-CH_2-CH=CH=S-SR' (R'= GR cysteine-58) covalently bound to the enzyme (see Scheme 3(i)). Further evidence of the modification was observed by the presence of hydrogen-bonding that existed between ajoene's sulfoxide group and NH- group on alanine-34 in the near vicinity. This is thought to have a bearing on ajoene's activity towards GR inhibition. By comparison DATS did not show any inhibitory effects on GR,[36] this result implies a specificity of GR towards ajoene and particular the *Z*-isomer. The cysteine-58 nucleophilically attack the vinyl-S as opposed to the allyl-S which is a strange outcome as the allyl-S would be expected to be more electrophilic than the vinyl-S on electronic grounds. In an attempt to model the regioselectivity described, ajoene was reacted with free cysteine in the flask and it was indeed found that this yielded allyl-S-S-cysteine as a primary product (see Scheme 3(ii)).[37] Interestingly when 2 equivalents of cysteine are used in the reaction carried out in a neutral medium it formed two products, as the ajocysteine (3-((3-(allylsulfinyl)prop-1-enyl)disulfanyl)-2-aminopropanoic acid) and S-allylmercaptocysteine (see Scheme 3(iii)). Such results suggest that a secondary exchange process between the primary products may ensue.[35]

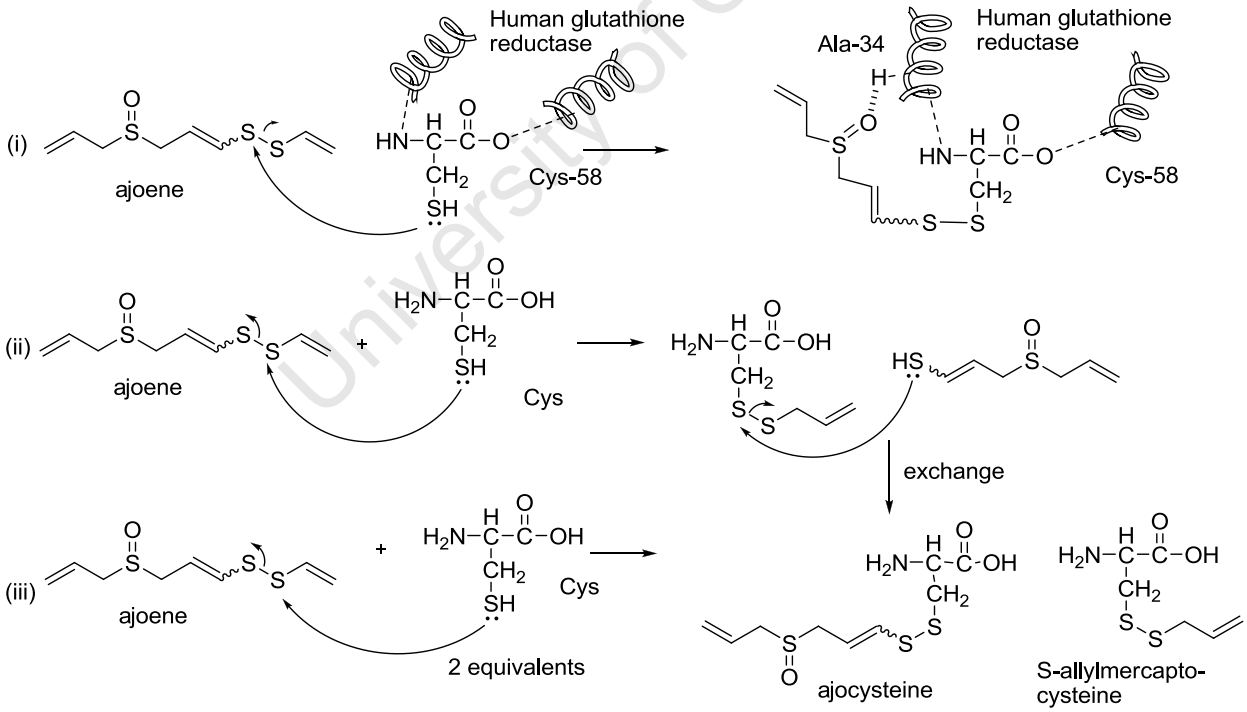

Scheme 3: (i) Ajoene reacting with a cysteine residue on GR and thus inhibiting it;[36] (ii) Reaction of ajoene with 1 equivalent of free cysteine;[35, 37] (iii) Ajoene reacting with 2 equivalents of cysteine to form two products.[36]

University of Cape Town

Gallwitz also demonstrated that ajoene-modified GR shows an elevated oxidase activity, in which blocking of cys-58 creates a shift in electron density that is directed to the flavin ring of the FAD co-factor resulting in an increased reduction of molecular oxygen to produce super-oxide radicals. The elevation of oxidative species coupled with their inability to promote reduction of glutathione created an unmanageable redox environment, resulting in activation of the mitochondrial caspase cascade. This depicts a likely mode of action for ajoene in inhibition of tumour proliferation and is also useful in rational anti-cancer drug design.[35, 36]

1.8 Summary

Garlic has been used for around 5000 years by ancient civilization to combat diseases. It was only in the last century that it was uncovered that the benefits were due to the OCS's that are in garlic. The OCS's have been described in detail and it was found that ajoene a stable rearrangement of allicin was the potent OCS that can be attributed to a lot of the therapeutic benefits outlined. Ajoene possess an array of therapeutic benefits, its anti-cancer properties were of most relevance to the current study and some of the benefits have been outlined. Interestingly ajoene has been shown to be a multi-target agent with the exact mode of action not clearly understood, however it is postulated that the mitochondrial caspase cascade may be directly linked to its apoptosis induction capabilities.

University of Cape Town

Chapter 2: Synthesis aspects of Ajoene

2.1 Overview

The structure of ajoene appeared in the literature in 1984 in a paper published by Block and Apitz-Castro in which ajoene was prepared using a biomimetic synthesis.[41] This chapter serves to outline some of the advances made thus far in ajoene synthesis as well as limitations to the biomimetic synthesis published by Block.

2.2 Block's Biomimetic Synthesis

Block developed a synthetic protocol in the 1980's for ajoene by mimicking how it is formed in Nature. Readily available diallyl disulfide was converted via mono-oxidation by per-acetic acid into allicin, which was immediately heated in aqueous acetone to form ajoene. The mechanism of ajoene formation was described by Block as a self-condensation of allicin, (see Scheme 4),[8, 41] involving *S*-sulfenylation (step ii) followed by the elimination of allylsulfenic acid to form a vinylthionium ion as shown. Subsequent Michael addition with allylsulfenic acid as a nucleophile affords ajoene as a mixture of *E*/*Z* – stereoisomers.

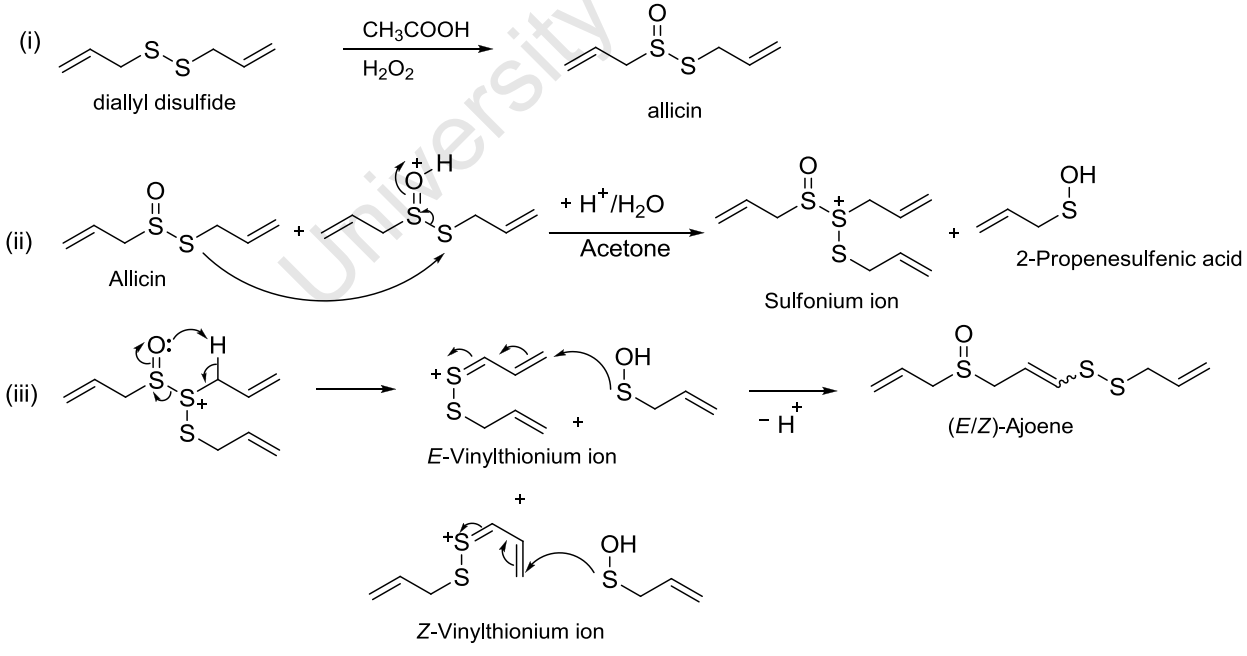

Scheme 4: The acid-catalysed rearrangement of allicin to form (*E*/*Z*)-Ajoene.

University of Cape Town

The biomimetic synthesis, however, has proven not to be a general protocol for synthesizing different analogues of ajoenes as it requires the R^2 group (see Figure 11 for general ajoene structure) to be an allyl group for providing the vinyl disulfide grouping. The R^1 in principle could be any grouping, but R^2 is determined by the vinyl disulfide group as observed from the mechanism and hence can't be varied independently. Another issue with the biomimetic synthesis is that the yield of ajoene is rather low, with 34 % being the highest reported yield in an *E*: *Z* ratio of 4: 1.[8, 41] It is known that the *Z*-isomer is more biologically active than the *E*-isomer, and thus it was crucial to develop a synthesis that provided a balance between yield and optimization of geometrical selectivity for the *Z*-isomer. Thus, a sequence was developed for accessing derivatives with variable end groups, which will now be described in detail.[42]

2.3 Terminally-substituted Ajoene analogues

Modern-day medicinal chemistry has been developed on the basis that a range of structurally related molecules can be created and tested to ultimately develop a SAR (structure-activity relationship) profile. The UCT (University of Cape Town) synthesis was developed on the basis of retaining the biologically active pharmacophore based on the vinyl disulfide and sulfoxide groups while replacing the terminal groups with various groups to achieve different analogues. A generalised structure of target ajoene analogues is depicted in Figure 11.[35]

For consistency in this thesis the ajoene analogues are drawn with the sulfoxide on the left-hand side of the molecule and the disulfide on the right as depicted in Figure 11. Thus, the "left-hand side of the molecule" denotes the R^1 group on the sulfoxide end, while the "right-hand side of the molecule" denotes the R^2 group on the disulfide end.

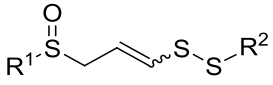

Figure 11: General structure of ajoene analogues.[42]

2.4 University of Cape Town (UCT) synthesis

A four-step synthetic protocol was developed at UCT to access terminally-substituted ajoene analogues, since the biomimetic synthesis only works with R^2 as an allyl group as already discussed. As the key step, the UCT strategy uses a moderately *Z*-stereoselective radical addition to generate the pivotal vinylthio functionality, which is shown in Scheme 5.[42]

University of Cape Town

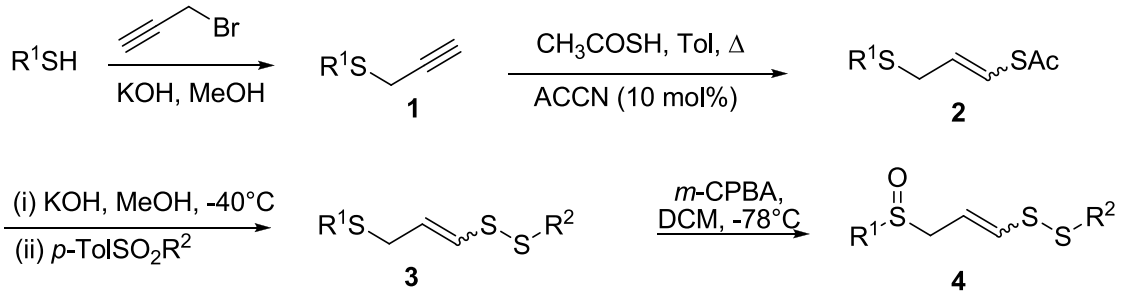

Scheme 5: Synthesis of doubly-end substituted ajoene analogues.

2.4.1 Step 1 - Propargylation

The first step starts with a thiol that is obtained commercially or via reaction of R^1X (X= halogen) with thiourea (see Scheme 6, step (i)) to form an isothiouronium salt. When subjected to potassium hydroxide hydrolysis, the latter forms a thiol, potassium halide and urea. In view of the pungent nature of thiols, it was more convenient to propargylate *in situ*. This was achieved by direct addition of propargyl bromide following the liberation of thiol from hydrolysis to form the desired propargyl thioether **1**.

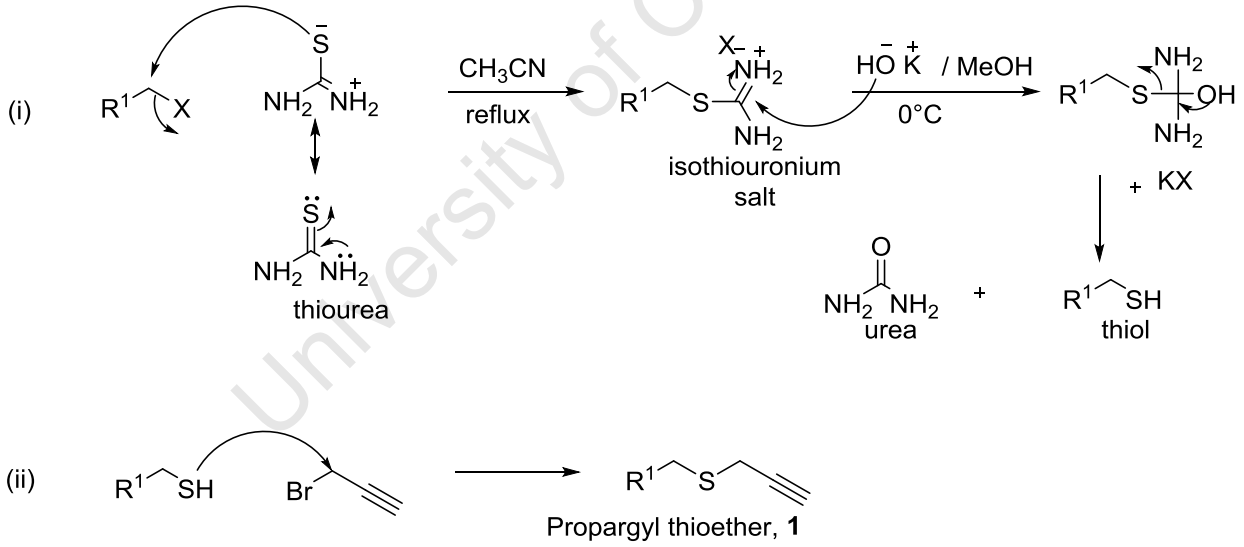

Scheme 6: (i) *in situ* preparation of thiol R^1SH; (ii) Propargylation of thiol.

2.4.2 Step 2 - Radical Addition

The second step involves the regioselective radical addition of thiolacetic acid to the terminus of the alkyne of **1** to form a vinyl thioacetate using ACCN (1,1`-azobis(cyclohexane-1-carbonitrile)) as radical initiator. The radical addition was the key step in the synthesis as it was at this point that the *Z*/*E* stereoselectivity was established, on the basis of a kinetic preference for the *Z*-isomer. This reaction

University of Cape Town

was developed by Kampmeier and colleagues in the 1960's involving regioselective radical addition of thiolacetic acid to 1-hexyne at its terminal position to afford the corresponding vinyl thioacetate. The reaction follows the classical initiation, propagation and termination sequence that is known in radical additions, (see Scheme 7).[44]

Upon heating to around 85 °C, the radical initiator ACCN undergoes thermal cleavage to yield an active α-cyano radical and nitrogen gas. The α-cyano radical then abstracts a hydrogen from thiolacetic acid to generate a thiyl radical, which adds regioselectively to the terminus of the propargyl thioether **1** on both steric as well as electronic control, the latter based on formation of the more stable radical intermediate. The newly formed radical abstracts a hydrogen on the thiolacetic acid to form a vinyl thioacetate, regenerating a new thiyl radical. The reaction is terminated by the dimerization of two thiyl radicals to form a disulfide diacetate. The *Z*-vinyl thioacetate radical provides easier access for the abstraction of the hydrogen in the second propagation step, and thus, the *Z*-product is kinetically favoured over the *E*-product.

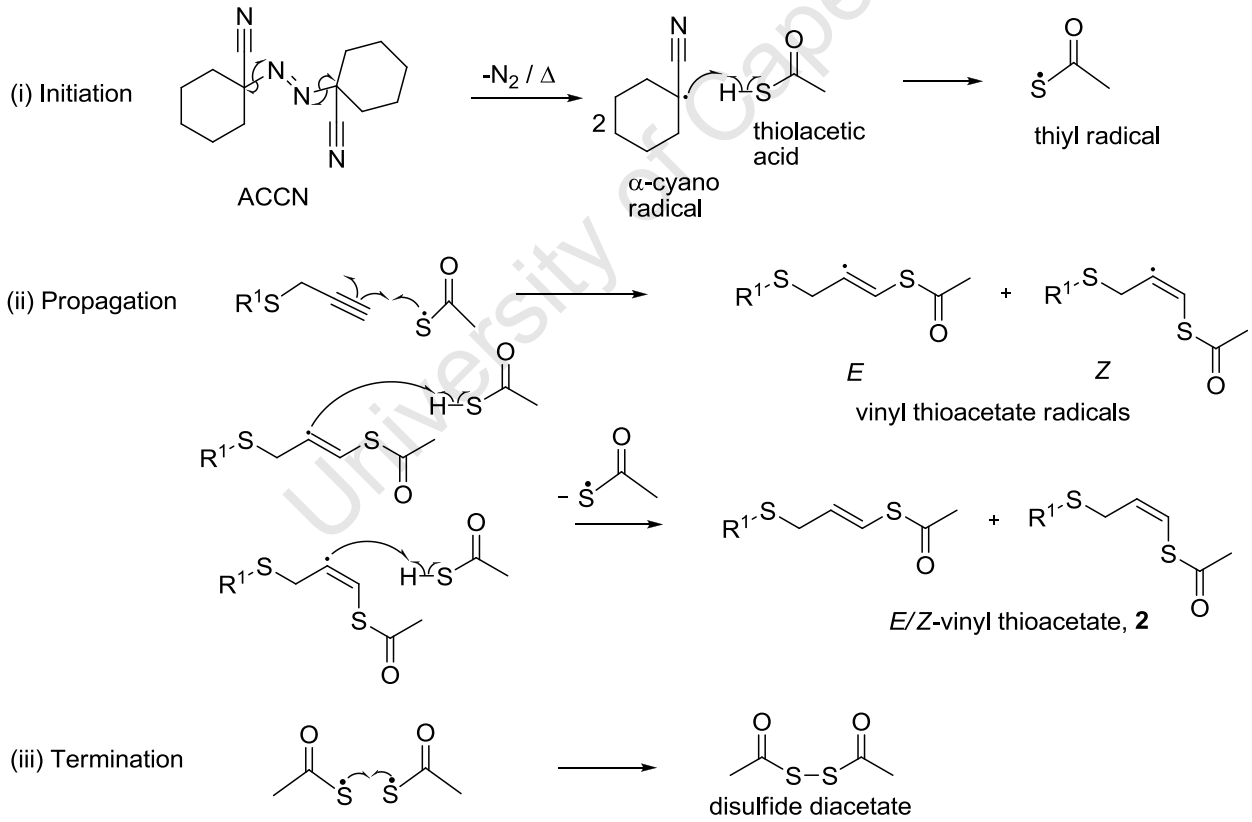

Scheme 7: Radical addition mechanism: (i) Initiation; (ii) Propagation; (iii) Termination.

University of Cape Town

2.4.3 Sulfenylating Agent

The right-hand side of the molecule is constructed from an *S*-tosyl sulfenylating agent derived itself from an appropriate R^2-halide. The thiosulfonate group, -S(SO_2)R, is analogous to the *O*-sulfonate ester (i.e. tosylate) that is used in S_N2 reactions, except that the thiosulfonate sulphur provides an electrophilic site for attack by soft nucleophiles, in contrast to the tosylate which makes the adjacent carbon electrophilic. The thiosulfonates are formed via nucleophilic substitution of an R^2-halide with potassium-thiotosylate, (see Scheme 8 (i)). However, it is important to use the appropriate equivalents of salt as further substitutions on the product are possible with an excess, (see Scheme 8 (ii)).

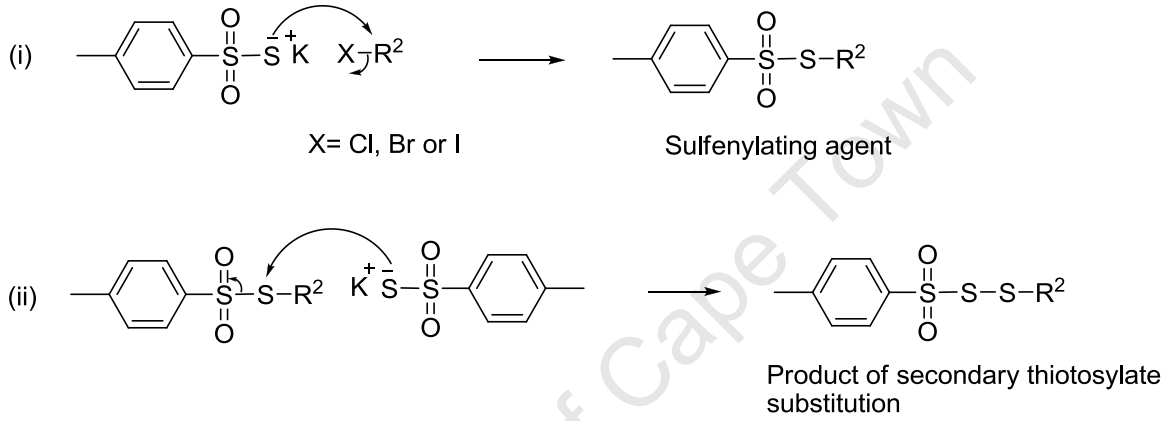

Scheme 8: Synthesis of the sulfenylating agent.

2.4.4 *S*-Sulfenylation Step

Hard-soft acid-base (HSAB) theory was applied in the design of this reaction. The vinyl thioacetate is subjected to deprotection by potassium hydroxide in methanol to form an enethiolate, analogous to an enolate except with S instead of O. This reaction has to be carried out at -40°C in order to retard the geometric isomerisation from the *Z*-isomer to the more stable *E*-isomer via a protonation, tautomerism (to the thioaldehyde), conformational switch, and re-deprotonation sequence. For addition of the sulfenylating agent the reaction is cooled to -78°C, whereupon the enethiolate rapidly displaces the sulfonate leaving group to form the desired disulfide via a soft-soft interaction between the two divalent sulfurs, (see Scheme 9).

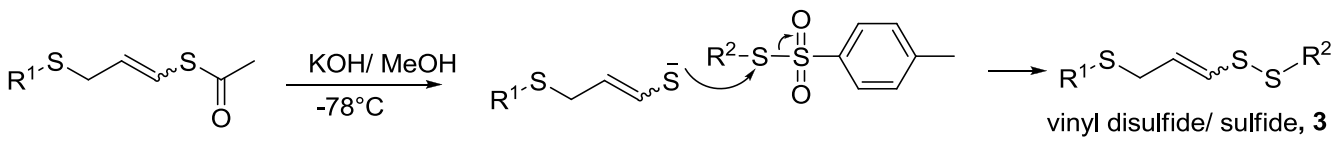

Scheme 9: Coupling of left-hand and right-hand fragments

University of Cape Town

2.4.5 Step 4 - Oxidation

The final step of the synthesis involves the chemoselective oxidation of the more nucleophilic sulfide of the vinyl disulfide / sulfide by limiting the *m*-CPBA (*meta*-chloroperbenzoic acid) oxidant to 1.1 equivalents as well as maintaining the reaction temperature below -60°C, (see Scheme 10). These conditions favour mono-oxidation to occur, on the sulfide sulfur.

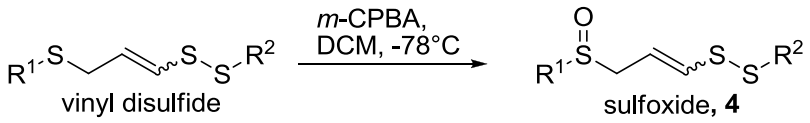

Scheme 10: Oxidation of the substituted-ajoene.

2.5 Summary

The synthetic route developed at UCT can be employed to synthesise a range of terminally-substituted ajoene analogues, although it was found that it could not be used to synthesise ajoene itself, which was explained by postulating that the vinyl radical cyclises onto the left-hand allyl group via a 5-*exo* or 6-*endo-trig* process, but this was not investigated further.[42] Han's group at Seoul National University have recently managed to synthesise the parent ajoene using the UCT method, but did not give a detailed account of their modified synthesis.[44]

Ajoene and its analogues are relatively stable to chromatography, and in cases where small R groups are used on the termini the *E*/*Z*- isomers can be separated, whereas large substituents, such as benzyl generally result in inseparable isomers. In the next section, SAR studies will be described.

2.6 Ajoene Analogues with Improved Water Solubility

2.6.1 Overview

A library of ajoene analogues were synthesized within our group and tested for their anti-proliferation activity on various cancer lines. We were particularly interested in an oesophageal cancer cell-line called WHCO1. Results of the SAR study are summarised in Table 1, where replacement of R^1 and R^2 were varied independently. Ajoene derivatives were tested either as separate isomers or as a mixture of isomers depending on the R group used. Anti-proliferation of the WHCO1 cell-line was determined by an MTT assay, which is a colourimetric assay in which live cells appear as purple due to intact mitochondrial reductase enzymes that reduce the MTT dye.

University of Cape Town

Initially, the R^1 substituents (**4a**- **4g**) were varied and it was identified that having an electron-releasing end-group with high lipophilicity provided an increased anti-proliferation activity, with *p*-methoxybenzyl as the most active substituent on R^1. The R^2 substituent was also optimised (**4j**-**5**) and it was found that *p*-methoxybenzyl also gave the best anti-proliferation of WHCO1 cells. Interestingly, having a *p*-fluorobenzyl substituent gave a significantly less active analogue suggesting that having electron-withdrawing groups on the terminus reduces the activity of the central pharmacophore. In cases where separation of isomers was possible it was found that the *Z*-isomer was slightly more active than the *E*-isomer by around 30%.[42] Hence, replacing both R^1 and R^2 by *p*-methoxybenzyl was identified as our most active analogue (see Figure 12), which resulted in an inseparable mixture that showed a twelvefold increase in activity (2.1 μM) relative to *Z*-ajoene (25 μM). The IC_{50} of this analogue is lower than that of the *in vitro* clinical range for the other chemotherapeutics, cisplatin (9.2 μM) and 5-fluororacil (7.9 μM) on the same cell-line.[35]

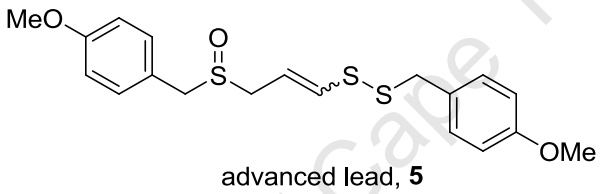

advanced lead, **5**

Figure 12: Advanced lead **5** identified in an SAR study.

Advanced lead **5** was tested for its ability to inhibit tumour growth in a nude-mouse model. However, owing to its lipophilic nature it was not possible to give oral doses and so it was decided to administer it through an intralipid vehicle. The test subjects were each inoculated with 2.50 x 10^6 WHCO1 cells delivered via subcutaneous injection and tumours were allowed to develop over the duration of the study.

At the end of the study it was found that there was no significant effect on tumour growth in the subjects that received drug treatment compared to the control subjects, and also that the drug had no negative effects on the health of the subjects. Advanced lead **5** that returned very good *in vitro* activity, was thus ineffective in reducing tumour sizes in an *in vivo* study. This may have been due to its lipophilic nature resulting in poor drug bio-availability, but it might also have been due to the drug degrading upon administration and thus not reaching the tumours. The latter possibility was further explored when advanced lead **5** was incubated in whole blood for two hours at 37°C and it was found that even after 15 minutes the compound could not be detected by HPLC (see, Figure 13). It may also be postulated that intraperitoneal injection may not have been the best choice for drug delivery. [35, 47]

University of Cape Town

Table 1: Effects of R^1 and R^2 substitution of WHCO1 cell proliferation.

Compound no.	Isomer	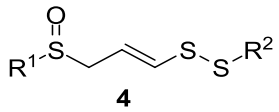 4		IC_{50} ± SD (μM)
		R^1	R^2	
Ajoene	*Z* *E*	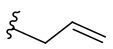	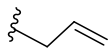	25.0 ± 2.8 39.0 ± 7.8
4a	*Z* *E*	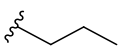	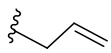	23.0 ± 4.2 37.0 ± 4.5
4b	*E/Z*		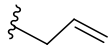	23.0 ± 6.7
4c	*Z* *E*	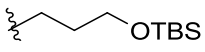	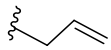	38.0 ± 5.9 27.0 ± 5.6
4d	*Z* *E*	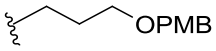	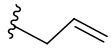	21.0 ± 0.6 18.0 ± 5.7
4e	*Z* *E*	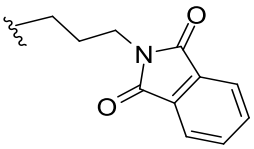	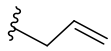	33.0 ± 1.4 68.0 ± 15
4f	*E/Z*	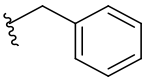	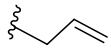	8.9 ± 1.2
4g	*E/Z*	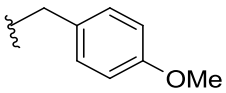	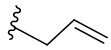	7.4 ± 0.7
4h	*Z* *E*	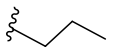	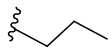	18.0 ± 4.1 24.0 ± 2.8
4i	*Z* *E*	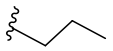	CH_3	26.0 ± 7.5 28.0 ± 7.2
4j	*E/Z*	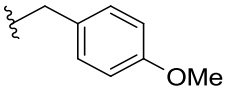	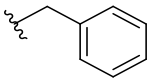	3.1 ± 1.1
4k	*E/Z*	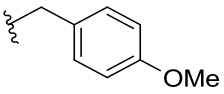	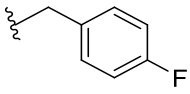	16. ± 1.1
5	*E/Z*	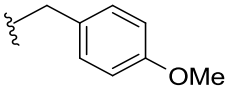	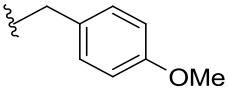	2.1 ± 0.4

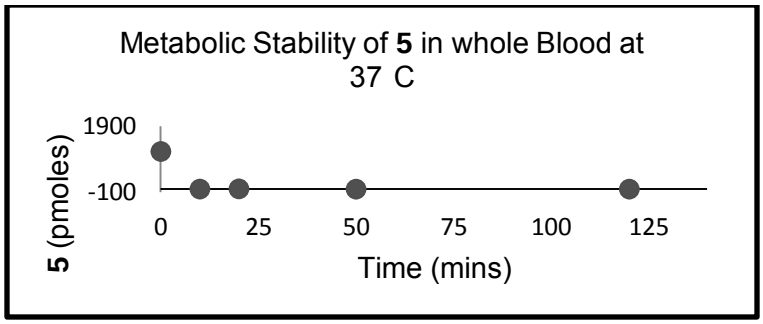

Figure 13: Metabolic stability of advanced lead **5**, as measured by HPLC.

The current project was aimed at addressing the first of these issues by introducing groups at the *para*-position of the benzyl substituents of **5** that would promote water-solubility. The new target should resemble analogue **5** as closely as possible in order to maximize activity and thus the proposed modified target was conceptualised as depicted in Figure 14. The next section serves to describe in detail the synthesis of ajoenes with substituents that promote an increased degree of aqueous solubility, their characterisation and also their biological evaluation.

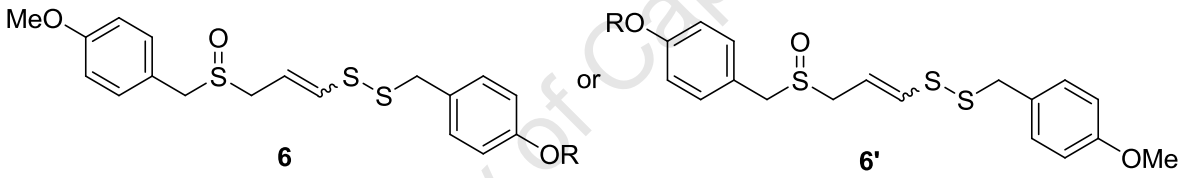

R= H, Water-soluble Group

Figure 14: Illustration of the target water-soluble ajoene, **6** and **6'**.

A second objective was to design the synthesis such that it is possible to place a radioactive ^{14}C-tag on one of the *p*-methoxy methyl groups in an attempt to track the movement and accumulation in nude mice xenografts using positron emission tomography (PET). In this case, the radiolabed ajoene analogue would still need to resemble **5** as depicted in Figure 15. This was done in collaboration with NTeMBI/ NECSA at the nuclear facilities at Pelindaba in South Africa

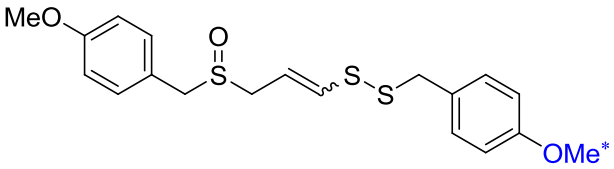

Radiolabeled lead, **7**

Figure 15: Illustration of targeted labelled analogue, **7**.

University of Cape Town

The UCT synthesis was employed to access the two target molecules and so it was decided to start the sequence by synthesis of an advanced intermediate that would allow placement of a radiolabeled tag and also a water-soluble group as the last step based on the availability of the tag. This required one of the aromatic groups to be a free phenol.

The synthesis began with attempts to synthesize ajoene 6' with a free phenol on the left-hand side of the molecule. A retrosynthetic analysis based on the UCT synthesis is shown in Scheme 11, which indentified synthons **8** and **9** as accessible from methyl *p*-hydroxybenzoate **12** and *p*-methoxybenzyl chloride **11** respectively. Reagent **9** had previously been synthesized within our group from the chloride **11**.

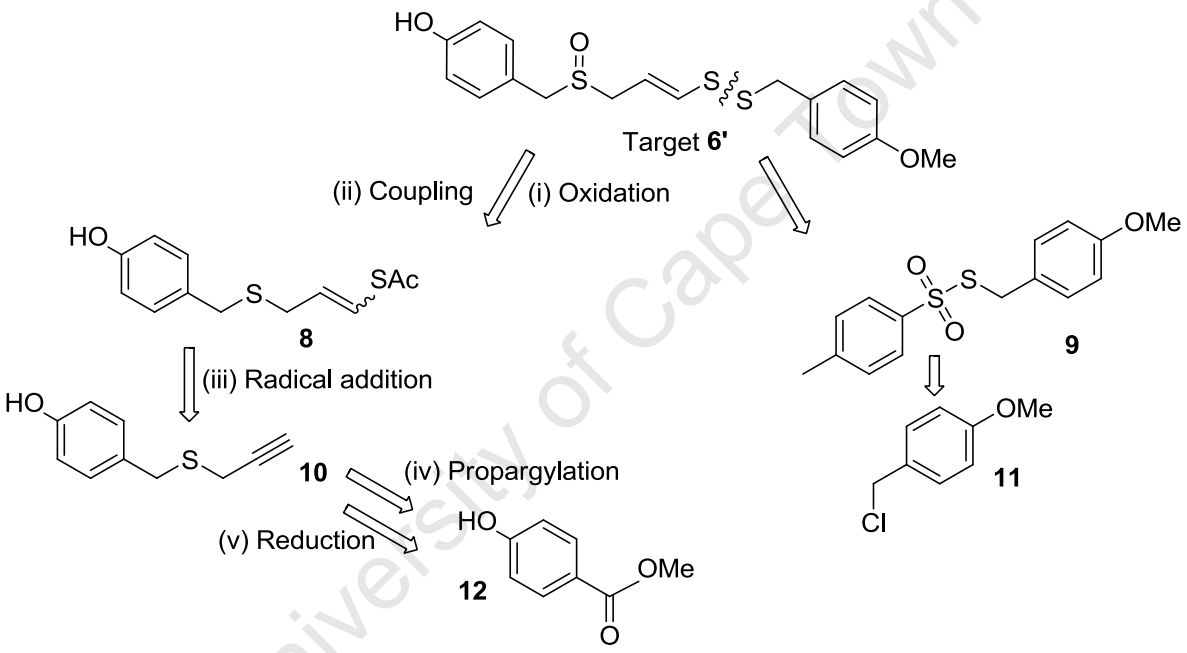

Scheme 11: Retrosynthetic analysis of target **6'**.

University of Cape Town

Chapter 3: Results and Discussions

3.1 Studies towards synthesis of Ajoene 6'

It was envisioned that synthon **8** could be synthesised from thiopropargylated phenol **10,** which in turn could be accessed via the commercially available phenolic ester **12**, (see Scheme 12).

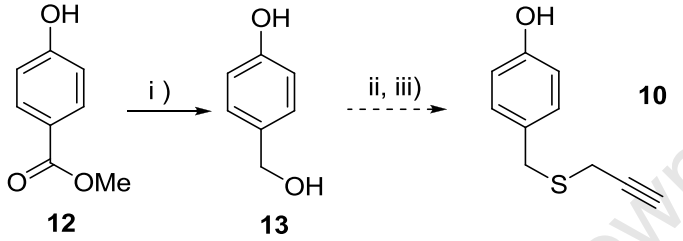

Scheme 12: (i) $LiAlH_4$ (LAH) / THF; (ii) $SOCl_2$/ $CHCl_3$; (iii) Thiourea/ Δ; KOH/ propargyl bromide

The first step began with an attempt to reduce commercially available methyl *p*-hydroxybenzoate **12** with 2 mol equivalents of LAH (Lithium aluminium hydride) to the corresponding benzylic alcohol **13**. The reaction turned out to be problematic and failed to produce an appreciable conversion as there was no formation of a polar spot upon TLC monitoring. Increasing the equivalents of LAH to 4 compared to the ester with heating also failed to improve conversion. This result was rationalised by assuming formation of the phenoxide *in situ* via deprotonation by the basic LAH resulting in the reduction in the electrophilicity of the ester carbonyl carbon via resonance delocalisation, (see Scheme 13). A degree of literature precedence exists on this problem.[45]

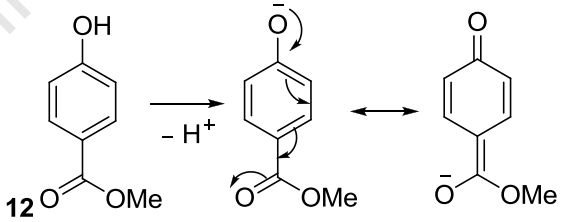

Scheme 13: Resonance delocalisation in the phenoxide ion of **12**.

The desired 4-hydroxybenzyl alcohol **13** was indeed commercially available which was adopted as the starting material. However attempts to convert the benzylic hydroxyl group into a better leaving group (Cl) using thionyl chloride in chloroform failed to give satisfactory results based on NMR data of the product formed, as the phenolic benzyl chloride was a highly reactive intermediate that rapidly

University of Cape Town

converted to a *p*-quinone methide with evolution of HCl (hydrochloric acid) gas as shown in Scheme 14. A similar result has been reported in the literature.[45, 48]

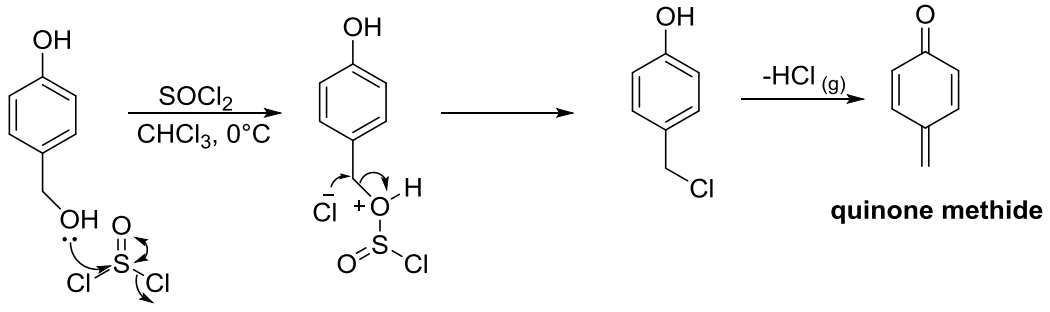

Scheme 14: Elimination of the target intermediate to form *p*-quinone methide.

At this point it was decided to attempt exploiting the S_N1 character of the benzylic position for direct substitution with a sulfur nucleophile. Thus, benzyl alcohol **13** was subjected to a classical S_N1 substitution using boron trifluoride etherate (BF_3: Et_2O) and thiolacetic acid in DCM. The reaction was expected to proceed via a *p*-quinone methide (as an attractive Michael acceptor) as shown in Scheme 15. The reaction involved addition of BF_3: Et_2O to benzyl alcohol **13** at 0°C, as the Lewis acid was very reactive. Reaction was allowed to progress for 30 minutes to facilitate formation of the *p*-quinone methide before adding thiolacetic acid dropwise to the mixture. The reaction was monitored by TLC, following the disappearance of the polar benzyl alcohol, which indicated that it had reached completion within the first hour. At this point the reaction was quenched with aq.$NaHCO_3$ (sodium bicarbonate). The desired thioacetate **14** was purified by column chromatography in 74% yield as a pungent oil and its structure confirmed by ^1H and ^{13}C NMR analysis in which **14** was shown to agree with the data.[49]

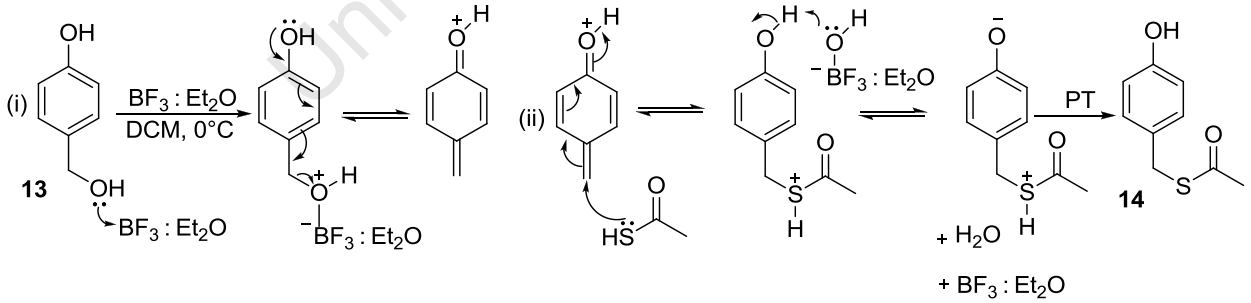

Scheme 15: S_N1 substitution to thioacetate **14** via a *p*-quinone methide.

The next step in the sequence involved hydrolysis of the acetate group of **14**, but unexpectedly, a prolonged treatment with KOH in EtOH or MeOH was necessary for full conversion of the thioacetate. However, only a 15% yield of the benzyl thiol was achieved. This was rationalised by invoking

University of Cape Town

deprotonation of the acidic phenolic hydroxyl group to the phenoxide ion, which retarded the facile hydrolysis of the thioacetate via electronic repulsion with the hydroxide ion.

From the findings described it was clear that using the *p*-hydroxybenzyl starting material to access the vinyl thioacetate **8** was problematic on account of the electronic connection between the *p*-hydroxyl group and the benzylic position. Thus, it was decided to lengthen the tether by one carbon atom in order to isolate these two functionalities electronically. Importantly, it was thought that adding an extra methylene group would have no drastic effect on the biological activity of the ajoene, since the pharmacophore resides within the vinyl disulfide and the sulfoxide.[35]

Commercially available methyl *p*-hydroxyphenylacetate **15** was successfully rapidly reduced with LAH in THF (tetrahydrofuran) at 0°C to alcohol **16** in high yield, corroborating our earlier findings about communication between the two sites. Thereafter, the primary hydroxyl group of **16** was converted to its iodide **17** using iodine and triphenylphosphine. The reaction involves formation of an alkoxyphosphonium ion of the more reactive hydroxyl group followed by substitution by iodide ion with expulsion of triphenylphosphine oxide. Imidazole was added to neutralise the HI which forms as a bi-product. The reaction was driven by formation of the triphenylphospine oxide and reached completion in an hour and a half as seen on TLC by the disappearance of the alcohol and formation of the less polar iodide together with the oxide. The resulting product was purified by chromatography in 90% yield, and could now be subjected to substitution to the propargylic sulfide **18**, (see Scheme 16).

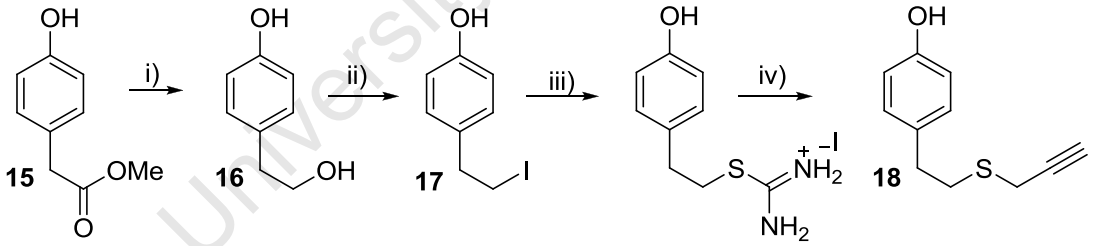

Scheme 16: (i) LAH/ THF (85%); (ii) I_2, Imidazole, PPh_3/ THF (90%); (iii) Thiourea, Δ, CH_3CN; (iv) KOH/ MeOH, Propargyl bromide.

Reaction of iodide **17** with thiourea proceeded to the isothiouronium salt with ease according to TLC as seen by the formation of a product spot that only migrated in a polar medium such as MeOH in DCM at a ratio of 1: 9. However, the propargylation step proved to be problematic, since the salt could not be hydrolyzed very readily. Once again, the problem encountered in the sequence may have been due to the formation of the phenoxide ion in the presence of the KOH, resulting in deactivation of the subsequent chemistry. At this point two other routes to achieve intermediate **18** were pursued as: (i) a

University of Cape Town

standard S_N2 substitution on the iodide **17** with thioacetate ion followed by base hydrolysis and propargylation, or (ii) substitution of **17** with a propargylthioate ion directly. Both sequences failed to give satisfactory results overall. The thiol derivative of **16** could be accessed from iodide **17** using sequence (i) above, but it could not be propargylated to intermediate **18**. As a last resort to prevent the phenoxide interference, the phenolic hydroxyl group of iodide **17** was protected with a TBDPS group, but this underwent deprotection when KOH or NaOMe in MeOH was used to facilitate the nucleophilic substitution at the iodide end.

It was decided to carry out a model study of other possible phenolic hydroxyl protecting groups, which revealed that: (i) the THP (tetrahydropyranyl) ether of 4-*tert*-butylphenol could be readily prepared but was rapidly removed by mild acids, (ii) silyl ethers were also tested and it was found that they were sensitive to hydroxide ion needed in the transformation of the isothiouronium salt and, (iii) a benzyl ether was not investigated as it requires removal by HX (X=halide) or H_2, Pd/C, which would not be compatible with vinyl thioacetate **8** later in the sequence.

All these results suggested that having a free phenol on the "left-hand side" of the molecule was very problematic as a lot of the reactions carried out invoked the usage of base, which created a phenoxide ion that ultimately deactivated any further chemistry on other functionality within the molecule.

3.2 Synthesis of Ajoenes, 6

Bearing in mind the challenges encountered with the previous target **6'** It was decided to switch to having the free phenol on the "right-hand side" of the molecule**,** so the new ajoene target was adopted as **6**, as depicted in Figure 15.

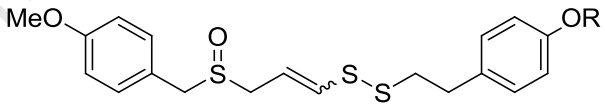

6, R = H

Figure 15: *p*-Methoxybenzyl / *p*-hydroxyphenethyl ajoene, **6**.

Retrosynthetic analysis of target **6**, according to the basic synthetic Scheme 17 identified synthons **23** and **19** which could be accessed from *p*-methoxybenzyl chloride **11** and the methyl *p*-hydroxyphenylacetate **15** respectively.

University of Cape Town

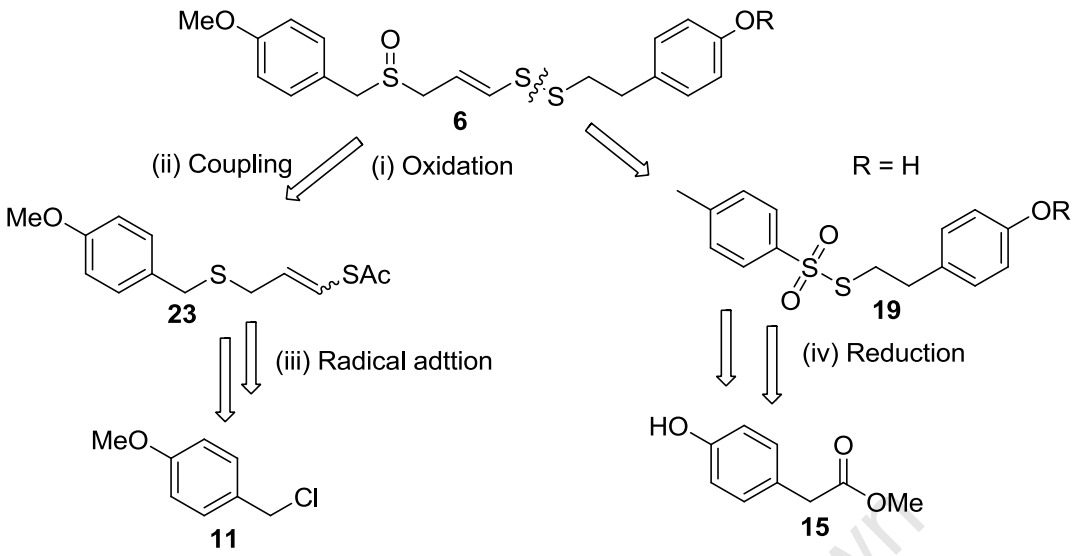

Scheme 17: Retrosynthetic analysis of the target ajoene molecule **6**.

3.2.1 Thiotosylate Sulfenylating Agent, 19

Our initial studies showed that a free phenol on the left-hand side of the molecule prevented further chemistry on other functionalities in the molecule, so it was decided to place the phenol group (for conversion to OR) on the disulfide end, making it part of the sulfenylating agent. The sulfenylating agent would be accessed by an S_N2 substitution reaction between iodide **17** and a thiotosylate group without invoking phenoxide generation because of the low basicity of the thiotosylate grouping. It was hoped that overall the free phenolic hydroxyl group wouldn't pose problems as before in order to avoid implementing a protection / deprotection sequence. The iodide **17** could be prepared from commercially available methyl *p*-hydroxyphenylacetate **15** via two steps that will be described next.

3.2.1.1 Alcohol, 16[39]

The alcohol **16** was synthesized by suspending LAH (3 mol equivalents) into THF at 0°C and slowly adding a solution of the methyl *p*-hydroxyphenylacetate **15** dissolved into a minimum amount of THF (see Scheme 18 (i)). The ester reduction was complete after 2 hours as evidenced by TLC analysis in which **16** appeared as a dominant polar spot relative to the ester starting material. 1M HCl was slowly added to the reaction mixture to quench the reaction and liberate the alcohol product from the aluminium salts formed in the reaction, and the resulting solution was filtered through Celite and the solid washed with EtOAc. Following drying of the filtrate, and removal of solvent, the residue crystallized from hexane to afford a clear crystalline solid in 85% yield.

University of Cape Town

The product was characterised primarily through ^{1}H and ^{13}C NMR data. The ^{1}H NMR of **16** revealed a singlet at 8.0 ppm corresponding to the phenolic OH, a pair of AB doublets at 7.05 ppm (H-3) and 6.74 ppm (H-2) characteristic for a *p*-substituted phenyl group, two methylene triplets at 3.69 ppm (H-6) and 2.71 ppm (H-5) and also a primary hydroxyl signal at 3.53 ppm.

The ^{13}C spectrum revealed absence of the carbonyl carbon, a downfield resonance at 156.6 ppm corresponding to C-1 bonded to oxygen and the other quaternary resonance at 131.1 corresponding to C-4. The signals for C-2 and C-3 on the aromatic ring were observed at 116.0 ppm and 130.8 ppm respectively, and interestingly C-2 was more deshielded than C-3 due to the shielding effect caused by mesomeric donation of the phenol hydroxyl into the phenyl ring (see Figure 16). Resonances at 64.3 ppm and 39.6 ppm corresponded to the two methylene carbon C-6 and C-5 respectively. All the carbon signals were successfully correlated with associated protons by HSQC analysis.

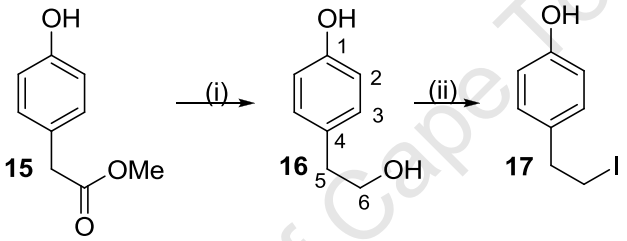

Scheme 18: (i) LAH/ THF/ 2 hrs/ 0°C; (ii) I_2, Imidazole, PPh_3/ THF/ 2 hrs/ 0°C

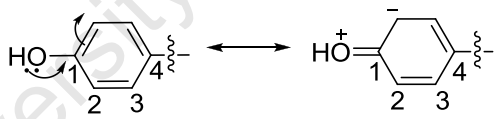

Figure 16: Mesomeric effect on the phenol ring.

3.2.1.2 Iodide, 17[40]

The next step involved the conversion of the primary hydroxyl group to the corresponding iodide. Alkyl halides are very useful intermediates for carbon-carbon bond formation via substitutions or radical reactions, and iodides are the most reactive of the alkyl halides. There are many methods described in the literature to achieve this transformation such as: BF_3:Et_2O / NaI, P_4 / I_2, $SOCl_2$-DMF / KI, MgI_2 and HI. However, these procedures suffer from one or more drawbacks such as low yields, long reaction times, drastic reaction conditions and tedious work-up procedures. A simple, mild and high-yielding procedure was employed in our transformation using iodine, triphenylphosphine and imidazole as described (*vide supra*) to afford the iodide **17** in 90%, (see Scheme 18, step (ii)).

University of Cape Town

The ^{1}H NMR for **17** revealed the diagnostic AB doublets characteristic of *p*-substituted phenyl groups at 7.06 ppm and 6.78 ppm, as well as a broad singlet at 4.84 ppm corresponding to the phenol OH, two methylene triplet signals at 3.31 ppm and 3.10 ppm corresponding to H-6 and H-5 respectively. The iodination was confirmed by the disappearance of the primary hydroxyl signal and an upfield shift of the H-6 triplet.

The ^{13}C NMR spectrum revealed two aromatic signals at 129.8 ppm and 115.6 ppm corresponding to C-3 and C-2 respectively, two methylene carbons at 39.5 ppm (C-5) and 6.4 ppm (C-6). The signal for C-6 offered further evidence for iodide formation in terms of the electron withdrawing oxygen being replaced by a highly shielding iodine.

3.2.1.3 Phenolic Thiotosylate tether, 19

In the last step in the synthesis of **19** (see Scheme 19), the desired sulfenylating agent was prepared by stirring iodide **17** with potassium thiotosylate (1.2 equivalents) in DMF at room temperature for 2 hours. At this point, TLC analysis indicated reaction completion by virtue of the formation of a more polar product relative to the starting iodide **17**, after which the DMF was removed under vacuum. The resulting residue was suspended into water and extracted into EtOAc, which was washed to remove residual DMF and dried over $MgSO_4$. Solvent evaporation afforded a pure clear oil **19** in 96% according to ^{1}H NMR analysis.

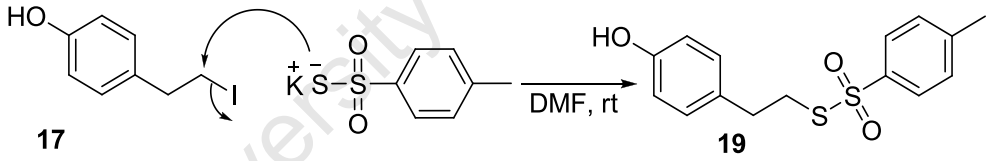

Scheme 19: Phenolic sulfenylating agent **19**.

The ^{1}H NMR of **19** revealed two sets of AB doublets in the aromatic region corresponding to two aromatic groups as H-4, H-3, H-9 and H-10 (see Figure 17 for numbering). A broad singlet at 3.38 ppm was observed for the phenol hydroxyl, two methylene triplets for H-7 and H-6 and another singlet at 2.45 ppm for H-1. Finally, the distinct aliphatic singlet for the H-1 methyl group provided evidence of a successful coupling reaction to form **19**.

The ^{13}C NMR spectrum of **19** revealed four aromatic singlets for the C-H carbons of which two belonged to the phenol ring and the other two to the thiotosylate core. In addition, four relaxed quaternary carbons were observed together with 3 aliphatic carbons at 37.6 ppm, 34.4 ppm and 21.8 ppm corresponding to C-7, C-6 and C-1 respectively. The significant downfield shift for C-6 (6.4 to 34.4

University of Cape Town

ppm) offered more evidence of coupling and consistent with the formation of a C-S bond. The IR spectrum of **19** indicated the presence of the tosylate group (-RSO_2R-) at 1228 cm^{-1} and also a phenol (ArOH) at 3152 cm^{-1}. High resolution mass spectrometry (HRMS) corroborated the molecular weight as found, (ES) *m/z*: 309.0615 $[M+H]^+$, $C_{15}H_{17}O_3S_2$ requires 309.0619, thus confirming product formation.

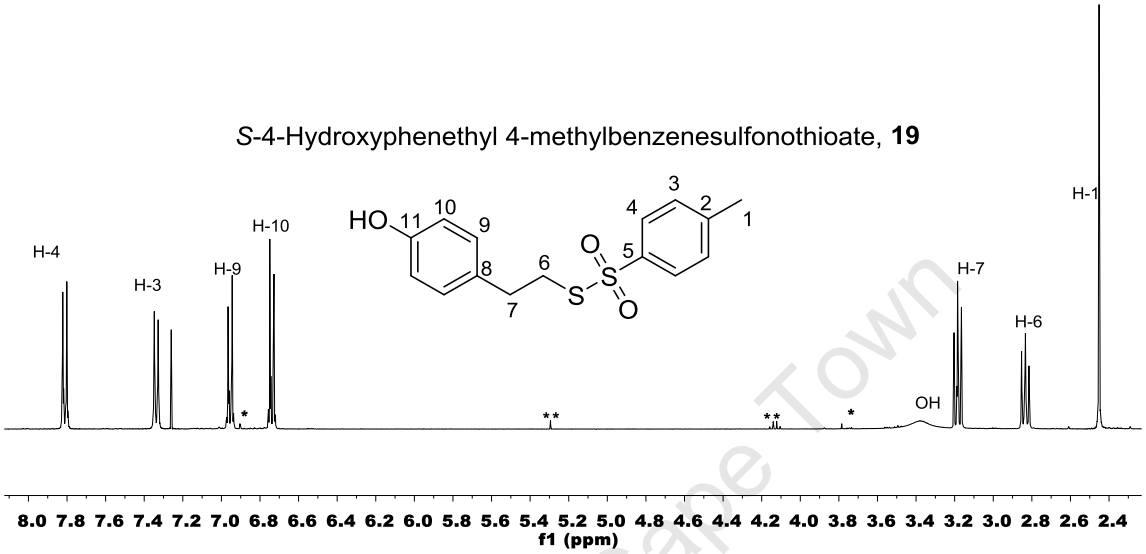

Figure 17: ^1H NMR spectrum of **19** in chloroform-d_3. **: Solvent impurities, *: impurity

University of Cape Town

3.2.2 PMB Vinyl thioacetate, 23[35]

With the right-hand fragment in hand we then turned our attention to the left-hand fragment. From the retrosynthetic analysis it was identified that the required vinyl thioacetate **23** could be accessed in two steps from commercially available *p*-methoxybenzyl chloride **11** as the starting material. The synthesis of **23** will now be described in detail.

3.2.2.1 PMB Alkyne, 22[35]

Adhering to the UCT synthesis as described previously in Chapter 2, the synthesis of the desired vinyl thioacetate **23** intermediate (see Scheme 20) began with the preparation of the *p*-methoxybenzyl thiol **21** which was achieved from commercially available *p*-methoxybenzyl chloride **11** using the thiourea methodology. The reaction was initiated by refluxing **11** with thiourea (1.2 mol equivalents) in acetonitrile. The donation of the lone pair on nitrogen enhances the nucleophilicity of the thiourea sulfur, which undergoes nucleophilic attack on the reactive benzyl halide to form the isothiouronium salt **20**. The salt **20** proved to be very polar and only migrated slightly on TLC in a polar medium such as MeOH in DCM at a ratio of 1: 9. The reaction progress was monitored by the disappearance of the *p*-

methoxybenzyl chloride and had reached completion within an hour and a half. Upon cooling, the thiouronium salt crystallised out of solution, and it was then filtered and washed twice with ice-cold acetonitrile and dried. The salt **20** was carried forward to the subsequent step without any further purification, in which it was dissolved in degassed MeOH at 0°C containing 2.5 equivalents of KOH. Therafter, propargyl bromide was added for the *in situ* propargylation of the thiol. Urea was produced in the reaction as a by-product. It was necessary to use 2.5 equivalents of KOH to completely hydrolyse the isothiouronium salt **20** to the corresponding thiol as well as to neutralise the HBr generated from the propargylation step. The propargylation step proved to be rapid, and reached completion within 40 minutes as seen by the appearance of a less polar product spot on TLC compared to the salt **20**. The product was purified by column chromatography to afford the alkyne **22** as a light-yellow pungent oil in 90% yield over the two steps.

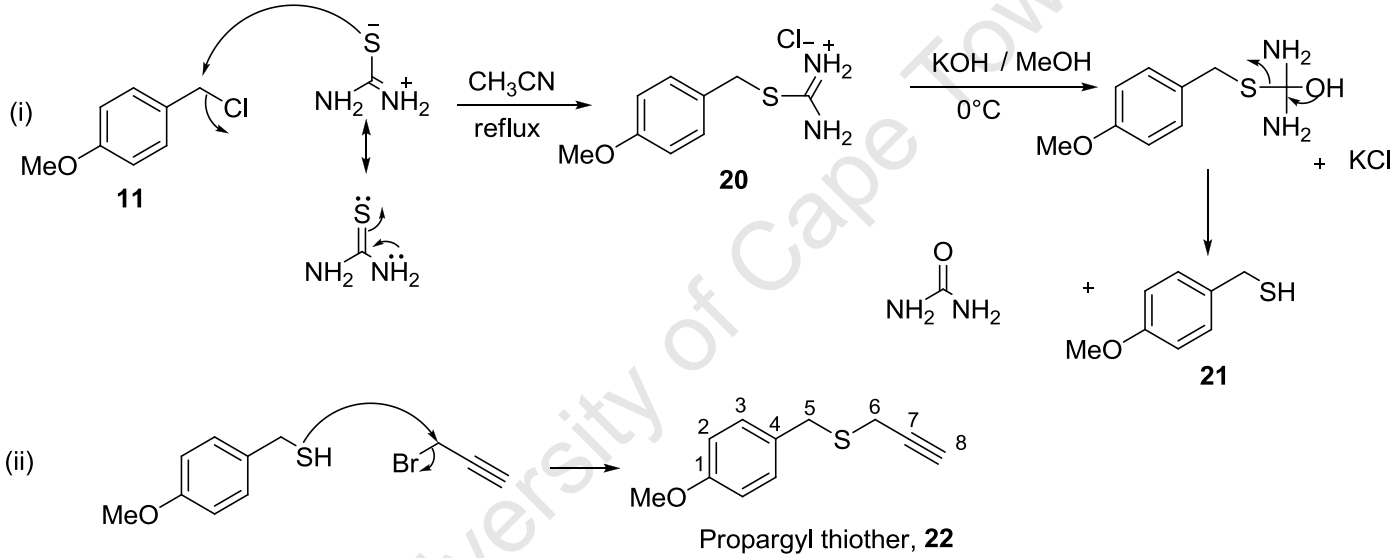

Scheme 20: Synthesis of the propargyl thioether **22**.

Evidence for propargylation was given by the appearance of a doublet at 3.08 ppm for H-6 that integrated for two protons, as well as a triplet at 2.28 integrating for one proton corresponding to H-8. Interestingly, the two signals had a common coupling of 2.6 Hz that indicated transmission through the triple bond C-6 and C-8. Analysis of the ^{13}C NMR spectrum of **22** revealed the alkyne carbons resonating at 80.1 ppm and 71.3 ppm corresponding to C-7 and C-8 respectively. Two methylene signals were observed at 34.9 ppm and 18.4 ppm corresponding to C-5 and C-6 respectively.

University of Cape Town

3.2.2.2 Vinyl thioacetate, 23[35]

The second step in the synthesis of vinyl thioacetate **23** involved the regioselective addition of thiolacetic acid to the terminus of alkyne **23** (see Scheme 21). The reaction was carried out by dissolving alkyne **23** in dry, degassed toluene and heating to 85°C. The radical initiator ACCN (0.1 equivalents) was added to the solution followed by the drop-wise addition of thiolacetic acid (1.2 equivalents) in toluene over 20 minutes. The temperature was cautiously maintained at 85°C, as it was thought that higher temperatures would favour further additions of thiolacetic acid to form the bis-substituted **23a** product. After an hour, TLC analysis revealed the formation of a more polar spot and substantial depletion of the starting alkyne **22**. Upon cooling, saturated aqueous sodium carbonate was added to the solution to quench any remaining thiolacetic acid. The toluene solvent was removed under vacuum and the residue extracted into DCM and dried over $MgSO_4$. The product was purified by column chromatography to afford vinyl thioacetate **23** in 62% yield as a ~ 1:1 mixture of *Z*: *E* isomers that were inseparable.

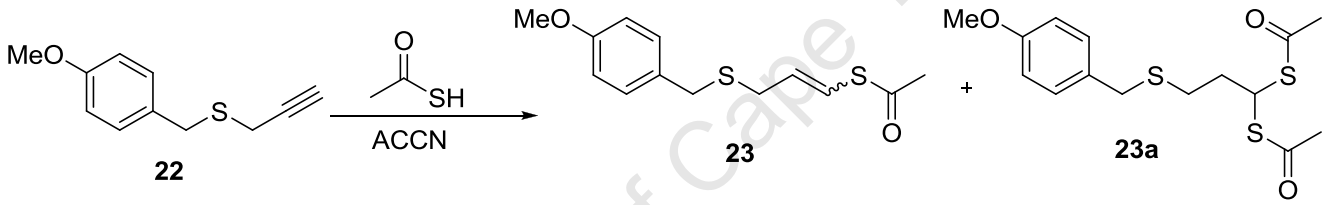

Scheme 21: Regioselective radical addition of thiolacetic acid to form vinyl thioacetate **23**.

The ^{1}H NMR spectrum of **23** revealed overlapping signals for both isomers that could not be distinguished easily. However, two vinyl doublets of triplets (allylic coupling to H-5) were observed downfield at 6.67 ppm and 6.50 ppm corresponding to H-3 of the *E*- and *Z*-isomers respectively (see Figure 18 for numbering) proving that addition had taken place on the terminus of alkyne **22**. The two isomers displayed different vicinal coupling constants between H-3 and H-4, which were 15.6 Hz for the *E*- and 9.6 Hz for the *Z*-isomer respectively. The H-4 signals were observed as an overlapping doublet of triplets ranging between 5.80 ppm and 5.87 ppm as they coupled to both H-5 and H-3. The H-5 peak appeared as a set of doublet of doublets accounting for both isomers that experienced coupling to both the vicinal H-4 and the allylic H-3. Other peaks were used to correctly identify the product included two acetyl singlets at 2.38 ppm and 2.36 ppm.

The ^{13}C NMR spectrum showed all the 26 required carbon signals (13 for each isomer) whereby two downfield signals were observed at 193.1 ppm and 191.4 ppm corresponding to the thioacetate carbonyl (C-2) of the *E*- and *Z*-isomers respectively. 2 sets of: two aromatic C-H carbons, two aromatic quaternary carbons, two vinyl carbons, three aliphatic signals and also the methoxy signals at 55.4 ppm

University of Cape Town

were observed for the two isomers. As the latter couldn't be separated by chromatography, HSQC was used to assign the signal for each one.

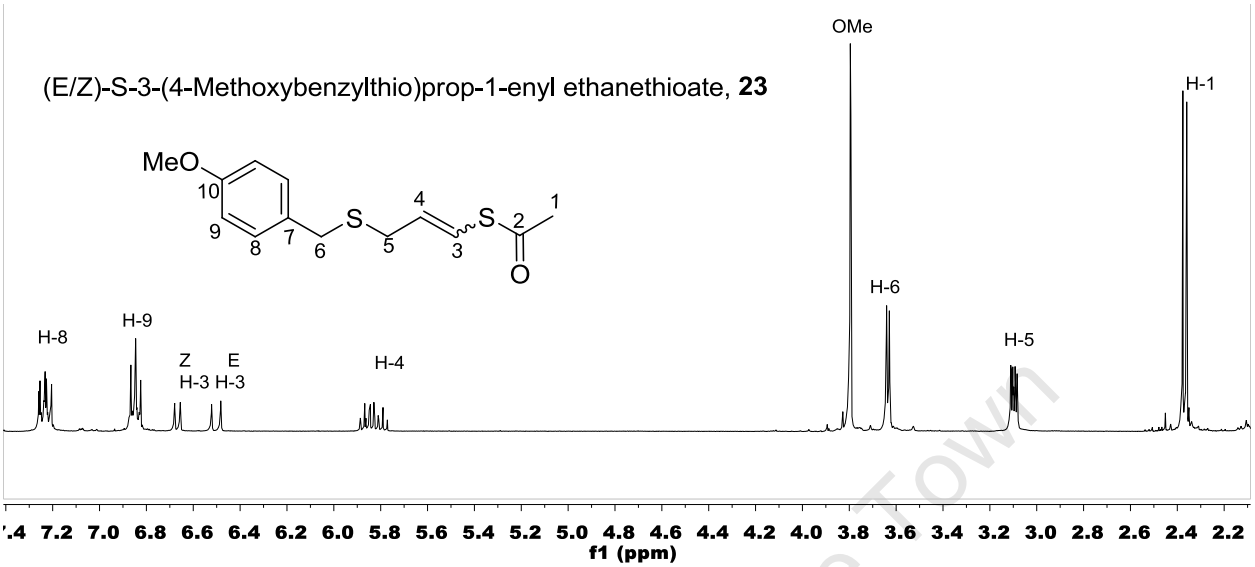

Figure 18: ^{1}H NMR spectrum of **23** in chloroform-d_3.

3.2.3 PMB-phenol Disulfide, 25

The coupling (see Scheme 22) of vinyl thioacetate **23** with the sulfenylating agent **19** to afford the core vinyl disulfide pharmacophore was a critical step in the synthesis of the target molecule **6**. This was achieved by vinyl thioacetate deprotection to its corresponding enethiolate ion **24** by hydrolysis with KOH in MeOH at -40°C. The reaction was kept at -40°C to retard the highly reactive enethiolate **24** from forming side products or reducing the possibility of tautomerism to the thermodynamically more stable *E*-isomer. The reaction was allowed to proceed for 45 minutes at -40°C after which it was cooled further to -78°C before adding the sulfenylating agent **19** (1.3 equivalents) dissolved in DCM (as a co-solvent) to the reaction mixture. TLC analysis was performed after an hour to reveal a dominant, more polar spot than the vinyl thioacetate, with reduction in intensity of the spot for the sulfenylating agent. Overall, it was found that an hour and a half for this step was sufficient time to achieve good yields. The reaction was quenched at -10°C with saturated ammonium chloride prior to being extracted, and the residue purified by column chromatography to afford the coupled product **25** as a 5:4 mixture of *E/Z*-isomers in a 73% yield.

University of Cape Town

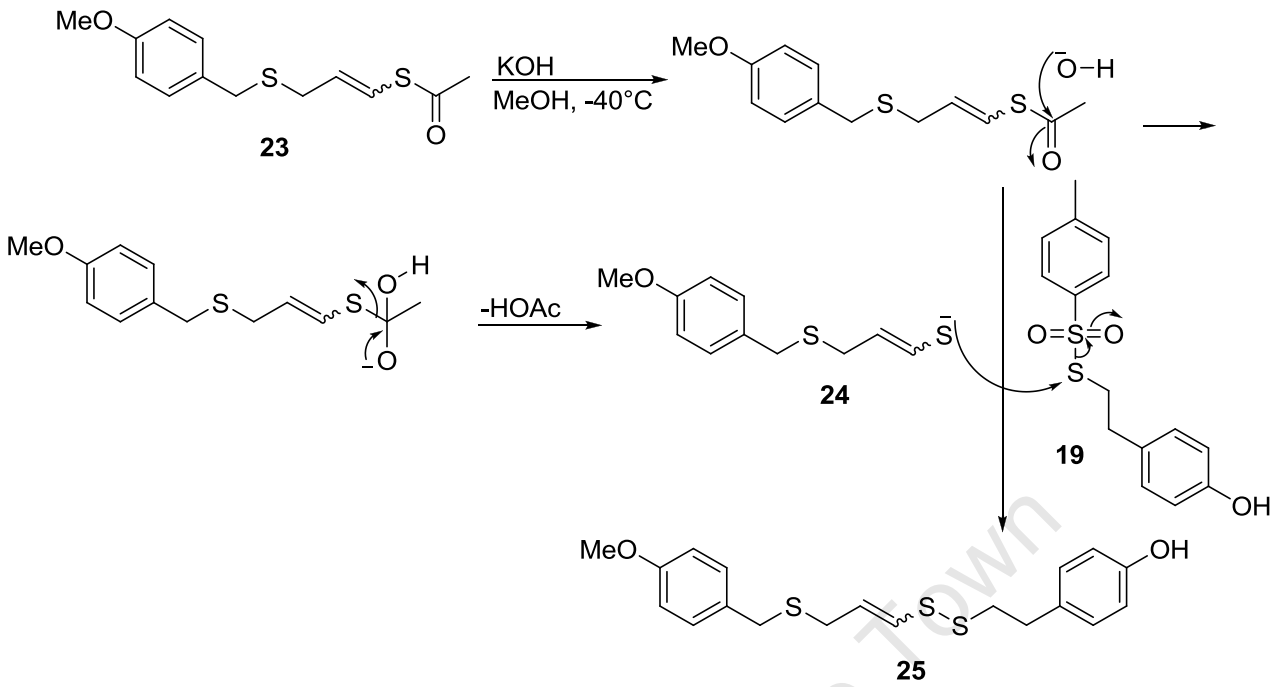

Scheme 22: Coupling of **19** and **23** to form vinyl disulfide **25**.

Surprisingly, there appeared to be a slight geometry reversal about the double bond, from ~ 1:1 in the vinyl thioacetate **23** to 5:4 (*E/Z*) in the vinyl disulfide **25**. The following (see Scheme 23) serves as a proposed pathway to explain the geometry shift. The enethiolate may undergo proton exchange with methanol to form the enethiol, which tautomerises to the corresponding thioaldehyde. Subsequent free rotation about the C-1/C-2 single bond to minimise steric strain followed by a second tautomerism to the thermodynamically more stable *E*-enethiol, followed by deprotonation by methoxide would then produce the *E*-enethiolate for reaction with the sulfenylating agent to form the stable *E*-vinyl disulfide **25**.

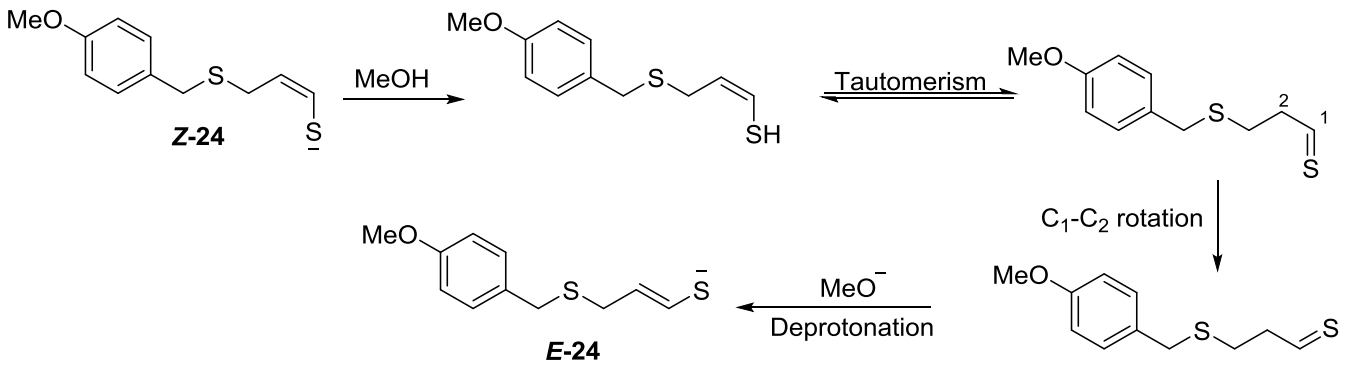

Scheme 23: A mechanism for enethiolate **24** tautomerism.

University of Cape Town

The structure of **25** was confirmed by its ^{1}H NMR spectrum (see Figure 19), which revealed the characteristic signals from both coupling partners. However, the *S*-acetyl methyl peaks of each isomer of the vinyl thioacetate group were not present at 2.38 ppm and 2.36 ppm, nor were the thiotosylate aromatic and methyl protons at 7.81, 7.34 and 2.45 ppm respectively. Interestingly, the signal for H-3 of the *E*-isomer (5.88 ppm) was slightly more downfield than that of the *Z*-isomer (5.70 ppm); this was a larger difference than that observed in **23**. The isomers were again distinguished by their coupling constants for H-4 which was 14.6 Hz and 9.6 Hz for the *E*- and *Z*-isomers respectively. H-3 has two vicinal couplings, while H-4 has an allylic and a vicinal coupling. Lastly, the four aromatic signals for the phenyl groups were observed.

The ^{13}C NMR of **25** revealed two downfield peaks at 158.8 ppm and 154.3 ppm corresponding to C-14 and C-10 respectively. Four C-H aromatic carbon peaks were observed at 130.2, 129.9, 115.6 and 114.1 ppm each corresponding to C-12, C-8, C-9 and C-13. Both C-9 and C-13 experienced shielding by the phenol and methoxy groups respectively. Two quaternary carbons were observed at 132.2 ppm and 130.7 ppm corresponding to C-7 and C-11 respectively. Two vinyl signals were observed, whereby their peaks were correlated to their corresponding proton signals by HSQC. Four aliphatic signals were also observed within their excepted regions and also methoxy signal. The product was obtained as a mixture of isomers in which some peaks overlapped and could not be assigned to individual isomers. However, all the required 38 carbons were identified (19 for each isomer). The IR spectrum of **25** indicated the presence of the ArOH hydroxyl group at 3152 cm^{-1} offering further evidence that coupling had taken place. High resolution mass spectrometry (HRMS) found (ES): *m/z*: 379.0849 [M+H]$^{+}$, $C_{19}H_{23}O_2S_3$ requires 379.0860, thus confirming product formation.

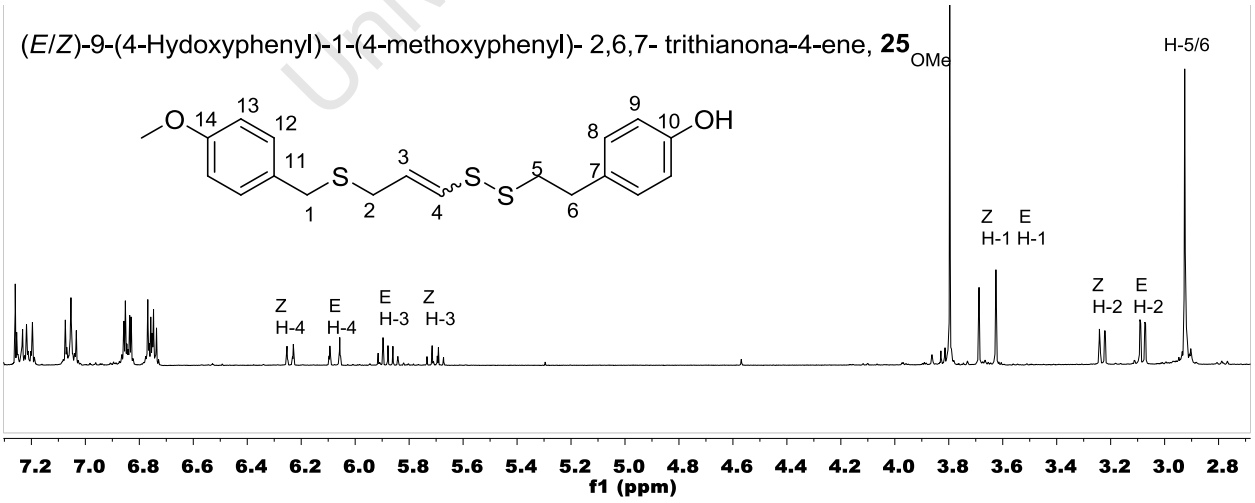

Figure 19: ^{1}H NMR spectrum of **25** in chloroform-d_3.

University of Cape Town

3.2.4 PMB-phenol Sulfoxide, 26

The final step in the synthesis of the target sulfoxide **26** (see Scheme 24), involved the chemoselective oxidation of the sulfide **25** precursor. The oxidizing agent as *m*-CPBA (*meta*-chloroperbenzoic acid) displayed selectivity towards the sulfide over the vinyl disulfide functionality, which may be attributed to the greater nucleophilicity of the sulfide.

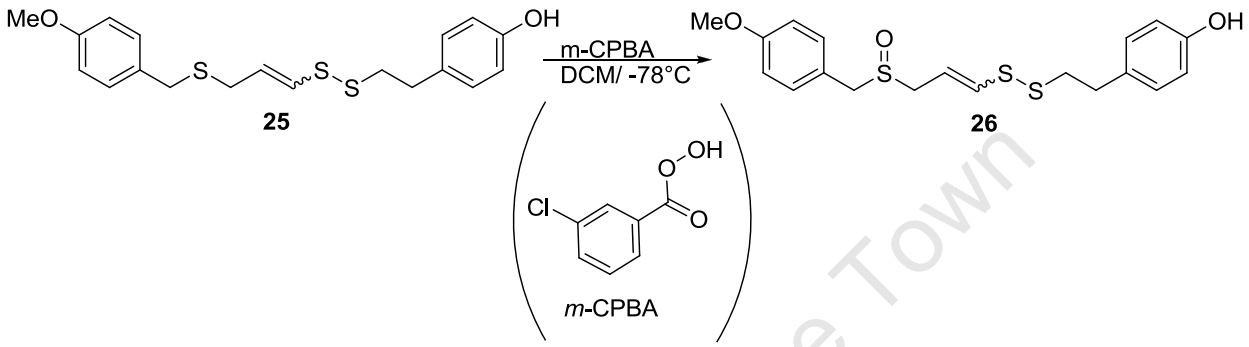

Scheme 24: Chemoselective oxidation of disulfide **25** to form the sulfoxide **26**.

It was decided to use a slight excess of *m*-CPBA since one equivalent did not seem to promote full conversion of the starting material. This required that the temperature be kept below -60°C throughout the reaction to prevent over-oxidation. TLC analysis after an hour and a half indicated the appearance of a single, very polar spot that was believed to the sulfoxide product, along with the disappearance of sulfide **25**. The reaction was quenched by the addition of saturated aqueous sodium carbonate, and the resulting solidified mixture allowed to warm up to room temperature. The residue was extracted and purified using column chromatography (EtOAc: Hexane = 75:25), to afford **26** as a 4:3 mixture of *Z/E* isomers as a clear oil in a yield of 68%. Minor bi-products were formed during the work-up which may have accounted for the modest yield observed. There was a slight geometrical shift of *E* to *Z* from 5:4 in sulfide precursor **25** to 3:4 in **26**, and this may have been due to isomer differences in oxidation reactivity, particularly given the possibility of secondary oxidations (three sulfurs) occurring.

The ^{1}H NMR spectrum of sulfoxide **26** displayed significant deshielding effects compared to precursor **25** (see Figure 20). The downfield shift of H-1 from 3.63 and 3.69 ppm in **25** to two singlets at 3.94 and 3.96 ppm for the *E*- and *Z*-isomers respectively in **26**, supported the site of oxidation as the sulfide sulfur. Similarly whereas the H-2 protons in the disulfide precursor **25** were observed as a doublet of doublets that appeared at 3.08 and 3.23 ppm for the *E*- and *Z*-isomers respectively, those for sulfoxide **26** appeared more towards 3.50 ppm. The sulfoxide has inherent chirality at the sulfur atom (see Figure

University of Cape Town

21 **i**), which creates a non-equivalent environment on C-2 and hence these protons H-2a and H-2b experience germinal coupling as diastereotopic protons. Thus, both H-2a and H-2b were observed as a double doublet of doublets (see Figure 21 **ii**) based on germinal, vicinal and allylic coupling. It would be thought that the protons on C-1 would manifest a diastereotopic relationship by virtue of being (α-) alpha to the chiral sulfoxide, but they did not split into the expected AB splitting pattern. Oxidizing from **25** to **26** also resulted in a significant downfield shift in H-4 for both isomers from 6.08 ppm to 6.28 ppm for the *E*-isomer and 6.24 ppm to 6.56 ppm for the *Z*-isomer as a result of the resonance effect experienced between the sulfoxide and the vinyl double bond.

The ^{13}C NMR spectrum further supported the oxidation reaction, whereby there was a downfield shift of the methylene carbons α- to the sulfoxide. Thus, C-1 shifted from 35.6 ppm to 56.9 ppm in the *Z*-isomer and 34.8 ppm to 56.3 ppm in the *E*-isomer, while C-2 as the other carbon α- to the sulfoxide shifted from 29.5 ppm to 49.6 ppm in the *Z*-isomer and 32.9 ppm to 52.9 ppm in the *E*-isomer Interestingly, an upfield shift was observed for the carbon β- to the sulfoxide (C-3) which may be attributed to the shielding effect of the sulfoxide's oxygen. Also, C-11 as β- to the sulfoxide on the other side shifted from 130.7 ppm to 121.3 ppm for the *E*-isomer and 130.7 ppm to 121.4 ppm for the *Z*-isomer. The ^{13}C was slightly complex due to the presence of the isomers; however, through HSQC analysis all the observed peaks were accurately correlated to their corresponding protons. All the required nineteen carbons were observed for each isomer. The IR spectrum of **26** indicated the presence of the ArOH hydroxyl group at 3152 cm^{-1}. High resolution mass spectrometry (ES) revealed a molecular ion peak (Figure 22) at 393.0646 corresponding to $[M-H]^+$, which provided confirmatory evidence for the formation of the product, as $C_{19}H_{21}O_3S_3$ requires 393.0653.

University of Cape Town

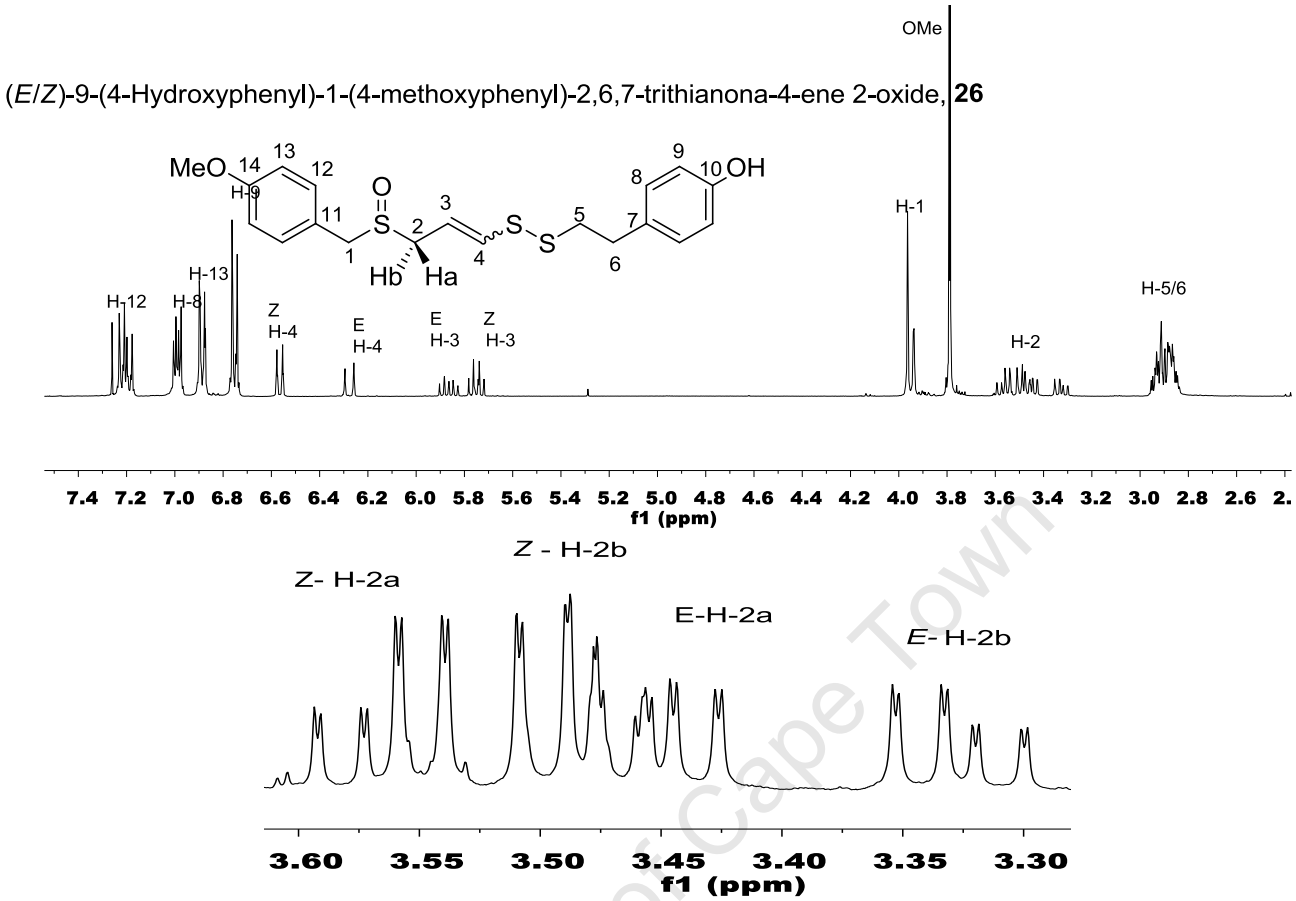

Figure 20: ^{1}H NMR of **26** in chloroform-d_3.

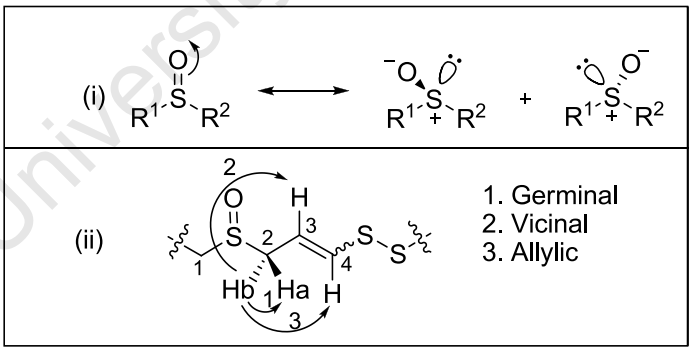

Figure 21: (i) Inherent chirality of sulfoxide moiety. (ii) The (1) germinal, (2) vicinal and (3) allylic coupling of H-2a and H-2b.

University of Cape Town

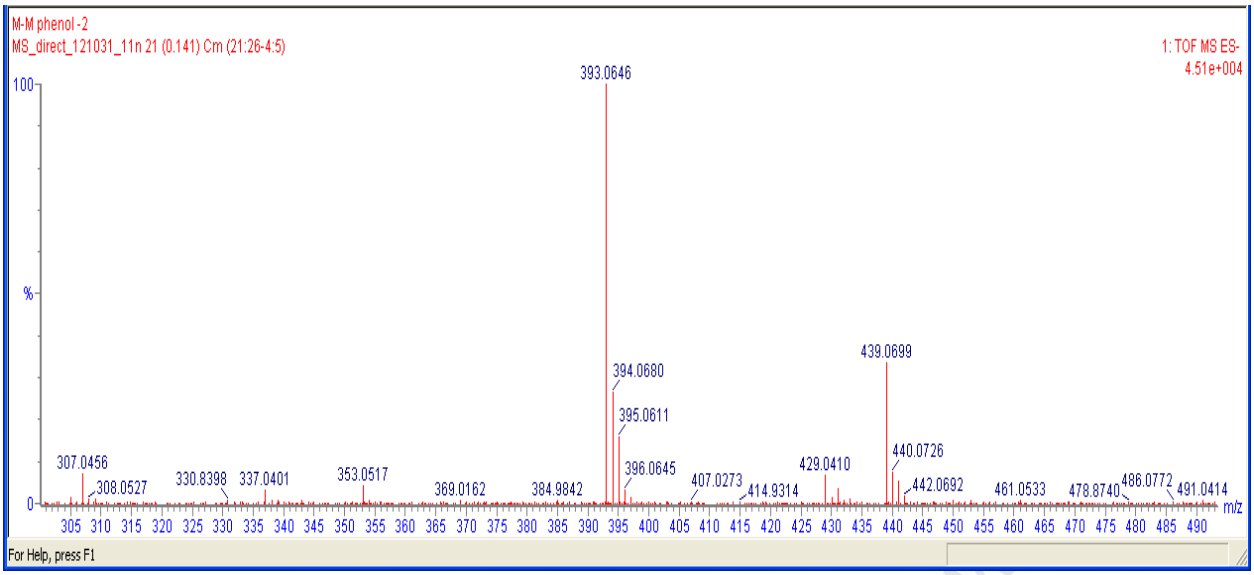

Figure 22: High resolution mass spectrum of **26**.

University of Cape Town

Chapter 4: Increasing the Aqueous Solubility of Substituted Ajoenes

4.1 Introduction

Following the successful synthesis of sulfoxide **26** (**6**, R = H), attention was then turned towards substituting the phenolic hydroxyl group with substituents that would promote the aqueous solubility of the ajoene molecule. The substituents were chosen as acetyl, methoxycarbonylmethylene as well as the corresponding amide based on hydrogen-bonding characteristics as well as ease of introduction. For simplicity the new targets are referred to as PMB-acetate **27**, PMB-Ester **28** and PMB-Amide **29** (see Figure 23). Their synthesis and characterisation will be described next.

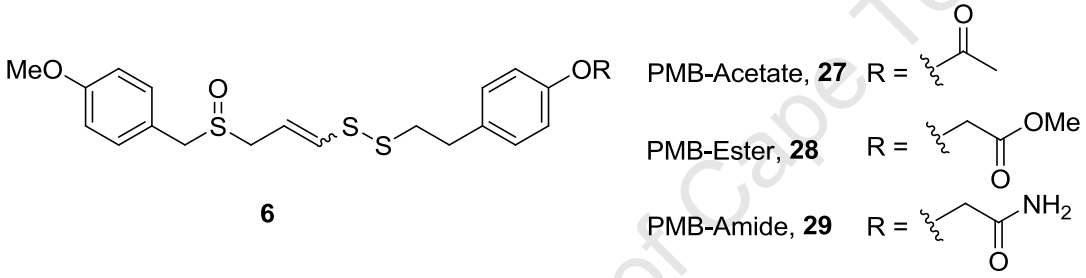

Figure 23: Ajoene targets with increased aqueous solubility.

4.2 PMB-Acetate, 27

The first target, **27,** was prepared by acetylation of the free phenol (see Scheme 25), by dissolving sulfoxide **26** into DCM and adding NEt_3 (triethylamine) as the base, DMAP (dimethylaminopyridine) (0.1 equivalents) as an acyl transfer agent followed by the addition of acetyl chloride (1.3 equivalents) at -20°C. TLC analysis revealed the formation of a less polar product spot within 20 minutes of reaction time accompanied by complete consumption of the starting material. The reaction proceeds rapidly due to the formation of a highly electrophilic, positively charged *N*-acylpyridinium intermediate species formed between DMAP and acetyl chloride, which reacts fast (faster than acetyl chloride itself) with the phenol via a nucleophilic acyl substitution reaction (S_NAc). 1M HCl was added to the reaction mixture to remove the NEt_3 and DMAP and the solution extracted with ethyl acetate before being washed by aqueous sodium bicarbonate to remove acidic residues. The residue obtained after extraction and drying was purified by column chromatography to produce **27** as a yellow solid as a 3:4 mixture of *Z/E* isomers in 88% yield. Numerous recrystallizations (from EtOAc) failed to give the correct elemental

University of Cape Town

combustion analysis, in which the best outcome was C found as 53.45% and H as 6.33% when C 57.77% and H 5.54% were required. The sample was left on the vacuum pump for several hours, was a single spot on TLC but returned a ^{1}H NMR spectrum that showed a small impurity in the highfield region – see Figure 24. Similarly, the melting point was found to be fairly sharp at 45 - 47°C (there are isomers). Final confirmation of structure was provided by ^{1}H and ^{13}C NMR spectroscopy, IR and HRMS.

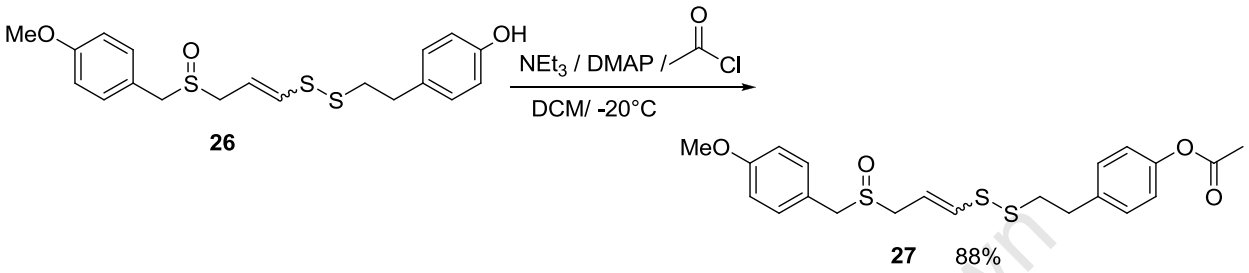

Scheme 25: Substitution of PMB-phenol **27** by acetyl chloride.

The ^{1}H NMR spectrum for the PMB-acetate **27** (see Figure 24) confirmed that the desired substitution had been achieved owing to signals of the phenol **26** being observed, together with a new singlet at 2.28 ppm for both *Z*/*E*-isomers corresponding to the acetyl methyl group of the acetate. The aromatic signals for H-12 and H-8 overlapped between 7.17 and 7.24 ppm, while the shielded H-9 and H-13 resonances *ortho* to the electron-releasing oxygen-based groups were clearly separated and with H-13 assigned as the most upfield of the two owing to the greater donating ability of the methoxy group.

In the ^{13}C NMR spectrum, a peak at 169.6 ppm was observed corresponding to the ester carbonyl carbon C-1`. An upfield shift of C-10 was observed from 155.2 ppm (in **26**) to 149.5 ppm due to the new acetyl group. There was a downfield shift from 131.0 ppm to 137.3 ppm experienced by C-7, and further evidence to support product formation was a new aliphatic signal at 21.2 ppm for the C-2` ester methyl group. In addition, the presence of the carbonyl was confirmed by a carbonyl stretch in the IR spectrum at 1700 cm^{-1}. HRMS (ES) revealed a molecular ion peak at 437.0910 corresponding to $[M+H]^{+}$, thus providing confirmatory evidence for the product as $C_{21}H_{25}O_4S_3$ requiring 437.0915.

University of Cape Town

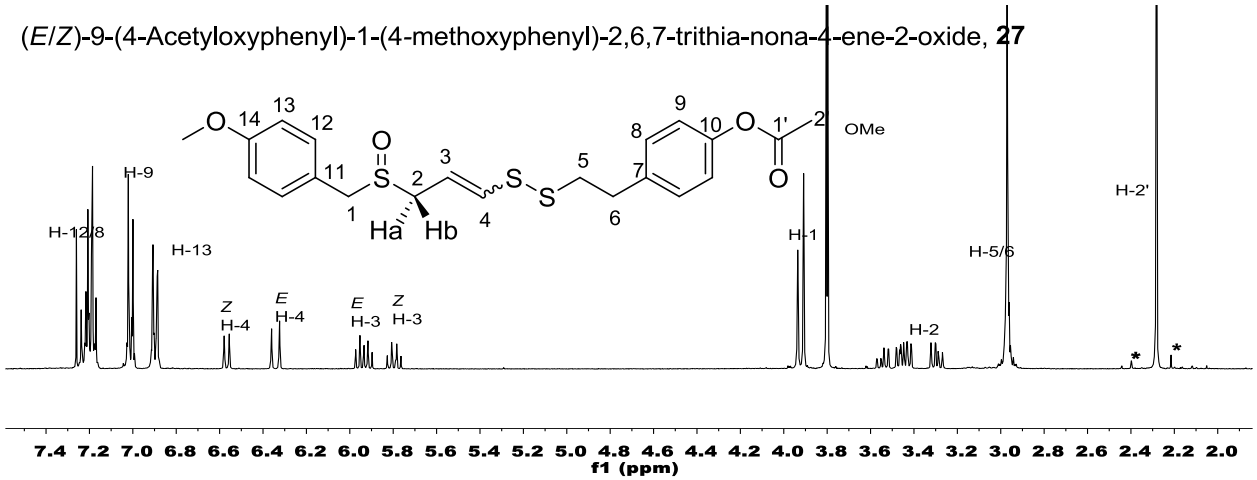

Figure 24: ^{1}H NMR of **27** in chloroform-d_3. *: impurity

4.3 PMB-Ester, 28

The second target was accessed via *O*-alkylation of the sulfoxide **26** through an S_N2 reaction (see Scheme 26). The sulfoxide was dissolved into THF and NaH (sodium hydride) added to the solution at -20°C. This afforded the sodium phenoxide ion with evolution of hydrogen gas, which was then reacted with methyl bromoacetate (1.4 equivalents). The reaction was allowed to warm to room temperature over 45 minutes, which produced one major product spot (by TLC) that was only marginally less polar than the starting material, and in which a double TLC development was required for it to become visible. The chemoselectively displayed in the substitution reaction, i.e attack at the methylene rather than the ester carbonyl was due to the greater electrophilicity of the methylene carbon due to the presence of two electron-withdrawing groups. This, coupled with the weaker C-Br bond compared with the C-O bond, steered the reaction. Aqueous ammonium chloride was added to quench the reaction and the product extracted with ethyl acetate, which was dried over $MgSO_4$ and the residue after solvent evaporation purified by column chromatography to afford **28** as a clear oil and as a 1:1 mixture of *Z/E* isomers in 85% yield.

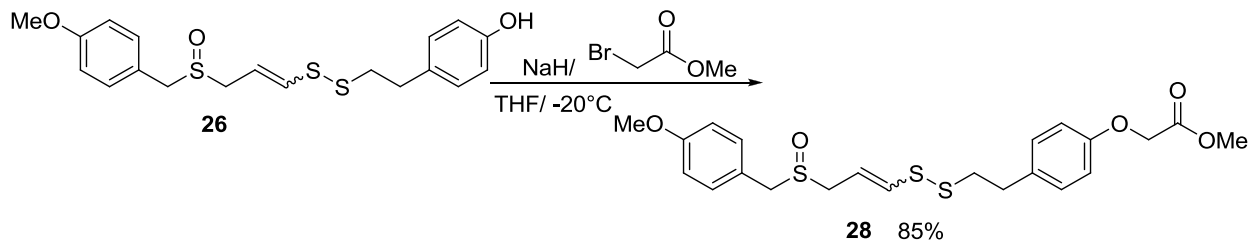

Scheme 26: Chemoselective synthesis of PMB-ester, **28**.

University of Cape Town

The ^{1}H NMR spectrum for the PMB-ester **28** revealed an interesting upfield shift of the H-9 signal (see Figure 24 for numbering) from 7.01 ppm in acetate **27** to 6.83 ppm in **28**, which was attributed to the greater donating ability of the oxygen in ester **28** compared to that of the acetate **27**, where there is resonance with the carbonyl group. A set of new methylene singlets observed downfield at 4.60 ppm and 4.61 ppm offered evidence for a successful *O*-alkylation. This was supported by the appearance of additional methoxy signals at 3.80 ppm corresponding to the ester. All the other signals for the core structure were also observed and used in discerning the structure of the product.

In the ^{13}C NMR spectrum of **28**, a peak was observed at 169.5 ppm corresponding to the ester carbonyl carbon for both *Z*/*E*- isomers. A signal for the methylene C-1` was observed at 65.6 ppm which offered evidence that it was adjacent to an electron-withdrawing oxygen. The methoxy C-1" signal was observed at 52.3 ppm. HSQC was used to identify all the 38 signals required for both isomers (19 each) correlating to their corresponding protons. In addition, the presence of the carbonyl was confirmed by a distinct carbonyl stretch in the IR spectrum at 1700 cm^{-1}. HRMS (ES) revealed a molecular ion peak at 467.1004 corresponding to $[M+H]^+$ (see Figure 25), providing confirmatory evidence for the product, since $C_{22}H_{27}O_5S_3$ requires 467.1021. The peak at 489.0828 is due to $[M+Na]^+$ as a result of using electronspray ionization.

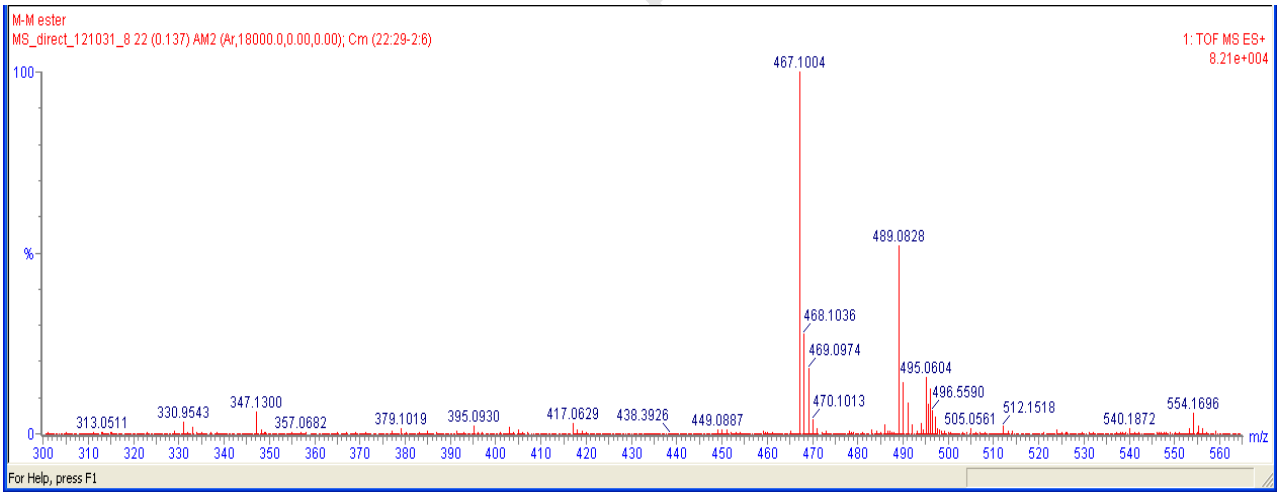

Figure 25: High-resolution mass spectrum of **28**.

University of Cape Town

4.4 PMB-Amide, 29

For synthesis of amide **29** it was initially thought that the reaction could be carried out in the same manner as synthesis of the PMB-ester **28**, except to change the electrophile to 2-iodoacetamide, (see Scheme 27 i), formed from iodide exchange on 2-chloroacetamide. This reaction, however, proved to be much slower as it was observed that after 45 minutes at room temperature only ~10-20% of the starting material had been converted into a more polar product, as seen by TLC analysis. Allowing the reaction to proceed longer at room temperature, did not improve the conversion. It was evident that the phenoxide ion had formed as hydrogen gas was evolved upon NaH addition, and thus it was assumed that this was not the reason for the rate reduction but rather the subsequent *O*-alkylation. The reaction was also refluxed at 65°C, which unexpectedly caused a fragmentation of the ajoene molecule at the S-S bond, confirmed by ^{1}H NMR analysis of the isolated products.

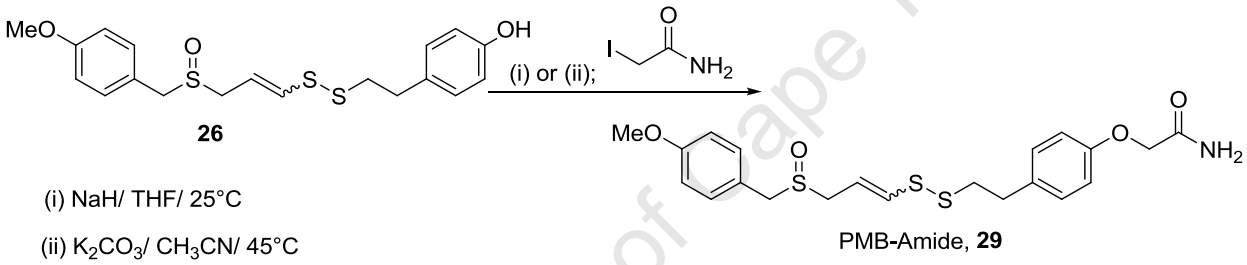

Scheme 27: Synthesis of the PMB-amide, **29**.

From a room-temperature reaction as shown in Scheme 27 (i), the PMB-amide was isolated as a solid in 15% yield as a 1:12 mixture of *Z/E* isomers. Noticeable was the major geometrical shift of *Z* to *E* from 3:4 in the sulfoxide **26** to 1:12 in the PMB-amide **29**. It was postulated that this may have been due to one of the relatively acidic protons α- to the sulfoxide undergoing deprotonation by the NaH to form a delocalised allylic anion. Such a species (see Scheme 28) might then have a reduced energy barrier to rotation of the C-3-C-4 double bond resulting in overall isomerization to the favoured *E*-form with less steric strain compared to the *Z*-. Protonation (eg on work-up) would then regenerate the allyl sulfoxide in preference to the less stable vinyl sulfoxide isomer.

University of Cape Town

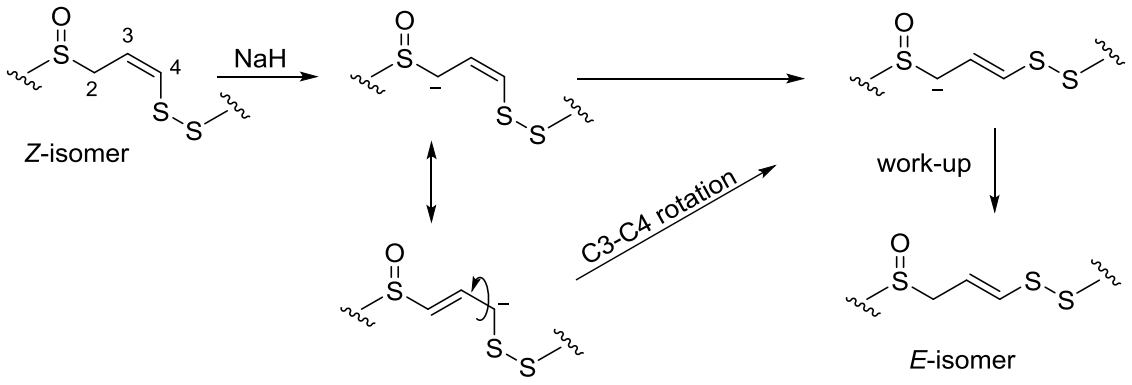

Scheme 28: Geometrical shift Suggested mechanism for isomerisation of PMB-amide **29**.

It is known that the *Z*-isomers of ajoenes are biologically more active and thus it was crucial to use a synthetic route that would retain Z-configuration integrity.[35] Thus, other bases to access PMB-amide **29** were considered and so a weaker base was used, since the rate-determining step was presumably the alkylation step.

K_2CO_3 (potassium carbonate) in acetonitrile was chosen as an appropriate base for reaction. To this end, the sulfoxide **26**, K_2CO_3, and 2-iodoacetamide (2.0 equivalents) were dissolved into acetonitrile at room temperature and the reaction mixture was heated to 45°C (see Scheme 27 (ii)), as it had been noticed that the reaction was not progressing at room temperature in a similar experiment. The potassium phenoxide was thought to be more reactive than its sodium counterpart, but TLC monitoring only showed significant starting material consumption at 10 hours at (room temperature). Heating the reaction at 45°C overnight in an attempt to consume all the starting material did not improve the conversion, and thus at this point the reaction was quenched with aqueous sodium bicarbonate and the product isolated in the conventional manner using extraction followed by chromatography to afford the amide **29** as a 3:1 mixture of *Z/E* isomers as a light-yellow solid in an improved 45% yield. The aforementioned explanation of the isomerization when using sodium hydride as base is supported by this result in that K_2CO_3 is too weak to deprotonate α- to the sulfoxide. The *Z*-isomer enrichment may be explained by the repeated chromatography as well as problems with separating the *E*-isomer from unreacted 2-iodoacetamide, which had the same polarity. The reduced reactivity in the reaction compared to that for **28** may be attributed to the nature of the electrophile, as the amide group is not as electron-withdrawing as its ester counterpart owing to back-donation by nitrogen. This results in a lower electrophilicity of the α-methylene carbon. Multiple recrystallizations failed to give satisfactory

University of Cape Town

combustion analysis data but the melting point was found to be quite sharp at 86 - 88°C. Overall confirmation of structure was provided by ^{1}H and ^{13}C NMR spectroscopy, IR and HRMS.

The ^{1}H NMR spectrum for the PMB-amide **29** resembled that of the PMB-ester **28**, except two diagnostic NH amide peaks were observed as two broad singlets at 6.53 and 5.72 ppm indicating their existence in different magnetic environments, since amides have partial double-bond character with restricted rotation about the C-N bond. Methylene singlets were observed at 4.47 ppm corresponding to H-1' for both isomers (see Figure 26 for numbering). As with the other derivatives **27** and **28**, diagnostic signals for the allyl sulfoxide moiety (H-2 to H-4) could be readily identified for each isomer.

The ^{13}C NMR spectrum offered more evidence for a successful *O*-alkylation, whereby it revealed a downfield peak at 171.0 ppm corresponding to the amide carbonyl C-2' for both isomers. Two sets (for the isomers) of four C-H aromatic peaks were observed at 131.3, 129.8, 115.0 and 114.7 ppm each corresponding to C-12, C-8, C-9, and C-13 respectively. Two sets of four quaternary carbons were observed at 160.0, 156.7, 133.0 and 121.7 ppm corresponding to C-14, C-10, C-7 and C-11 for both *E*/*Z*-isomers. Similarly, two sets of two vinyl carbons were observed corresponding to C-3 and C-4, and also the four aliphatic carbons as C-1, C-2, C-5 and C-6. The methylene C-1' carbon adjacent to the phenolic oxygen resonated at 65.6 ppm. HSQC was used to identify all 21 carbons (as 17 resonances) for each isomer, correlating to their respective protons. The amide carbonyl was also identified by IR spectroscopy in which a carbonyl stretch was observed at 1688 cm^{-1}, as well as NH stretches at 3524 and 3401 cm^{-1}. High resolution mass spectrometry (ES) revealed a molecular ion peak (Figure 27) at 452.1026 corresponding to $[M+H]^{+}$, which provided confirmatory evidence for the formation of the product, as $C_{21}H_{26}NO_4S_3$ requires 452.1024.

4.5 Overview and Comments

The synthesis of an ajoene analogue with an amide group substituent on the "right" side of the molecule proved to be a non-trivial task. The success of the synthesis is attributed to long reaction times using a mild base, and repeated chromatography was required to purify the product from unreacted excess 2-iodoacetamide, which had the same polarity as the product making it difficult to monitor the reaction progress with ease. The other analogues were successfully achieved in good yields via an assisted O-acylation using DMAP for the acetate analogue and a nucleophilic substitution (O-alkylation) for the ester analogue.

The biological activity and aqueous solubility of each analogue were evaluated and the results are reported in the next Chapter.

University of Cape Town

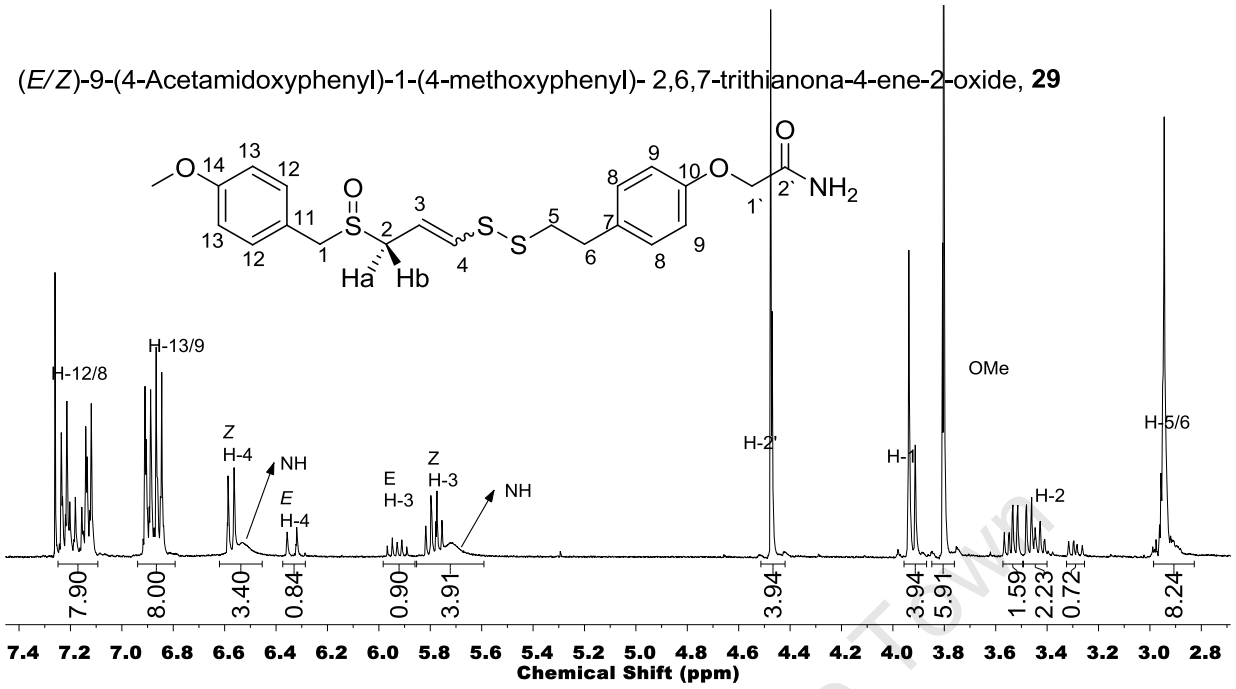

Figure 26: ^{1}H NMR spectrum of PMB-amide **29** in chloroform-d_3.

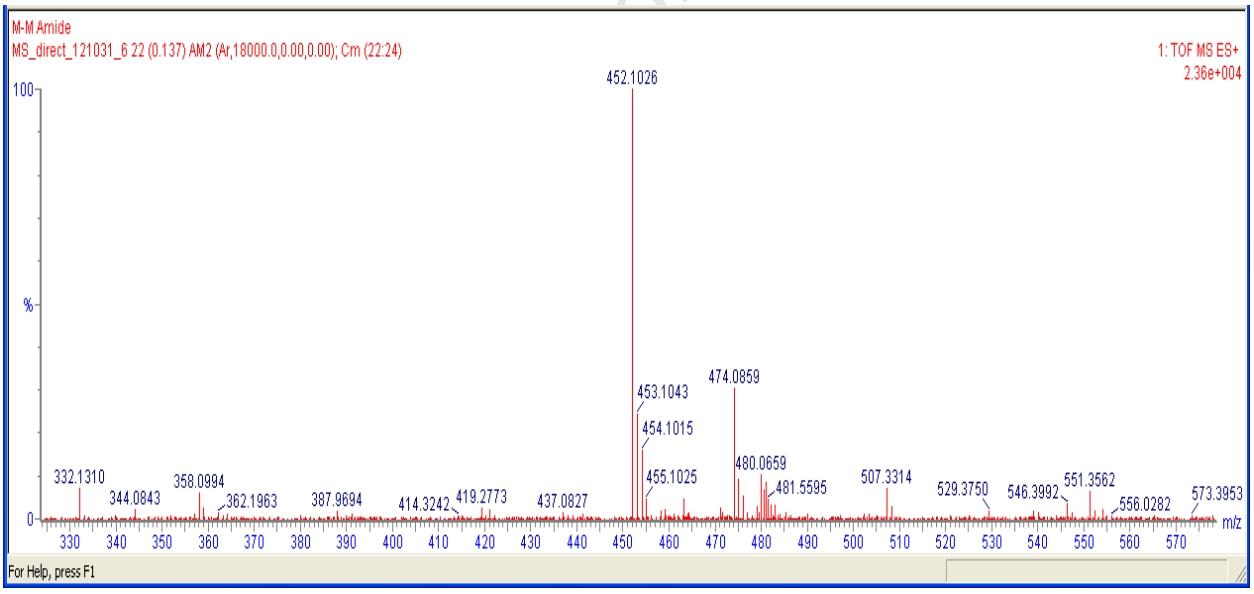

Figure 27: High-resolution mass spectrum of **29**.

of Cape Town

Chapter 5: Biological and Solubility Evaluation of the Substituted Ajoenes

5.1 Determination of the IC_{50} of Ajoene analogues

To determine whether the novel ajoene analogues displayed any tumour-cell cytotoxic effects, each analogue was tested against two cancer cell lines for its capability to inhibit cell proliferation. The assay employed 3-(4,5-dimethylthiazol-2-yl)-2,5-diphenyltetrazolium bromide (MTT) to evaluate the extent to which each compound affected cell viability by spectrophotometrically measuring the reduction of yellow tetrazolium MTT to the crystalline purple formazan (see Scheme 29). The mitochondrial reductase enzymes in metabolically active cells are known to facilitate this reduction, and thus the concentration of formazan falls away as cells are killed by the ajoene being tested. The MTT reagent was added to cells that had been previously treated with varying concentrations of each ajoene analogue for a few days and the resulting formazan was solubilised in a 10% aqueous sodium lauryl sulfate (SLS) solution. The concentration of the formazan dye was measured spectrophotometrically using a scanning multi-well plate reader as an absorbance at 595 nm. A dose-response curve was then generated, from which an IC_{50} value for each compound was extrapolated. The IC_{50} is defined as the compound concentration required to inhibit 50% of the (cancer) cell population.[50]

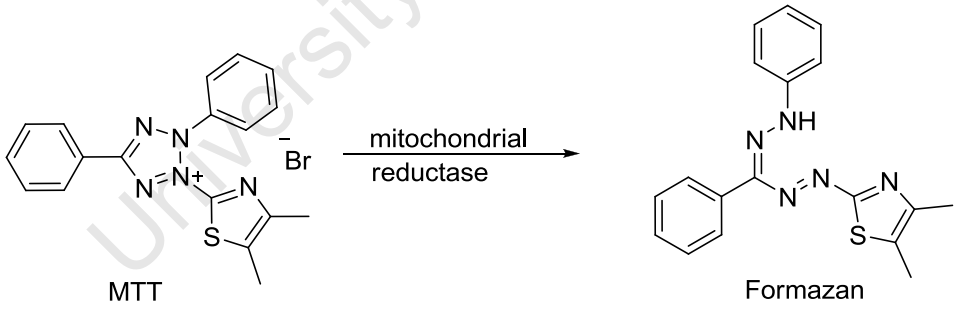

Scheme 29: Reduction of MTT to formazan by viable cells.

The analogues were each assayed for their ability to inhibit cell proliferation in two cancer cell-lines, namely: An A375 human malignant melanoma epithelial cell-line and a WHCO1 oesophageal epithelial cancer cell-line, which had displayed good sensitivity to other ajoene analogues synthesized previously in our group.[35] Since the ajoene analogues were synthesized as a non-separable mixture of *E*/*Z*-isomers they were tested as such.

University of Cape Town

The IC_{50} values for each ajoene analogue tested are shown in Table 2. The activities of all the new synthesized analogues were comparable to the advanced lead **5** that had been identified in an SAR study conducted within our group.[35] It is important to note that the results of the assay were influenced by the cell density, as treating cells that had reached (or near) full confluence returned a less pronounced effect. This finding supported the suggestion proposed by Xiao and co-workers that ajoene and related compounds are selective for mitotic cells and as such, all the IC_{50} values were determined only on growing cells.[51]

The IC_{50} values of the new analogues against the WHCO1 cell-line were each comparable to that of the *bis*-PMB **5** (2.5 μM) used as the prototype, again offering further evidence that the cancer cell anti-proliferation activity of ajoene resides within the vinyl disulfide/sulfoxide core.[35] The newly formed analogues had enhanced polar character due to substitution by polar groups on the right-hand terminus; these did not have any detrimental effects on the anti-proliferation activity. The PMB-ester **28** with a methoxycarbonylmethylene substituent was the most active of the four new analogues against both the WHCO1 (1.7 μM) and A375 cell-lines (9.3 μM) (see Table 2 and 3 for representative IC_{50} curves).

Table 2: IC_{50} Data for Ajoene Analogues (in μM)

Analogue as *E*/*Z*-mixture	A375	WHCO1
Bis-PMB, **5**	9.4	2.5 ± 0.7; $^{n = 3}$
PMB-Phenol, **26**	9.4	1.9 ± 0.8; $^{n = 3}$
PMB-Acetate, **27**	16.5	3.6 ± 0.04; $^{n = 3}$
PMB-Ester, **28**	9.3	1.7 ± 0.9; $^{n = 3}$
PMB-Amide, **29**	13.0	7.7 ± 1.7; $^{n = 3}$

n = number of repeated experiments

The next section discusses the solubility studies and the animal study carried out on one of the analogues.

University of Cape Town

Table 3: Representative dose-response Curves for the Ajoene Analogues

Analogue	A375	WHCO1
PMB-Phenol, **26**	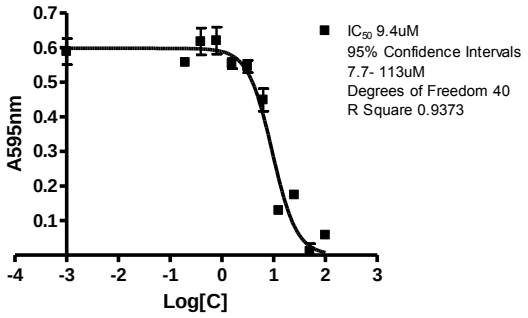	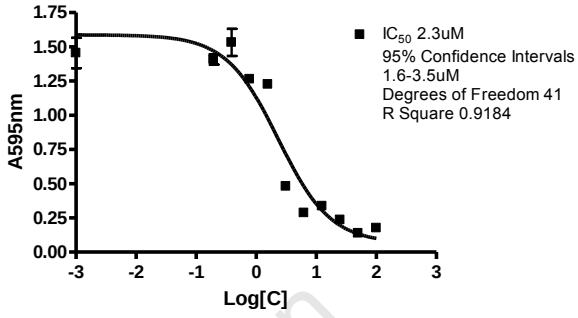
PMB-Acetate, **27**	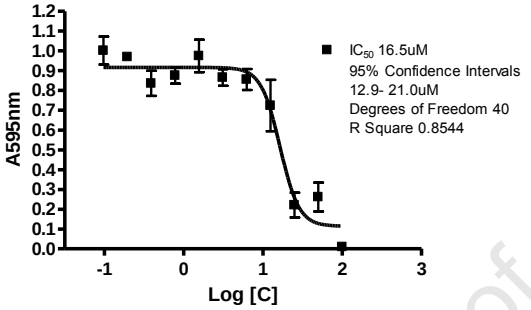	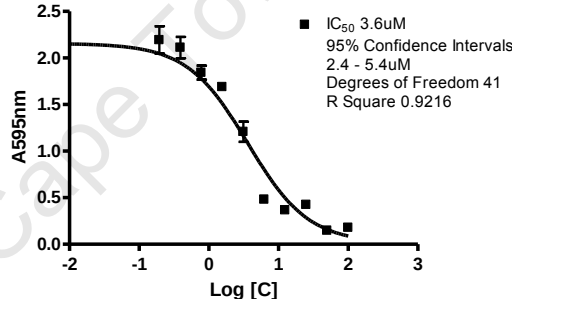
PMB-Ester, **28**	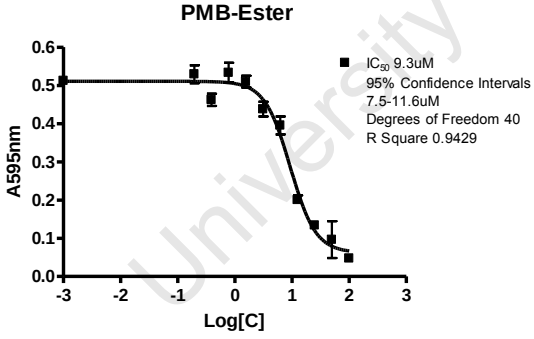	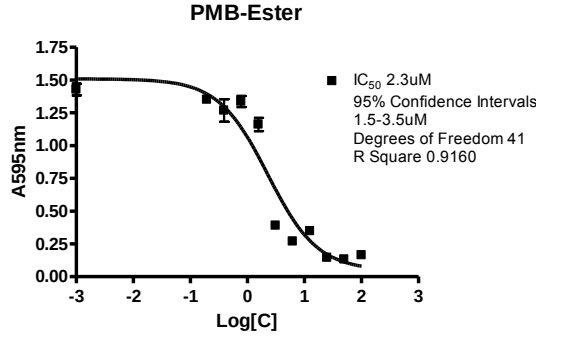
PMB-Amide, **29**	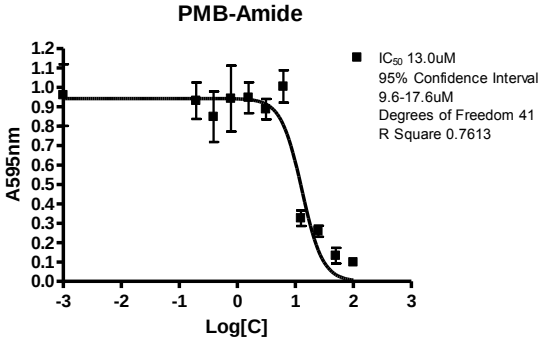	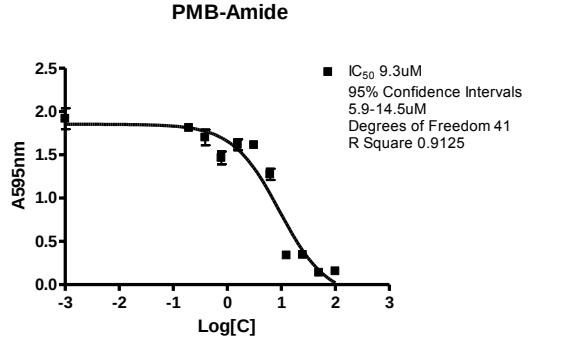

University of Cape Town

5.2 Assessment of Aqueous Solubility by Measuring Turbidity

The turbidimetric solubility assay used in this work was developed by Van de Hulst and Hongve, which is used in modern times by the pharmaceutical industry in the rapid screening of libraries (allied with Lipinski rules).[59] It is based on the fact that precipitated particles formed at the onset of solubility scatter light resulting in an Absorbance that can be measured. The intensity of the scattered light is dependent on the concentration of scattering particles, and the turbidity is measured using a UV-vis spectrophotometer at 620 nm. Testing of a compound required dissolving it in high purity DMSO then added to an aqueous solvent (0.01 M Phosphate-buffered saline (PBS) at pH 7.4) to evaluate its solubility. The point at which the solution becomes turbid is regarded as that at which the compound is insoluble in the PBS solution and it is at this point that particle precipitation leads to an increase in absorbance (from 0) related to the concentration of the sample.[56, 57]

Sample preparation starts by making up a stock of the test compound in high purity DMSO into a 300 μl solution of 10 mM. A predilution plate is made up in a 96 well-plate with solutions with 10, 8, 4, 2, 1, 0.5, 0.25 and 0mM of the stock in 100 μl in triplicate and these are used to make up the test solutions. To prepare 200 μl of each solution containing 200, 160, 80, 40, 20, 10, 5 and 0 μM in both DMSO and PBS, 4 μl of each of the predilution solutions was added to 196 μl of both DMSO and PBS in triplicate. The samples were incubated for 2 hours at 37°C and analysed on the SpectraMax 340PC UV-vis spectrophotometer, and the results are summarised in Figure 28.

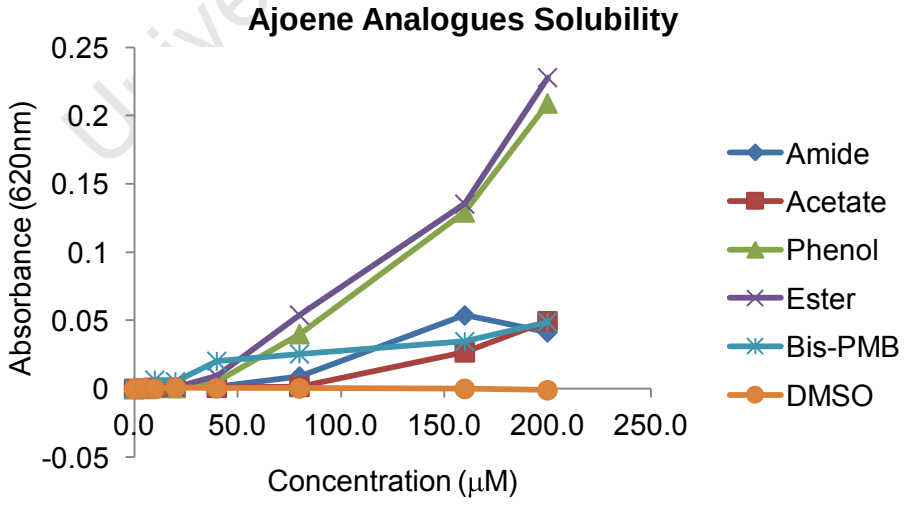

Figure 28: Turbidimetric aqueous solubility of ajoene analogues.

University of Cape Town

Turbidimetric analysis of the new analogues indeed revealed an increase in aqueous solubility compared to the *bis*-PMB, which became turbid at a concentration of about 20 μM. Surprisingly, the scattering with increased concentration of this analogue (as seen from the increase in A) did not increase as much as that of the phenol and the ester analogues which become turbid at similar concentrations. Reasons for the discrepancy are unclear at this stage.

The amide **29** and acetate **27** analogues were the most soluble of the four analogues from this thesis, as their scattering (A > 0) was observed at a concentration of 40- 50 μM indicating their promoted solubility in the aqueous medium as compared to the *bis*-PMB, which may be attributed to their hydrogen-bonding characteristics.

5.3 Animal study (*in vivo*)

The study was conducted by Dr Catherine Kaschula from the UCT IIDMM (Institute of Infectious Diseases and Molecular Medicine) to assess the *in vivo* activity of the PMB-amide **29**, which was chosen to be a suitable candidate based on its polar nature. Based on the solubility data, the latter was considered as having a good enough solubility for delivery into the mouse subject, since one of the objectives was to enhance the aqueous solubility of the ajoene molecules. There are reports in the literature that suggest that compounds with phenols may be toxic to subjects as they form reactive metabolites. Similarly, phenolic acetates (**27**) could be hydrolysed to the phenol, and the PMB-ester **28** could also be hydrolysed (to its acid form), which would also probably be toxic. All these factors suggested that the other three analogues were not as suitable candidates as amide **29**.[52]

The study comprised of 20 nude mice, which each received a subcutaneous injection of 2.50 x 10^5 A375 cells (in 100 μL of PBS) into their hind right quarter. The mice were split into two groups of 10 mice assigned to the treatment or the control group and the tumours were allowed to grow for 21 days. The test mice each received PMB-amide (8mg/kg) from the day of inoculation every day for the duration of the study by intraperitoneal injection, in which the drug was solubilised easily into a solution of 2.5% chondroitin, 10% DMSO and PEG400. The tumours were measured twice weekly and recorded as a tumour volume (volume calculated by: (length^2 x height)/2).[53] Upon completion of the study on day 21, the mice were sacrificed (halothane inhalation), the tumours were removed and accurately weighed to determine if there had been any size reduction during the course of the study (see Figure 29).

University of Cape Town

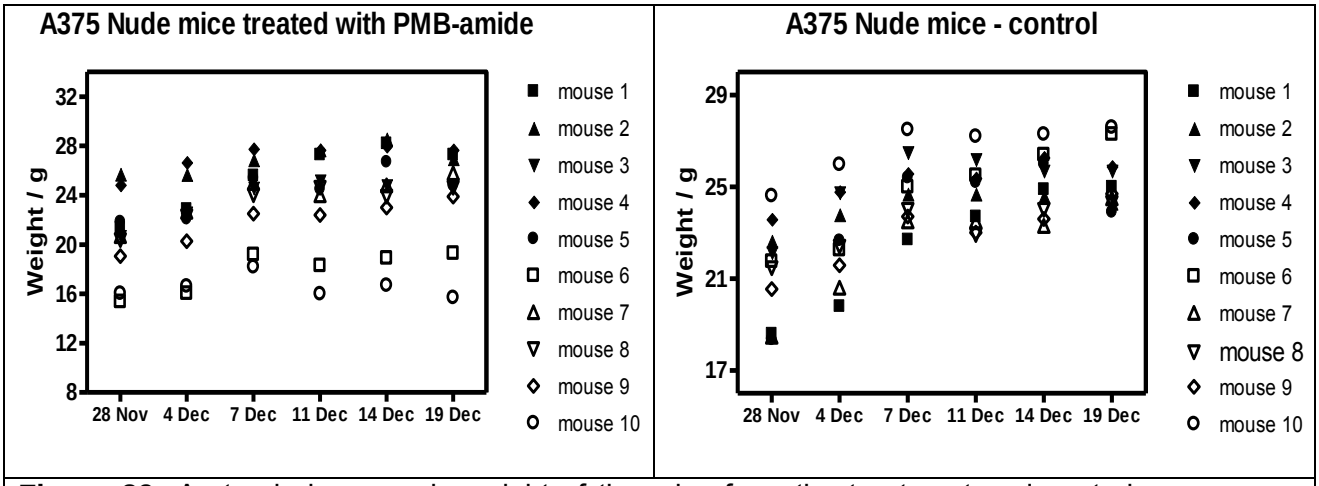

Figure 29: A steady increase in weight of the mice from the treatment and control groups was observed over the duration of the study which indicated that the drug was not cytotoxic to the mice.

The results revealed that treatment with the PMB-amide had no significant effect on the tumour growth (see Figure 30) when compared with their control counterparts. From the collected data, it was apparent that there was no tumour volume reduction observed in the treatment group; rather the tumours steadily grew over time (see Figure 30 (i)). A similar result was observed for mice that were treated with the advanced lead (*bis*-PMB) **5** that had also returned excellent *in vitro* activity.

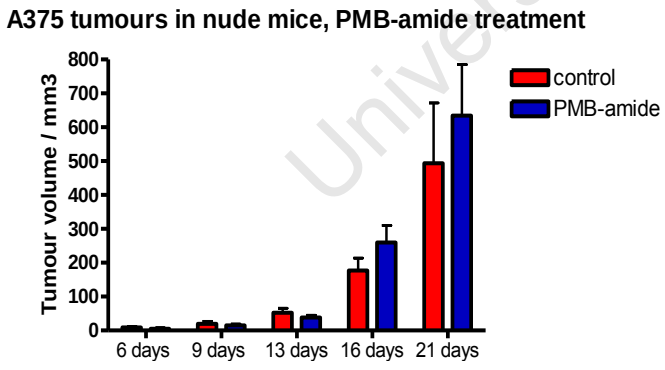

(i)

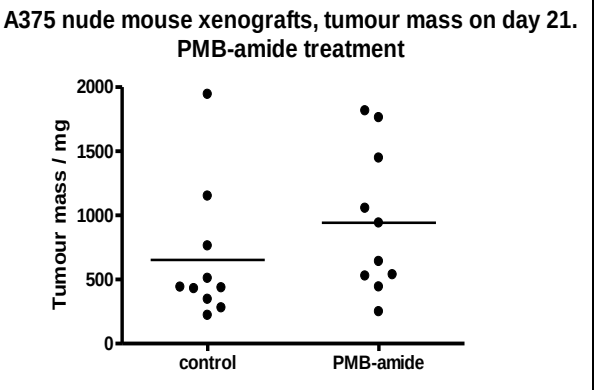

(ii)

Figure 1: **Figure 30:** (i) Growth of tumours - Treated vs Untreated. Tumour size were measured by calipers (volume calculated by: (length^2 x height)/2) [53]; (ii) Tumour size as measured by weight of tumour obtained from biopsy.

University of Cape Town

The PMB-amide was ineffective at reducing tumour growth in the nude mice, yet it still had good *in vitro* activity. Upon initial design of this compound it was thought that its precursor *bis*-PMB **5** was ineffective due to its poor-bioavailability as a result of poor solubility in the intralipid solution used for drug delivery. The PMB-amide had a twofold increase in inherent solubility into the delivery solution compared to the *bis*-PMB **5** and as such it was administered in a solubilised form. Thus, the poor-bioavailability due to solubility was ruled out as an explanation for the failure. The two studies involving both *bis*-PMB and the PMB-amide have shown that administering of the drug via intraperitoneal injection is not the best method and as such oral or intravenous administration should be considered. However, owing to time constraints the other two methods could not be attempted. Other experiments were carried out in an attempt to explain the ineffectiveness of the two compounds in reduction of tumours in nude mice and these were carried out at the Department of Pharmacology, UCT. The *bis*-PMB **5** was incubated with mouse whole blood *in vitro* at 37°C and the amount of compound present in the sample monitored over three hours by removing an aliquot and analysing it by liquid chromatography-mass spectrometry (LC/MS), which gave a peak area as a reflection of ajoene derivative concentration. Concurrently, red blood cells (RBC) and blood plasma were separated and the same experiment conducted, and the results analysed, which are summarised in Figure 31.[54]

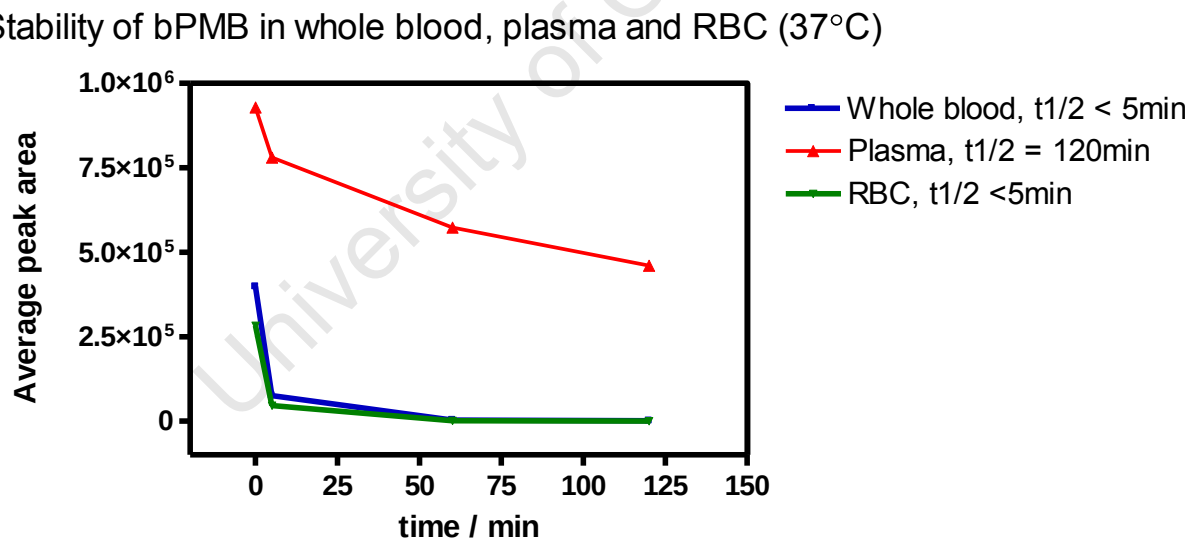

Figure 31: Metabolic stability of bis-PMB in blood.

The results from Figure 31 indicate that the *bis*-PMB incubated in both the whole blood and the red blood cells had strong affinity towards them and as such could not be detected in the two samples by LC/MS beyond 5 minutes of incubation, whereas in plasma alone it had a half-life of two hours. This data suggests that the *bis*-PMB possibly binds to the red blood cells and is thus not available for

University of Cape Town

delivery into the tumours when it is administered via intraperitoneal injection. However, further investigation needs to be carried out to support this hypothesis and to also evaluate exactly which receptors are likely responsible for the interaction observed. A study conducted by Apitz-Castro showed that ajoene (with the same vinyl disulfide/sulfoxide pharmacophore) has affinity towards the fibrinogen receptor, which is found in human platelets and prevents platelet aggregation. Thus, it is likely that the *bis*-PMB might bind to similar receptors reversibly, but this is still to be proven.[55]

5.4 Ajoene analogues as Chemosensitizing agents

The analogues described in this thesis were also tested in Professor Pani's lab at the University of Cagliari (Institute for Virology and Microbiology) in Sardinia, for the possibility of chemosensitization defined as the reintroduction of sensitivity of an established anti-cancer drug towards a drug-resistant cancer strain. Hassan had shown that ajoene inhibits the anti-apoptotic bcl-2 protein in acute myeloid leukaemia (AML) cells resulting in the release of cytochrome c into the cytosol and the activation of caspase-3 which ultimately leads to an apoptotic response.[12b] In the study they observed that addition of ajoene with two chemotherapeutic drugs fludarabine and cytarabine promoted sensitivity of the drug towards drug-resistant AML strains and this was attributed to inhibition of over-expression of anti-apoptotic bcl-2 proteins by ajoene. Interestingly, the ajoene on its own failed to promote either the inhibition of the bcl-2 or the induction of apoptosis in the AML cells implying that ajoene's anti-tumour activity wasn't a prerequisite for chemosensitization.

The cytotoxicity of a library of ajoene analogues synthesized (**5**, **26-29** as well as some ajoenes with alkyl end-groups) was analysed against hematologic and solid tumour cell-lines by an MTT assay as described in section 5.1 above and the results shown in Table 4. The analogues were not potent towards the CRL-7065 to the SK-MES-1 cell-lines as the required concentration to inhibit 50% growth was >30 μM. On the other hand they showed very good activity for the human acute T-lymphoblastic leukemia cells (CCRF-CEM), CCRF-SB, and the KB^{WT}, kB^{MDR} and the KB^{V20C} cell-lines, particularly in comparison with established agents like Doxorubicin and Etoposide (see Table 4). Interestingly, the PMB-allyl **32**, acetate **27**, ester **28** and PMB-phenol **26** were the more potent analogues tested, in which each of this group of analogues contained a lipophilic *p*-methoxybenzyl group that presumably promoted good permeability into the cells. The KB^{WT} and the human nasopharyngeal carcinoma (which has stepwise selection for resistance with increasing concentration of vincristine) (KB^{V20C}) cell-lines were selected for a chemosensitization assay, whereby the analogues were mixed with two chemotherapeutic drugs Vincristine (VCR) and doxorubicin (DOXO).[58]

University of Cape Town

Table 4: Cytotoxicity against hematologic and solid tumor cell lines°.

Compound	CRL-7065 [a] CC_{50}	DU-145 [b] CC_{50}	Hela [c] CC_{50}	HEP-G2 [d] CC_{50}	SK-MEL-28 [e] CC_{50}	SK-MES-1 [f] CC_{50}	CEM [g] CC_{50}	SB [h] CC_{50}	KB^{WT} [i] CC_{50}	KB^{MDR} [j] CC_{50}	KB^{7D} [k] CC_{50}	KB^{V20C} [l] CC_{50}
(E) Ajoene, **4**	>30	>30	>30	>30	>30	>30	5.4 ± 0.5	6.3	30.8 ± 5	50.7 ± 17.2		35.8 ± 1.6
(*Z*) Ajoene, **4**	>30	>30	>30	>30	>30	>30	6.2 ± 0.7	6.4	22.0	34.1 ± 12.4		22.0 ± 2.4
(*E*)Propyl-Allyl, **30**	>30	>30	>30	>30	>30	>30	2.3 ± 0.2	5.7	13.2 ± 1.1	28.8 ± 5.5		18.8 ± 1.1
(*Z*)Propyl-Allyl, **30**	>30	>30	>30	>30	>30	>30	3.1 ± 0.4	5.7	23.1 ± 2.6	34.9 ± 5.3		23.3 ± 1.3
(*E*) *Bis*-Propyl, **31**	>30	29.45	>30	>30	>30	>30	2.6 ± 0.5	6.0	19.6	37.7 ± 10.9		23.6 ± 1.2
(*Z*) *Bis*-Proply, **31**	>30	29.32	>30	>30	>30	>30	2.6 ± 0.5	3.2	14.4 ± 1.7	31.3 ± 3		16.7 ± 2.3
(*E*/*Z*) PMB-Allyl, **32**	>30	16.4	27.46	>30	>30	>30	1.3 ± 0.4	3.5	7.8 ± 0.6	13.8 ± 1.9		8.5 ± 1.7
(*E*/*Z*) *Bis*-PMB, **5**	>30	11.83	13.34	>30	>30	>30	0.8 ± 0.2	0.2	4.5 ± 1.3	7.4 ± 1.5		5.4 ± 1.0
(*E*/*Z*) PMB-Acetate, **27**	>30	>30	9.65	>30	>30	>30	0.8 ± 0.1	3.1	3.5 ± 1.3	8.2 ± 0.7		4.8 ± 1.3
(*E*/*Z*) PMB-Ester, **28**	>30	>30	>30	>30	>30	>30	5.4	5.1	11.9 ± 1.7	21.8 ± 2.1		12.1 ± 1.3
(*E*/*Z*) PMB-Phenol, **26**	>30	>30	>30	>30	>30	>30	0.8 ± 0.1	3.1	4.4 ± 1.3	8.0 ± 1.2		5.4 ± 1.2
[p]**6-MP**							2.1±0.4	1.4±0.7				
[q]**CDDP**							1.0±0.2	1.4±0.2				
Vincristine		0.015		2.6	>4	0.015	0.004±0.0008	0.012±0.0003	0.004±0.002	0.95±0.2	0.09±0.01	0.40±0.08
Doxorubicin		0.44		0.3	1.1	0.21	0.12±0.06	0.05±0.03	0.4±0.08	≥20	3.3±1	2.2±0.7
[r]**Etoposide**		4.6		7.6	7.8	2.04			3.3±1.1	≥100	≥100	7.6±2.5

°Data represent mean values for three independent determinations.
[a]CC_{50} : Compound concentration (μM) required to reduce the viability by 50%, as determined by the MTT method.
[b]CRL-7065: skin fibroblasts
[c]DU-145: human prostate carcinoma;
[d]Hela: human cervical adenocarcinoma;
[e]HEP-G2: human hepatocellular carcinoma;
[f]SK-MEL-28: human skin malignant melanoma;
[g]SK-MES-1: human squamous cell lung carcinoma;
[h]CCRF-CEM: human acute T-lymphoblastic leukemia;
[i]CCRF-SB: human acute B-lymphoblastic leukemia;
[j]KB^{WT}: human nasopharyngeal carcinoma, wild type;
[m]KB^{MDR}: human nasopharyngeal carcinoma, multidrug resistent infected with a retroviral vector containing a full-length cDNA for the human MDR1 gene that conferred the full MDR phenotype;
[n]KB^{7D}: human nasopharyngeal carcinoma, stepwise selection for resistance with increasing concentration of etoposide;
[o]KB^{V20C}: human nasopharyngeal carcinoma, stepwise selection for resistance with increasing concentration of vincristine;
[p]6-MP: 6-mercaptopurine
[q]CDDP: Cis-platinum
[r]Etoposide: VP16
[ ] = increased cytotoxicity [fold]

University of Cape Town

The results showed both a synergistic and also an antagonistic effect when the analogues were mixed with the drugs DOXO and VCR. When compounds (*E*/*Z*)-ajoene **4**, **30** (propyl - allyl) and the (*E*/*Z*)-*bis*-propyl **31** analogues were mixed with the two drugs and tested against the KB^{V20C} cell-line which has resistance to VCR the results indicated an increase in resistance, i.e. negative chemosensitization. Reasons for this antagonism are unclear. The opposite effect was observed for the PMB-allyl **32** to the PMB-Phenol **26**. For the former, the CC_{50} of Vincristine (the concentration required to reduce viability by 50% of the KB^{V20C} cells) was 0.85 μM which decreased by eighteen fold to 0.047 μM when 6.67 μM of the PMB-allyl was combined with VCR. Of importance is that 6.67 μM was below the CC_{50} of the PMB-allyl **32** of 8.5 μM, meaning that the reduced CC_{50} of the drug in combination was not due to the ajoene derivative. This result indicated a synergy (positive chemosensitization) as it had been shown that the analogue alone had a CC_{50} of 8.5 μM (see Table 4 and Figure 32).

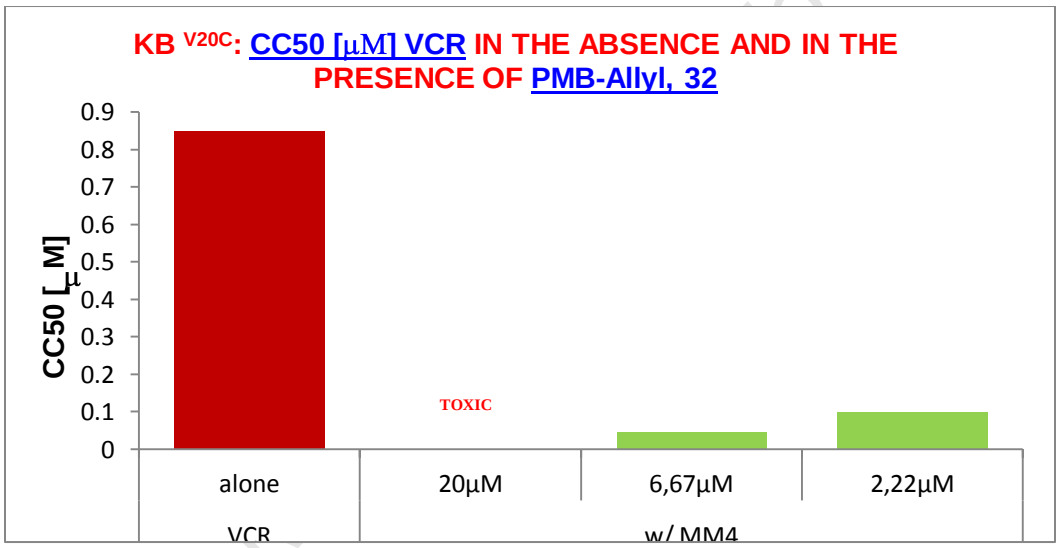

Figure 32: Representation of the chemosensitization effect of Vincristine and PMB-allyl against a VCR-resistant cancer cell-line.

In the case when the PMB-allyl concentration was lowered to 2.22 μM the required VCR was 0.1 μM showing that the synergistic effect as expected is ajoene-concentration dependent. This was still a healthy reduction in the CC50 of the drug.

Similarly, the PMB-Ester **28** showed positive chemosensitization towards both DOXO (Doxorubicin) as well as VCR in KB^{WT} (human nasopharyngeal carcinoma, wild type), with significant reductions in CC_{50} of the drugs at 8.33 μM of **28** which is below the CC_{50} of **28** (11.9 μM) in this cell-line, see Figure 33.

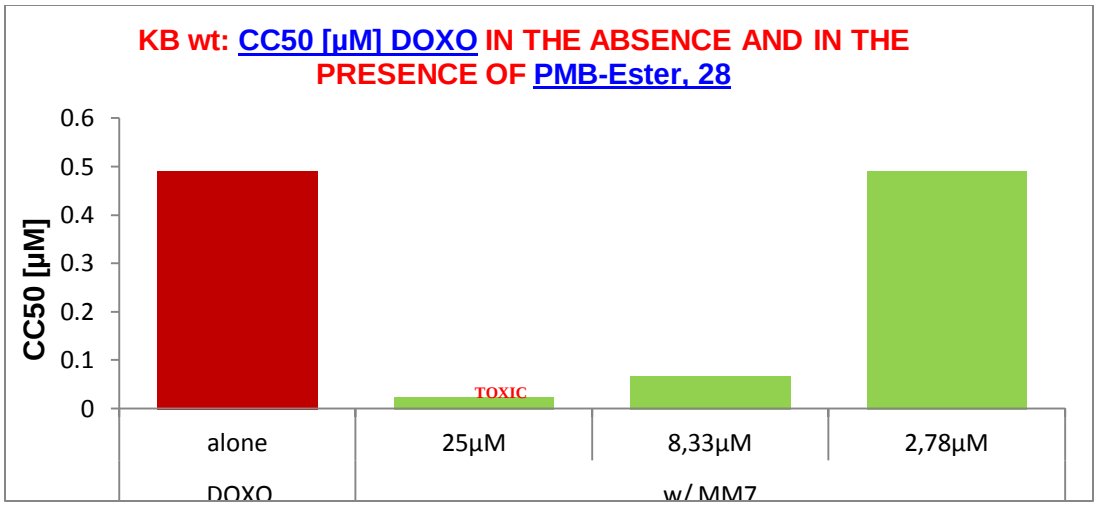

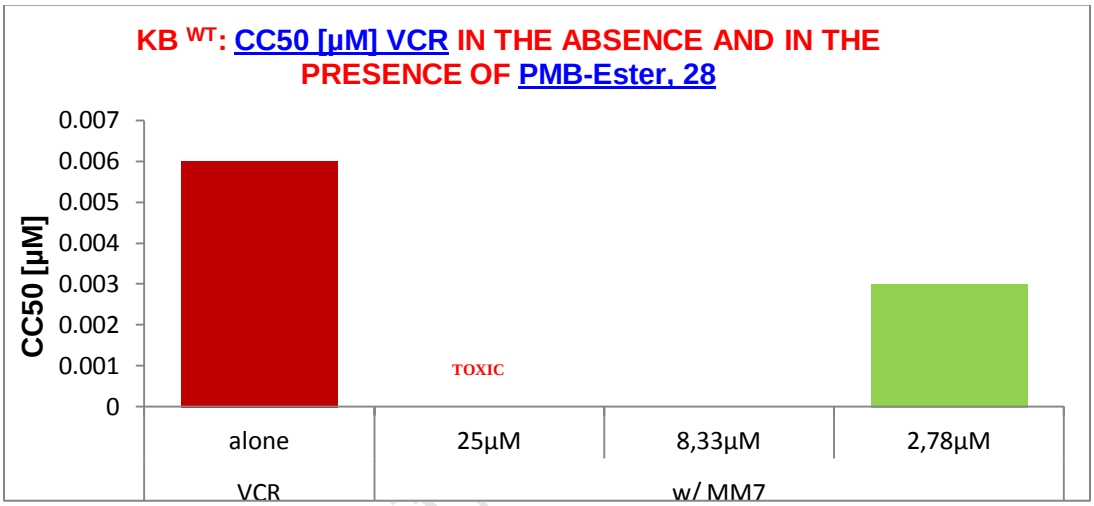

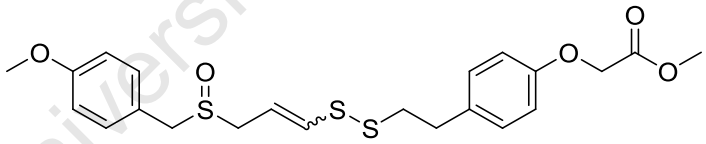

PMB-Ester

University

Figure 33: The comparison of CC_{50} when PMB-Ester **28** is combined with both DOXO and VCR in KB^{WT}.

In addition, The PMB-phenol **26** showed significant chemosensitization activity at 3.33 µM against the VCR-resistant cell-line KB^{V20C}, and importantly at a concentration below its own CC_{50} (5.4 µM in this cell-line, see Table 4 and Figure 34). In this regard it is useful to have a derivative with a relatively high CC_{50}.

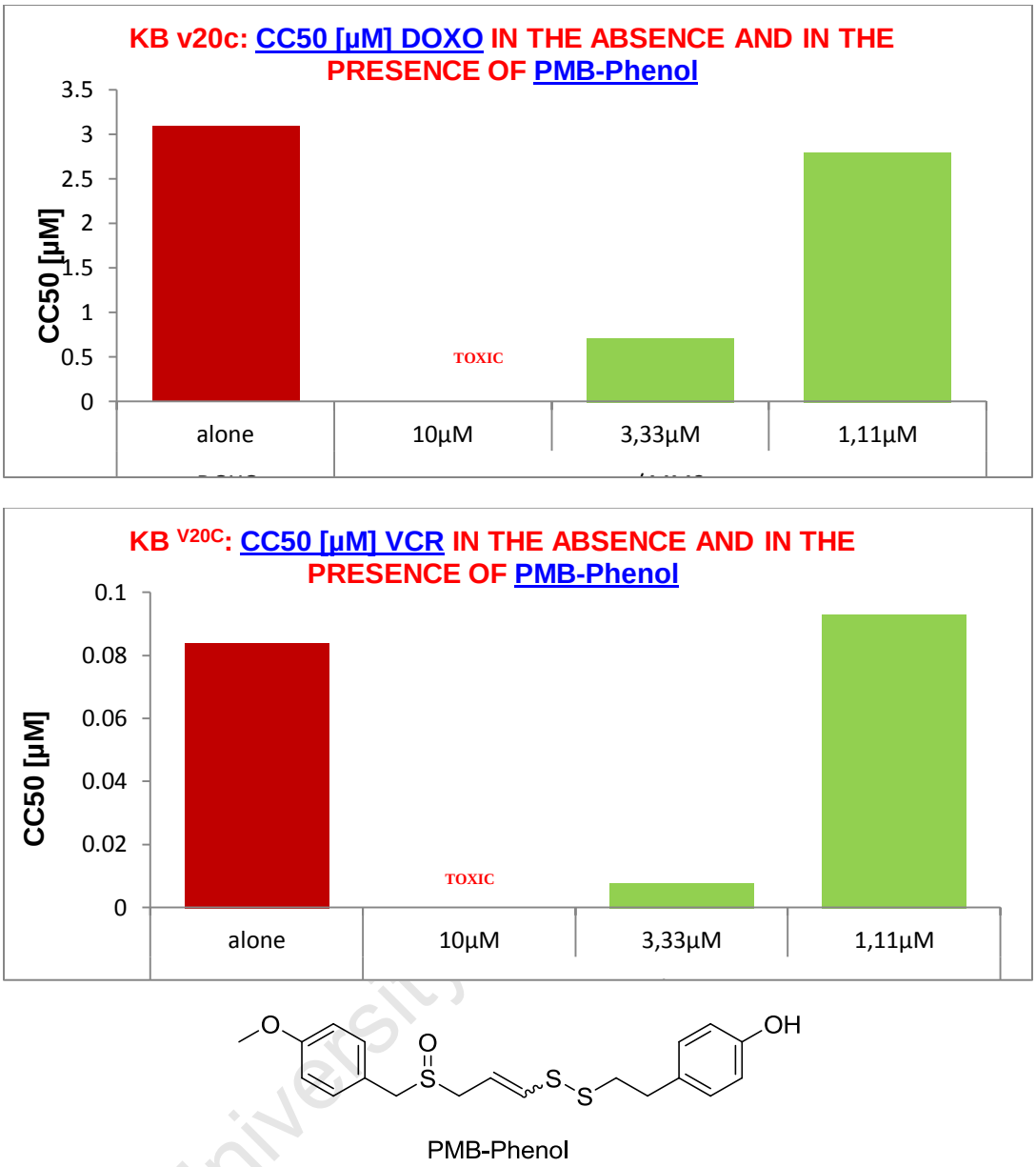

Figure 34: The comparison of CC_{50} when PMB-Phenol is combined with both DOXO and VCR.

These results show how addition of ajoene analogues switch on the sensitivity of the tumour cells towards the drug resulting in a reduction in the concentration of VCR required to achieve 50% inhibition. Mechanistic and structural reasons for this are unclear at this stage but an empirical observation is that all positive ajoene chemosensitizers had at least one *p*-methoxybenzyl group in their structure. This observation aids in the future design of chemosensitizing agents.[12b, 30]

University

5.5 Overview and Comments

All the synthesized ajoene analogues displayed good *in vitro* activity that was comparable to that of *bis*-PMB **5** which their design was based on. However, the analogue that was chosen for the *in vivo* assay returned a disappointing inability to reduce tumour growth in nude mice. Based on solubility studies, this is not believed to be due to poor solubility but rather either instability in blood and/or binding to red-blood cells. The compounds also demonstrated their ability as chemosensitization agents towards tumour cell-lines that are resistant to some marketed drugs such as Doxorubicin and Vincristine, which was attributed to the presence of at least one lipophilic *p*-methoxybenzyl substituent at the ajoene termini.

University of Cape Town

Chapter 6: Summary and Future work

The current thesis was aimed at improving the aqueous solubility of ajoene analogues for biological evaluation purposes. An SAR study identified *bis*-PMB **5** as the advanced lead that returned excellent *in vitro* activity, but failed to reduce tumour growth in an *in vivo* assessment. This was rationalised by identifying poor solubility of **5** as well as high reactivity of **5** as possible reasons. To this end, four new analogues were successfully synthesised in this thesis namely: PMB- Phenol **26**, PMB- Acetate **27**, PMB- Ester **28** and the PMB-Amide **29.** Each returned an improved aqueous solubility as compared to the *bis*-PMB in which the acetate and amide analogues were the most soluble of the new analogues. Each of these analogues also had good *in vitro* activity that was comparable and superior to that of the *bis*-PMB (2.5 μM) against the WHCO1 cell-line, with the PMB-Ester being the most active (1.7 μM).

The PMB-Amide **29** was chosen for the *in vivo* study in a nude-mouse model, which disappointingly failed to reduce tumour growth. This excluded poor solubility as a cause of the absence of bioactivity *in vivo*. Evidence suggested that **29** was binding to red-blood cells and not reaching the tumours. Future work will include administering the drugs via intravenous injection which would bypass the delivery problem. Various analogues were also tested for their ability to act as chemosensitization agents for the clinically approved chemotherapeutic drugs Doxorubicin and Vincristine against a drug-resistant cell-line. It was observed that analogues containing at least one *p*-methoxybenzyl substituent switched on the sensitivity of the tumours towards the drugs.

It was thought that labelling the ajoene analogue would offer a unique opportunity to visualize the movement and localization of ajoene in cancer cells. However, attempts (not described in the thesis) to label the PMB-Phenol **26** with a radioactive ^{14}C-tag failed to give the desired labeled products. A full investigation (at NECSA in Pelindaba, SA) could not be carried out owing to the lack of time. In the future, a different radioactive tag could be used to evaluate the localisation and metabolic fate of the ajoene analogue. An analogue with a radioactive amide substituent would prove to be very useful, see Figure 35.

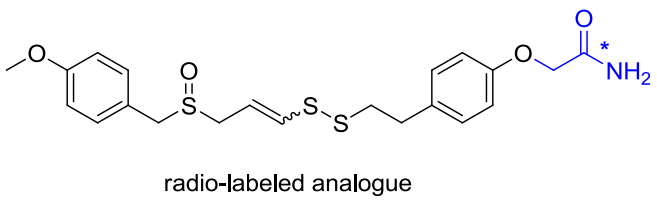

radio-labeled analogue

Figure 35: Proposed radio-labeled analogue.

University of Cape Town

Chapter 7: Experimental Section

7.1 General synthetic methods

Thin Layer chromatography (TLC) was employed to monitor reaction progress utilising aluminium-backed plates that are coated with silica-gel F_{254}. Compounds on TLC plates were visualised using ultra-violet light (254 nm), iodine vapour, or by spraying with a 2.5 % solution of anisaldehyde in a mixture of sulfuric acid and ethanol (1:10 v/v) and heating at 150 °C. Column chromatography was carried out using silica-gel (35-70 μm) on Biotage automated columns. Infrared spectra were recorded in chloroform or neat on an FT-IR spectrophotometer. Melting points were obtained using a Reichert-Jung Thermovar hot-stage microscope and are uncorrected. Elemental analyses were performed using a CHN elemental analyser. ^{1}H and ^{13}C NMR spectra were recorded at 400 MHz for ^{1}H and 101 MHz for ^{13}C in deuteriochloroform ($CDCl_3$) unless stated otherwise. Chemical shifts are quoted using residual chloroform (δ 7.26 in ^{1}H NMR and δ 77.16 in ^{13}C NMR) as an internal reference. All the chemical shifts are reported in ppm and coupling constants are quoted in Hz. High-resolution mass spectra were recorded on a Waters API Q-TOF Ultima machine, at the Mass Spectrometry Service, School of Chemistry, University of Stellenbosch.

All reagents and chemicals were commercially available. All the solvents used were purified and freshly distilled using standard methods prior to use. Degassed methanol as stated refers to purging the solvent with nitrogen gas to remove oxygen.

University of Cape Town

4-(2-Hydroxyethyl)phenol, **16**[39]

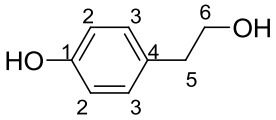

$LiAlH_4$ (690.0 mg, 18.16 mmol) was suspended in THF (10 mL) at -20° C under N_2, and methyl 2-(4-hydroxyphenyl) ethanoate (1.00 g, 6.52 mmol) dissolved in THF (2 mL) added drop-wise to the rapidly stirring solution. The reaction was allowed to proceed for 2 hours after which a more polar spot was observed on TLC. Following the reaction 1M HCl (8 mL) was added slowly at 0° C to quench any remaining $LiAlH_4$ and the solution was stirred for 20 minutes. The resulting solution was filtered through Celite, which was washed with EtOAc (40 mL) following drying of the extracts over $MgSO_4$ and the solvent removed under vacuum, the residue was crystallised from hexane to afford **16** as a clear crystalline solid (828.0 mg, 92%):

R_f = 0.3 (EtOAc: Hexane = 50:50); Mp (Hexane):86-88 °C, lit[39] Mp: 87-89 °C; IR ν_{max}/ cm-^{1} (KBr): 3391 (ROH), 3152 (ArOH); δ_H (400 MHz,d_6-acetone) : 8.00 (1H, brs, OH), 7.05 (2H, d, *J* = 8.4 Hz, H-3), 6.74 (2H, d, *J* = 8.4 Hz, H-2), 3.69 (2H, t, *J* = 7.1 Hz, H-6), 3.53 (1H, brs, OH'), 2.71 (2H, t, *J* = 7.1 Hz, H-5); δ_C (101 MHz, d_6-acetone): 156.6 (C-1), 131.1 (C-4), 130.8 (C-3), 116.0 (C-2), 64.3 (C-6), 39.6 (C-5).

4-(2-Iodoethyl)phenol, **17**[40]

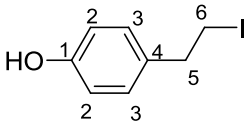

The alcohol **16** (800.0 mg, 5.77 mmol), imidazole (789.0 mg, 11.54 mmol), triphenylphosphine (3.041 g, 11.54 mmol) and iodine (2.943 g, 11.54 mmol) were dissolved in THF (7 mL) under N_2 at 0°C. The reaction mixture was allowed to warm up to room temperature over 2 hours, after which the alcohol spot had disappeared on the TLC (EtOAc: Hexane =30:70) and replaced by a less polar spot corresponding to the iodide. The solution was diluted with EtOAc (20 mL), and then saturated sodium thiosulphate (5 mL) was added. The contents were transferred into a separating funnel, the aqueous layer was further extracted with EtOAc (10 mL x 3), and the combined extracts were washed with 1 M HCl (10 mL), sodium bicarbonate (15 mL) and lastly brine (20 mL). Following drying over $MgSO_4$ and solvent removal under vacuum the residue was

University of Cape Town

purified by column chromatography (EtOAc: Hexane = 7:93) to afford **17** as a colourless solid (1.385 g, 97%):

R_f = 0.7 (EtOAc: Hexane = 30:70); Mp (Hexane) :112-113 °C, lit[40] Mp: 111-112°C; IR v_{max}/ cm^{-1} ($CHCl_3$): 3152 (ArOH), 500 (C-I); δ_H (400 MHz,$CDCl_3$) : 7.06 (2H, d, *J* = 8.6 Hz, H-3), 6.78 (2H, d, *J* = 8.6 Hz, H-2), 4.84 (1H,brs, OH), 3.31 (2H, t, *J* = 7.7 Hz, H-6), 3.10 (2H,t, *J* = 7.7 Hz, H-5); δ_C (101 MHz, $CDCl_3$): 154.6 (C-1), 133.2 (C-4), 129.8 (C-3), 115.6 (C-2), 39.7 (C-5), 6.4 (C-6).

S-4-Hydroxyphenethyl 4-methylbenzenesulfonothioate, **19**

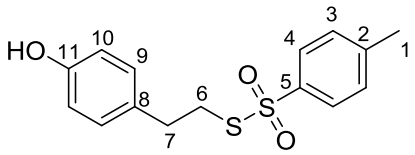

4-(-2-Iodoethyl)phenol **17** (1.350 g, 5.45 mmol) and potassium thiotosylate (1.604 g, 7.08 mmol) were dissolved in DMF (3 mL) and stirred at room temperature. The reaction was allowed to proceed for 2 hours, whereupon a spot-to-spot conversion was observed on TLC (EtOAc: Hexane = 20: 80), with the resulting product more polar than the starting 4-(-2-iodoethyl)phenol. The solution was then suspended in water (30 mL), which was extracted with EtOAc (15 mL x 3). The combined extracts were washed with water (20 mL x 2) to remove any residual DMF. Following drying over $MgSO_4$ and solvent evaporation a product as a clear oil was afforded **19**, which was pure by ^{1}H NMR spectroscopy (1.613 g, 96%):

R_f = 0.4 (EtOAc: Hexane = 30: 70); IR v_{max}/cm^{-1} ($CHCl_3$): 3152 (ArOH), 1228 (O=S=O); HRMS (ES) *m/z*: 309.0615 [M+ H]$^+$, $C_{15}H_{17}O_3S_2$ requires 309.0619; δ_H (400 MHz, $CDCl_3$) 7.81 (2H, d, *J* = 8.5 Hz, H-4), 7.34 (2H, d, *J* = 8.5 Hz, H-3), 6.95 (2H, d, *J* = 8.5 Hz, H-9), 6.74 (2H, d, *J* = 8.5 Hz, H-10), 3.38 (1H, brs, OH), 3.18 (2H, t, *J* = 7.6 Hz, H-7), 2.83 (2H, t, *J* = 8.6 Hz, H-6), 2.45 (3H, s, H-1); δ_C (101 MHz, $CDCl_3$): 154.7 (C-11), 144.9 (C-2), 142.3 (C-5), 131.0 (C-8), 130.0 (C-3), 129.9 (C-4), 127.2 (C-9), 115.7 (C-10), 37.6 (C-7), 34.4 (C-6), 21.8 (C-1).

University of Cape Town

(4-Methoxybenzyl) prop-2-ynyl sulfane, **22**[35]

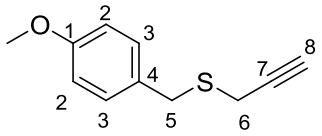

Thiourea (270.0 mg, 4.20 mmol) was dissolved in acetonitrile (7 mL) under N_2 atmosphere and 4-methoxybenzyl chloride (0.43 mL, 3.20 mmol) was added to the solution which was then refluxed for 2 hours. Reaction progress was monitored by TLC which showed formation of a more polar spot corresponding to the isothiouronium salt intermediate. The reaction was cooled in an ice-bath to afford a solid product that was filtered on a Bűchner funnel. The product was washed with ice-cold acetonitrile (25 mL) and dried further on the high vacuum pump to afford the crude isothiouronium salt (700.0 mg, 94%), R_f = 0.1 (EtOAc: Hexane = 2:3).

The isothiouronium salt (700.0 mg, 3.02 mmol) was added to a rapidly stirring solution of potassium hydroxide (423.0 mg, 7.54 mmol) dissolved in degassed methanol (7 mL) at -20°C. After 30 minutes a less polar spot was observed on TLC (EtOAc: Hexane = 5:95) corresponding to the thiol. Propargyl bromide (0.47 mL, 80% in toluene, 5.29 mmol) was added drop-wise into the mixture and the reaction was warmed up gradually to room temperature. One major product spot on TLC was formed (EtOAc: Hexane = 5:95), which was less polar than the *p*-methoxybenzyl chloride. The methanol was removed under vacuum, water (10 mL) was added and the residue was extracted into DCM (3 x 15 mL). The combined extracts were dried with $MgSO_4$, solvent was removed under vacuum and the residue purified on silica-gel with (EtOAc: Hexane = 3:97) to afford **22** as a pungent oil, (522.0 mg, 90%):

TLC: R_f = 0.4 (EtOAc: Hexane = 5:95); IR ν_{max}/cm^{-1} ($CHCl_3$): 3304 (C≡C<u>H</u>); δ_H (400 MHz, $CDCl_3$) : 7.26 (2H, d, *J* = 8.8 Hz, H-3), 6.86 (2H, d, *J* = 8.8 Hz, H-2), 3.83 (2H, s, H-5), 3.80 (3H, s, OMe), 3.08 (2H, d, *J* = 2.6 Hz, H-6), 2.28 (1H, t, *J* = 2.6 Hz, H-8); δ_C (101 MHz, $CDCl_3$) 158.9 (C-1), 130.2 (C-3), 129.5 (C-4), 114.1 (C-2), 80.1 (C-7), 71.3 (C-8), 55.4 (OMe), 34.9 (C-5), 18.4 (C-6).

University of Cape Town

(E/Z)-S-3-(4-Methoxybenzylthio)prop-1-enyl ethanethioate, **23**[35]

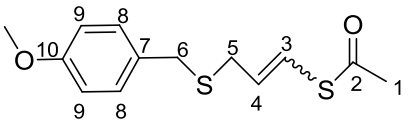

Alkyne **22** (522.0 mg, 2.72 mmol) was dissolved in toluene (7 mL) and the solution heated to 85°C under N_2. ACCN (68.0 mg, 0.27 mmol) used as a radical initiator was added to solution directly followed by the drop-wise addition of thiolacetic acid (0.23 mL, 3.26 mmol) in toluene (1 mL). The reaction was carefully monitored by TLC (EtOAc: Hexane = 10:90), which revealed the formation of a more polar spot corresponding to the thioacetate after one hour. Allowing the reaction to progress a further 45 minutes in an attempt to consume all the starting material indicated the formation of an even more polar spot believed to be the bis-substituted product, **23a**. The solution was therefore cooled to room temperature and saturated sodium carbonate (5 mL) was added to quench unreacted thiolacetic acid. Following removal of the toluene under vacuum, the remaining residue was extracted into DCM (10 mL x 3) and the combined extracts were washed with brine (10 mL x 2) then dried over $MgSO_4$. The solvent was removed under vacuum and the resulting residue was purified by column chromatography (EtOAc: Hexane = 10:90) to afford the ethanethioate product **23** as a ~ 1:1 mixture of *Z*: *E* isomers and as a light-yellow oil (450.0 mg, 62%):

(*E/Z*) mixture: TLC $R_{f=}$ 0.6 (EtOAc: Hexane = 10:90); IR ν_{max}/cm^{-1} ($CHCl_3$): 1700 (C=O), 663 (C-S)

***E*-isomer**: δ_H (400 MHz, $CDCl_3$): 7.23 (2H, d, *J* = 8.3 Hz, H-8), 6.86 (2H, d, *J* = 8.3 Hz, H-9), 6.50 (1H, dt, *J* = 15.6, 1.4 Hz, H-3), 5.81 (1H, dt, *J* = 15.6, 7.5 Hz, H-4), 3.80 (3H, s, OMe), 3.63 (2H, s, H-6), 3.08 (2H, dd, *J* = 7.5, 1.2 Hz, H-5), 2.36 (3H, s, H-1); δ_C (101 MHz, $CDCl_3$) : 193.1 (C-2), 158.9 (C-10), 130.5 (C-4), 130.3 (C-8),130.0 (C-7), 119.5 (C-3), 114.1 (C-9), 55.4 (OMe), 34.6 (C-6), 33.3 (C-5), 30.5 (C-1).

***Z*-isomer**: δ_H (400 MHz, $CDCl_3$): 7.22 (2H, d, *J* = 8.3 Hz, H-8), 6.84 (2H, d, *J* = 8.3 Hz, H-9), 6.67 (1H, dt, *J* = 9.6, 1.2 Hz, H-3), 5.86 (2H, dt, *J* = 9.6, 7.5 Hz, H-4), 3.80 (3H, s, OMe), 3.64 (2H, s, H-6), 3.10 (2H, dd, *J* = 7.5, 1.2 Hz, H-5), 2.38 (3H, s, H-1); δ_C (101 MHz, $CDCl_3$): 191.4 (C-2), 158.9 (C-10), 130.3 (C-8), 130.2 (C-4),130.0 (C-7), 119.7 (C-3), 114.1 (C-9), 55.4 (OMe), 35.4 (C-6), 30.9 (C-5), 30.5 (C-1).

University of Cape Town

(*E*/*Z*)-9-(4-Hydoxyphenyl)-1-(4-methoxyphenyl)- 2,6,7- trithianona-4-ene, **25**

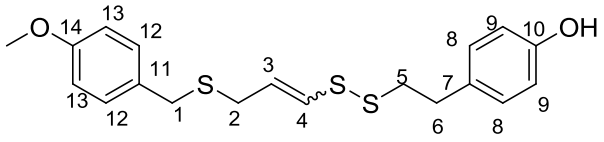

The vinyl thioacetate **23** (226.0 mg, 0.84 mmol) was dissolved in methanol (1.5 mL), the solution was cooled to -40°C and stirred under N_2. KOH (50.0 mg, 0.89 mmol) in degassed methanol (1 mL) was added slowly and the reaction left stirring for 45 minutes, after which it was cooled down to -78°C. Sulfonothioate **19** (336.3 mg, 1.09 mmol) dissolved in DCM (2 mL) was added and the reaction was allowed to stir for an hour at -78°C before being allowed to warm up, after which a more polar spot than the starting vinyl thioacetate was observed on TLC (EtOAc: Hexane = 20: 80). The reaction was quenched with saturated ammonium chloride (5 mL), the solvents were removed under vacuum on the rotary evaporator, and the resulting residue extracted into DCM (15 mL x 3). The combined extracts were washed with brine (15 mL x 2) and dried over $MgSO_4$. The product was purified using column chromatography (EtOAc: Hexane = 15: 85) to give a light-yellow oil **25** as a 5:4 mixture of *E*/*Z* isomers, (232.0 mg, 73%):

(E/Z) mixture: TLC R_f = 0.6 (EtOAc: Hexane = 15:85); IR ν_{max}/cm^{-1} ($CHCl_3$): 3152 (ArOH), 663 (C-S); HRMS (ES) *m/z*: 379.0849 [M+ H] $^+$, $C_{19}H_{23}O_2S_3$ requires 379.0860.

***E*-isomer**: δ_H (400 MHz, $CDCl_3$): 7.22 (2H, d, *J* = 8.5 Hz, H-12), 7.06 (2H, d, *J* = 8.5 Hz, H-8), 6.85 (2H, d, *J* = 8.5 Hz, H-13), 6.76 (2H, d, *J* = 8.5 Hz, H-9), 6.08 (1H, dt, *J* = 14.6, 1.1 Hz, H-4), 5.88 (1H, dt, *J* = 14.6, 7.4 Hz, H-3), 3.80 (3H,s, OMe), 3.63 (2H,s, H-1), 3.08 (2H, dd, *J* = 7.4, 1.2 Hz, H-2), 2.93 (4H, m, H-5/6); δ_C (101 MHz, $CDCl_3$): 158.8 (C-14), 154.3 (C-10), 132.2 (C-7), 130.7 (C-11), 130.2 (C-12), 129.9 (C-8), 128.3 (C-3), 128.0 (C-4), 115.6 (C-9), 114.1 (C-13), 55.5 (OMe), 39.9 (C-6), 34.8 (C-1 & 5), 32.9 (C-2).

***Z*-isomer**: δ_H (400 MHz, $CDCl_3$): 7.23 (2H, d, *J* = 8.5 Hz, H-12), 7.04 (2H, d, *J* = 8.5 Hz, H-8), 6.83 (2H, d, *J* = 8.5 Hz, H-13), 6.74 (2H, d, *J* = 8.5 Hz, H-9), 6.24 (1H, dt, *J* = 9.6, 1.0 Hz, H-4), 5.70 (1H, dt, *J* = 9.6, 7.6 Hz, H-3), 3.80 (3H, s, OMe), 3.69 (2H, s, H-1), 3.23 (2H, d, *J* = 7.6 Hz, H-2), 2.93 (4H, m, H-5/6); δ_C (101 MHz, $CDCl_3$): 158.8 (C-14), 154.3 (C-10), 132.4 (C-4), 132.2 (C-7), 130.7 (C-11), 130.2 (C-12), 129.9 (C-8), 128.2 (C-3), 115.6 (C-9), 114.1 (C-13), 55.5 (OMe), 40.7 (C-6), 35.6 (C-1), 34.8 (C-5), 29.5 (C-2).

University of Cape Town

(*E*/*Z*)-9-(4-Hydroxyphenyl)-1-(4-methoxyphenyl)-2,6,7-trithianona-4-ene 2-oxide, **26**

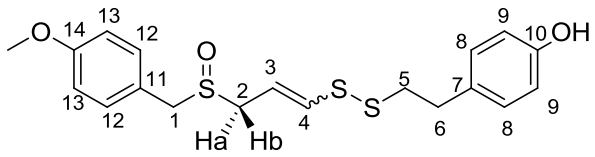

The phenol **25** (100.0 mg, 0.26 mmol) was dissolved into DCM (4 mL) and the solution stirred under N_2. The temperature was lowered to -78 °C using a liquid N_2/ acetone bath and *m*-CPBA (75.0 mg, 77% in H_2O, 0.34 mmol) was added to the reaction mixture. The reaction was allowed to proceed for 2 hours below -60 °C, producing a more polar product spot upon TLC monitoring (EtOAc: Hexane = 80:20). Saturated aqueous Na_2CO_3 (5 mL) was added at -60 °C and the reaction allowed to warm up to room temperature. The residue was extracted into DCM (10 mL x 3), the combined fractions were washed with brine (2 x 10 mL) and dried over $MgSO_4$. A number of minor products were observed to form during the work-up. The product was purified by column chromatography (EtOAc: Hexane = 75:25) to result in a yellow oil **26** as a 4:3 mixture of *Z/E* isomers, (70.0 mg, 68 %):

(*E*/*Z*) mixture: TLC R_f = 0.3 (EtOAc: Hexane = 80:20); IR ν_{max}/cm^{-1} ($CHCl_3$): 3152 (ArOH), 1325 (S=O), 663 (C-S); HRMS (ES) *m/z*: 393.0646 [M- H^+], $C_{19}H_{21}O_3S_3$ requires 393.0653.

***E*-isomer:** δ_H (400 MHz, $CDCl_3$): 7.19 (2H, d, *J* = 8.7 Hz, H-12), 6.99 (2H, d, *J* = 8.7 Hz, H-8), 6.89 (2H, d, *J* = 8.7 Hz, H-13), 6.75 (2H, d, *J* = 8.7 Hz, H-9), 6.28 (1H, dt, *J* = 14.6, 0.9 Hz, H-4), 5.86 (1H, dt, *J* = 14.6, 7.2 Hz, H-3), 3.94 (2H, d, *J* = 1.2 Hz, H-1), 3.79 (3H, s, OMe), 3.45 (1H, ddd, *J* = 13.2, 7.2, 0.9 Hz, H-2_a), 3.32 (1H, ddd, *J* = 13.2, 7.2, 0.9 Hz, H-2_b), 2.90 (4H, m, H-5/6); δ_C (101 MHz, $CDCl_3$): 160.0 (C-14), 155.2 (C-10), 135.1 (C-4), 131.4 (C-12), 131.0 (C-7), 129.8 (C-8), 121.3 (C-11), 116.3 (C-3), 115.8 (C-9), 114.7 (C-13), 56.3 (C-1), 55.4 (OMe), 52.9 (C-2), 40.3 (C-6), 34.8 (C-5).

***Z*-isomer**: δ_H (400 MHz, $CDCl_3$): 7.22 (2H, d, *J* = 8.7 Hz, H-12), 6.98 (2H, d, *J* = 8.7 Hz, H-8), 6.89 (2H, d, *J* = 8.7 Hz, H-13), 6.75 (2H, d, *J* = 8.7 Hz, H-9), 6.56 (1H, dt, *J* = 9.4, 1.0 Hz, H-4), 5.75 (1H, dt, *J* = 9.4, 7.3 Hz, H-3), 3.96 (2H, s, H-1), 3.79 (3H,s, OMe), 3.56 (1H, ddd, *J* = 13.2, 7.3, 1.0 Hz, H-2_a), 3.48 (1H,ddd, *J* = 13.2, 7.3, 1.0 Hz, H-2_b), 2.90 (4H, m, H-5/6); δ_C (101 MHz, $CDCl_3$): 160.0 (C-14), 155.2 (C-10), 139.0 (C-4), 131.4 (C-12), 131.0 (C-7), 129.7 (C-8), 121.4 (C-11), 118.0 (C-3), 115.8 (C-9), 114.7 (C-13), 56.9 (C-1), 55.4 (OMe), 49.6 (C-2), 40.8 (C-6), 34.8 (C-5).

University of Cape Town

(*E*/*Z*)-9-(4-Acetyloxyphenyl)-1-(4-methoxyphenyl)-2,6,7-trithia-nona-4-ene-2-oxide, **27**

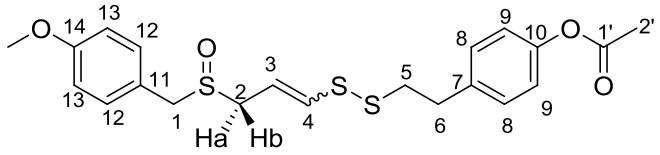

The oxide **26** (200.0 mg, 0.51 mmol) was dissolved into DCM (5 mL) under N_2, NEt_3 (103.0 mg, 1.02 mmol) was added to the solution, followed by DMAP (6.0 mg, 0.05 mmol). The temperature was lowered to -20 °C and acetyl chloride (52.0 mg, 0.66 mmol) was added slowly to the rapidly stirring solution and the reaction was allowed to stir for 20 minutes at this point TLC monitoring produced a less polar product spot (EtOAc: Hexane = 60:40). DCM (25 mL) was added and washed with 1M HCl (2 mL) to remove NEt_3 and DMAP, followed by the $NaHCO_3$ (5 mL) to neutralise the reaction mixture. The combined fractions were washed with brine (2 x 10 mL) and dried over $MgSO_4$. The resulting residue after solvent removal was purified by column chromatography (EtOAc: Hexane = 60:40) to afford a yellow solid **27** as a 3:4 mixture of *Z/E* isomers (196.0 mg, 88%)

(*E/Z*) mixture: TLC R_f = 0.4 (EtOAc: Hexane =60:40); Mp (Hexane): 45- 47 °C; IR ν_{max}/cm^{-1} ($CHCl_3$): 1700 (C=O), 1325 (S=O), 663 (C-S); HRMS (ES) *m/z*: 437.0910 $[M+ H]^+$, $C_{21}H_{25}O_4S_3$ requires 437.0915

***E*-isomer:** δ_H (400 MHz, $CDCl_3$): 7.20 (4H, m, H-8/12), 7.01 (2H, d, *J* = 8.8 Hz, H-9), 6.90 (2H, d, *J* = 8.8 Hz, H-13), 6.34 (1H, dt, *J* = 14.8, 1.0 Hz, H-4), 5.93 (1H, dt, *J* = 14.8, 7.4 Hz, H-3), 3.91 (2H, s, H-1), 3.80 (3H, s, OMe), 3.43 (1H, ddd, *J* = 12.0, 7.4, 1.0 Hz, H-2a), 3.29 (1H, ddd, *J* = 12.0, 7.4, 1.0 Hz, H-2b), 2.97 (4H, s, H-5/6), 2.28 (3H, s, H-2'); δ_C (101 MHz, $CDCl_3$): 169.6 (C-1'), 160.0 (C-14), 149.5 (C-10),137.3 (C-7), 134.3 (C-4), 131.3 (C-12), 129.7 (C-8), 121.9 (C-9), 121.7 (C-11), 117.4 (C-3), 114.7 (C-13), 56.6 (C-1), 55.5 (OMe), 53.0 (C-2), 39.5 (C-6), 35.0 (C-5), 21.2 (C-2').

***Z*-isomer**: δ_H (400 MHz, $CDCl_3$): 7.20 (4H, m, H-8/12), 7.01 (2H, d, *J* = 8.8 Hz, H-9), 6.90 (2H, d, *J* = 8.8 Hz, H-13), 6.57 (1H, dt, *J* = 9.4, 1.2 Hz, H-4), 5.80 (1H, dt, *J* = 9.4, 7.3 Hz, H-3), 3.94 (2H, s, H-1), 3.80 (3H, s, OMe), 3.54 (1H, ddd, *J* = 12.0, 7.3, 1.2 Hz, H-2a), 3.47 (1H, ddd, *J* = 12.0, 7.3, 1.2 Hz, H-2b), 2.97 (4H, s, H-5/6), 2.28 (3H, s, H-2'); δ_C (101 MHz, $CDCl_3$): 169.6 (C-1'), 160.0 (C-14), 149.5 (C-10), 138.3 (C-4), 137.2 (C-7), 131.4 (C-12), 129.7 (C-8), 121.8 (C-9), 121.7 (C-11), 118.8 (C-3), 114.7 (C-13), 57.1 (C-1), 55.5 (OMe), 49.7 (C-2), 40.4 (C-6), 35.1 (C-5), 21.2 (C-2').

University of Cape Town

(E/Z)-1-(4-Methoxyphenyl)-9-(4-(methoxycarbonylmethyloxy)phenyl)-2,6,7, -trithianona-4-ene-2-oxide, **28**

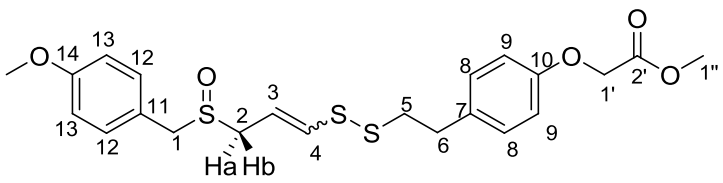

The oxide **26** (200.0 mg, 0.51 mmol) was dissolved into THF (5 mL) under N_2, and NaH (26.5 mg, 60% suspension in mineral oil, 0.66 mmol) added to the solution at -20 °C. The reaction was stirred for 15 minutes followed by the addition of methyl bromoacetate (109.0 mg, 0.714 mmol). The reaction was then allowed to warm up to room temperature over 45 minutes with TLC monitoring indicating the completion of the reaction by conversion of starting material to a less polar product spot (EtOAc: Hexane = 60:40). NH_4Cl (4 mL) was added to quench the reaction and the product was extracted into EtOAc (3 x 15 mL), which was dried over $MgSO_4$. The resulting product was purified by column chromatography (EtOAc: Hexane = 55:45) to afford **28** as a clear oil as a 1:1 mixture of *Z/E* isomers (195.0 mg, 85%):

(*E/Z*) mixture: TLC R_f = 0.4 (EtOAc: Hexane = 60:40); IR ν_{max}/cm^{-1} ($CHCl_3$): 1700 (C=O), 1325 (S=O), 663 (C-S); HRMS (ES) *m/z*: 467.1004 $[M+ H]^+$, $C_{22}H_{27}O_5S_3$ requires 467.1021

***E*-isomer:** δ_H (400 MHz, $CDCl_3$):7.19 (2H, d, *J* = 8.7 Hz, H-12), 7.11 (2H, d, *J* = 8.7 Hz, H-8), 6.89 (2H, d, *J* = 8.7 Hz, H-13), 6.83 (2H, d, *J* = 8.7 Hz, H-9), 6.34 (1H, dt, *J* = 14.6, 1.2 Hz, H-4), 5.93 (1H, dt, *J* = 14.6, 7.4 Hz, H-3), 4.60 (2H, s, H-1'), 3.91 (2H, s, H-1), 3.80 (3H, s, H-1"), 3.79 (3H, s, OMe), 3.43 (1H, ddd, *J* = 12.0, 7.4, 1.2 Hz, H-2a), 3.30 (1H, ddd, *J* = 12.0, 7.4, 1.2 Hz, H-2b), 2.93 (4H, s, H-5/6); δ_C (101 MHz, $CDCl_3$): 169.5 (C-2'), 160.0 (C-14), 156.7 (C-10), 134.4 (C-4), 133.1 (C-7), 131.3 (C-12), 129.8 (C-8), 121.8 (C-11), 117.2 (C-3), 115.0 (C-9), 114.7 (C-13), 65.6 (C-1'), 56.5 (C-1), 55.4 (OMe), 53.0 (C-2), 52.3 (C-1''), 39.8 (C-6), 34.8 (C-5).

***Z*-isomer**: δ_H (400 MHz, $CDCl_3$): 7.22 (2H, d, *J* = 8.7 Hz, H-12), 7.09 (2H, d, *J* = 8.7 Hz, H-8), 6.89 (2H, d, *J* = 8.7 Hz, H-13), 6.83 (2H, d, *J* = 8.7 Hz, H-9), 6.57 (1H, dt, *J* = 9.4, 1.2 Hz, H-4), 5.79 (1H, dt, *J* = 9.4, 7.2 Hz, H-3), 4.61 (2H, s, H-1'), 3.94 (2H, s, H-1), 3.80 (3H, s, H-1"), 3.79 (3H, s, OMe), 3.53 (1H, ddd, *J* = 12.0, 7.2, 1.2 Hz, H-2a) 3.47 (1H, ddd, *J* = 12.0, 7.2, 1.2 Hz, H-2b), 2.93 (4H, s, H-5/6); δ_C (101 MHz, $CDCl_3$): 169.5 (C-2'), 160.0 (C-14), 156.7 (C-10), 138.4 (C-4), 133.0 (C-7), 131.4 (C-12), 129.8 (C-8), 121.7 (C-11), 118.7 (C-3), 115.0 (C-9), 114.6 (C-13), 65.6 (C-1'), 57.1 (C-1), 55.5 (OMe), 52.3 (C-2), 52.3 (C-1''), 40.6(C-6), 34.8 (C-5).

University of Cape Town

(*E/Z*)-9-(4-Acetamidoxyphenyl)-1-(4-methoxyphenyl)- 2,6,7-trithianona-4-ene-2-oxide, **29**

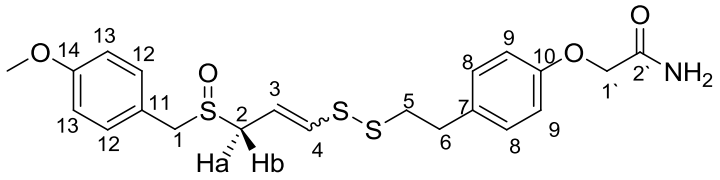

The oxide **26** (400.0 mg, 1.02 mmol) was dissolved in acetonitrile (8 mL) under N_2, and K_2CO_3 (282.0 mg, 2.04 mmol) and 2-iodoacetamide (377.0 mg, 2.04 mmol) were added to the solution at room temperature. The reaction was heated at 45°C and carefully monitored by TLC (EtOAc = 100%), which revealed the formation of a more polar spot corresponding to the amide product after 12 hours. Allowing the reaction to progress a further 12 hours in an attempt to consume all of the starting material did not show full conversion, so at this point the reaction was quenched with $NaHCO_3$ (4 mL) and the product extracted into EtOAc (15 mL x 3), which was dried over $MgSO_4$, and the solvent removed under vacuum. The residue was purified by column chromatography (MeOH: EtOAc= 5:95) to afford the amide product **29** as a 3:1 mixture of *Z/E* isomers as a colourless solid that was crystallized from methanol, (210.0 mg, 45%):

(*E/Z*) mixture: TLC R_f = 0.3 (EtOAc = 100%); Mp (methanol): 86-88 °C; IR ν_{max}/cm^{-1} ($CHCl_3$): 3524 and 3401 (NH_2), 1688 (C=O), 1325 (S=O), 663 (C-S); HRMS (ES) *m/z*: 452.1026 $[M+H]^+$, $C_{21}H_{26}NO_4S_3$ requires 452.1024.

***E*-isomer:** δ_H (400 MHz, $CDCl_3$): 7.22 (2H, d, *J* = 8.6 Hz, H-12), 7.13 (2H, d, *J* = 8.6 Hz, H-8), 6.90 (2H, d, *J* = 8.6 Hz, H-13), 6.85 (2H, d, *J* = 8.6 Hz, H-9), 6.53 (1H, brs, NH), 6.34 (1H, dt, *J* = 14.6, 1.2 Hz, H-4), 5.93 (1H, dt, *J* = 14.6, 7.4 Hz, H-3), 5.72 (1H, brs, NH), 4.47 (2H, s, H-2'), 3.91 (2H, s, H-1), 3.81 (3H, s, OMe), 3.43 (1H, ddd, *J* = 12.0, 7.4, 1.2 Hz, H-2a), 3.30 (1H, ddd, *J* = 12.0, 7.4, 1.2 Hz, H-2b), 2.93 (4H, s, H-5/6); δ_C (101 MHz, $CDCl_3$): 171.0 (C-2'), 160.0 (C-14), 156.1 (C-10), 134.4 (C-4), 133.4 (C-7), 131.3 (C-12), 130.1 (C-8), 121.8 (C-11), 117.3 (C-3),115.0 (C-13), 114.7 (C-9), 67.5 (C-1'), 56.6 (C-1), 55.5 (OMe), 53.0 (C-2), 39.7 (C-6), 34.7 (C-5).

***Z*-isomer:** δ_H (400 MHz, $CDCl_3$): 7.22 (2H, d, *J* = 8.6 Hz, H-12), 7.13 (2H, d, *J* = 8.6 Hz, H-8), 6.90 (2H, d, *J* = 8.6 Hz, H-13), 6.85 (2H, d, *J* = 8.6 Hz, H-9), 6.57 (1H, dt, *J* = 9.4, 1.2 Hz, H-4), 6.53 (1H, brs, NH), 5.79 (1H, dt, *J* = 9.4, 7.2 Hz, H-3), 5.72 (1H, brs, NH), 4.47 (2H, s, H-2'), 3.94 (2H, s, H-1), 3.80 (3H, s, OMe), 3.53 (1H, ddd, *J* = 12.0, 7.2, 1.2 Hz, H-2a) 3.47 (1H, ddd, *J* = 12.0, 7.2, 1.2 Hz, H-2b), 2.93 (4H, s, H-5/6); δ_C (101 MHz, $CDCl_3$): 171.0 (C-2'), 160.0 (C-14), 156.1 (C-10), 138.4 (C-4), 133.4 (C-7),131.4 (C-12), 130.1 (C-8), 121.8 (C-11), 118.7 (C-3),

University of Cape Town

114.0 (C-13), 114.7 (C-9), 67.5 (C-1'), 57.1 (C-1), 55.5 (OMe), 49.7 (C-2), 40.6 (C-6), 34.7 (C-5).

7.2 Biological Experimental

7.2.1 General

The cells used were A375 human malignant melanoma epithelial cell-line and WHCO1 oesophogeal epithelial cell-line.

All cells were grown in Dulbecco's Modified Eagle Medium (DMEM) that contained 10% heat-inactivated fetal bovine serum (FBS), 100 μg/ml penicillin and 100 μg/ml streptomycin that prevented contamination. All media, buffers and reagents were pre-incubated (unless otherwise stated) to 37 ^{o}C in a thermostat-controlled water bath.

The cells were cultured in 100 mm petri dishes and allowed to reach between 80-95 % confluence prior to being split. The splitting procedure that was done under a sterile hood involved removal of the growth media and a quick wash to remove excess media with phosphate buffer (PBS) (3-4 mL) at pH 7.4, followed directly by incubating the cells in 0.05% tripsen-EDTA (2 mL) for 2-3 minutes at 37°C. The trypsin was used to detach the cells from the surface of the dish, and it was then deactivated with the growth media (3 mL). The cells were then pelleted by centrifugation for 4 minutes at 40000 rpm using a Hettich EBA 20 centrifuge. The pellet was then resuspended into growth media (1 mL) and using and using 10% of the cells to propagate further.

7.2.2 Cell proliferation analysis

The anti-proliferation effects of the analogues on tumour cells was measured by the MTT (3-(4,5-Dimethylthiazol-2-yl)-2,5-diphenyltetrazolium bromide) proliferation kit (Roche, Mannheim, Germany). The MTT reagent is a yellow tetrazolium salt that is reduced by viable cells to form purple formazan crystals, which can easily be quantified by spectroscopy. The amount of the formazan formed is directly related to the number of metabolically active cells. Each experiment was performed in quadruplet which used 4 rows of the 96 well-plate (Costar, Corning Inc., USA).

University of Cape Town

The cells were plated in 135 μl of media in the cell density of 2500 cells/ well for both the A375 and WHCO1 cells. After plating, the cells were allowed to settle and grow in an incubator overnight at 37°C.

On day 2, a stock dilution series (see Table 5), ranging from 100 mM to 0 of drug prepared in high DMSO. Each dilution was further diluted 100 fold into media, after which 10 μl of the newly formed dilution was added to the cells (see Table 6), which gave a final drug concentration of 1 in 1000 of the original solutions and a 0.1% DMSO. The cells were then incubated with the drugs at 37°C, 5% CO_2 for 48 hours.

On day 4, 10 μl of the MTT reagent was added to each well and the cells incubated for a further 4 hours at 37°C and followed by the addition of solubilisation reagent (10% SLS on 0.01 M HCl) (100 μl) and lastly incubated overnight at 37°C.

Table 5: Dilution of drug stock (mM)

1	2	3	4	5	6	7	8	9	10	11
100	50	25	12.5	6.25	3.125	1.56	0.78	0.39	0.195	0

Table 6: Final drug concentration in each well (μM)

1	2	3	4	5	6	7	8	9	10	11
100	50	25	12.5	6.25	3.125	1.56	0.78	0.39	0.195	0

University of Cape Town

On day 5, the plates were read on a plate reader (EL800, Biotek Instruments, Winsooki, USA) at 595nm and the background absorbance of the media, drugs and MTT (without cells) was also recorded at 595 nm. The background absorbance (with media only) was then subtracted from each reading and the data was analysed using Graphpad Prism 4, using a non-linear regression analysis fitted to sigmoidal dose-response curve with A595nm- baseline vs Log C to obtain the IC_{50} at 95% confidence interval.

7.2.3 Animal Study

A375 cells were grown to 80% confluence, harvested and then suspended in PBS at 2.5 x 10^7 cells/ml. 100 μl of the suspension (2.50 x 10^6) was subsequently injected into the right hind posterior of each nude mice. At this point the mice were divided into two groups of 10 namely: the treatment group and the control group, and the treatment group each received the PMB-Amide at 8mg/kg administered every day for the duration of the study that lasted 21 days. The

drug doses were prepared by dissolving the test drug in 2.5% chondroitin, 10% DMSO and PEG400 to make up a solubilised solution and then administered to the mice intraperitoneally from day 1 until 21.

The treated mice were monitored for signs of discomfort following the administration of the test drug and as such their health, weight and tumour size (measured by calipers) carefully recorded. Upon completion of the study at day 21, the mice were sacrificed by halothane and weighed and tumours were carefully removed and their volumes determined by (lenght^2 x height)/2.[53]

Stock solutions for all experiments were made as follows:

PBS 10 X solution: 1.37M NaCl 27 mM KCl 43 mM $Na_2HPO_4.2H_2O$ (pH 7.4) 14 mM KH_2PO_4	PBS 1 X solution: 1 part "PBS 10X" in 9 parts distilled H_2O – mixed, autoclaved and stored at 4 ^oC.
SLS – Solubilisation: 10% SLS in 0.01M HCl	The MTT solution: 100mg of MTT in 20 ml PBS buffer. Stored in the dark at 4 ^oC.

University of Cape Town

References

1. E. A. Wilson and B. Demmig-Adams, *Nutr. Food. Sci*., 2007, **37**, 178-183.

2. S. Yoshida, S. Kasuga, N. Hayashi, T. Ushiroguchi, H. Matsuura and S. Nakagawa, *Appl. Environ. Microbiol*., 1987, **53**, 615-617.

3. L. D. Lawson, *Planta Med.*, 1992, **58**, 345-350.

4. E. Block, *Angew. Chem. Int. Ed.*, 1992, **31**, 1135-1174.

5. E. Block, *Sci. Am*., 1985, **252**, 114-119.

6. Phytomedicines of Europe: Chemistry and Biological Activity: A review of its medicinal effects and indicated active compounds, eds. L.D. Lawson and R. Bauer, American Chemical Society, Washington, 1998, pp. 177-209.

7. J. C. Harris, S. L. Cottrell, S. Plummer and D. Lloyd, *Appl. Microbiol. Biotechnol.*, 2001, **57**, 282–286.

8. E. Block, S. Ahmad, M. K. Jain, R. W. Crecely, R. Apitz-Castro and M. R. Cruz, *J. Am. Chem. Soc.*, 1984, **106**, 8295-96.

9. F. Rendu, D. Daveloose, J. C. Denouzy, N. Bourdeau, S. Levy-Toledano, M. K. Jain and R. Apitz-Castro, *Biochem. Pharmacol*., 1989, **38**, 1321-132.

10. Y. J-Yang, M. Della-Fera, C. Nelson-Dooley, and C. A. Baile, *Obesity*, 2006, **14**, 388-397.

11. S. R. Davis, R. Perrie and R. Apitz-Castro, *J. Antimicrob. Chemother*., 2003, **51**, 593-597.

12. (a) A. Arora, C. Tripathi and Y. Shukla, *Curr. Cancer Ther. Rev.*, 2005, **1**, 199-205.

(b) H. T. Hassan, *Leuk. Res*., 2004, **28**, 667-671.

(c) A. Powolny and S. V. Singh, *Cancer Lett*., 2008, **269**, 305-314.

13. http://www.who.int/mediacentre/factsheets/fs297/en/index.html

14. http://www.thymic.org/uploads/reference-sub/03chemopric.pdf

15. G. H. Williams and K. Stoeber, *J. Pathol.*, 2012, **226**, 352-364.

University of Cape Town

16. J. Sjöström, T. Mäkelä, Apoptosis and the Cell Cycle in Human Disease. *Wiley Online Library* 2006, pp. 1-6.

17. *The Eukaryotic Cell Cycle*, J. A. Bryant and D. Francis, Taylor & Francis, Abingdon, UK, Vol. 59, 2008.

18. *Programmed Cell Death in Animals and Plants*, J. A. Bryant, S. G. Hughes and J. M. Garland, BIOS Scientific Publishers limited, Oxford, 52nd edn., 2000.

19. C. Xu, B. Baily-Maitre and J. C. Reed, *J.Clin. Invest.*, 2005, **115**, 2656-2664.

20. S. Sundar Rajan, V. Srinivasan, M. Balasubramanyam and U. Tatu, *Indian. J. Med. Res.*, 2007, **125**, 411-424.

21.http://www.intechopen.com/books/phytochemicals-bioactivities-and-impact-on-health/naturally-occurring-organic-sulfur-compounds-an-example-of-a-multitasking-class-of-phytochemicals-in

22. Y. Shukla and N. Kalra, *Cancer Lett*., 2007, **247**, 167–181.

23. K. Ishikawa, R. Naganawa, H. Yoshida, N. Iwata, H. Fukuda, T. Fujino and A. Suzuki, *Biosci. Biotech. Biochem.*, 1996, **60**, 2086–2088.

24. K. Scharfenberg, R. Wagner and K. G. Wagner, *Cancer Lett*., 1990, **53**, 103-108.

25. M. Li, J.-R. Ciu, Y. Ye, J.-M. Min, L.-H. Zhang, K. Wang, M. Gares, J. Cros, M. Wright and J. Leung-Track, *Carcinogenesis*, 2002, **23**, 573-579.

26. P. Taylor, R. Noriega, C. Farah, J. M. Abad, M. Arsenak and R. Apitz, *Cancer Lett*., 2006, **239**, 298-304.

27. V. M. Dirsch, D. S. M. Antlsperger, H. Hentze, A. M. Vollmar, *Leukemia*, 2002, **16**, 74-83.

28. T. Nishikawa, N. Yamada, A. Hattori, H. Fukuda and T. Fujino, *Biosci. Biotechnol. Biochem*., 2002, **66**, 2221-2223.

29. C. M. L. J. Tilli, A. J. W. Stavast-Kooy, J. D. D. Vuerstaek, M. R. T. M. Thissen, G. A. M. Krekels, F. C. S. Ramaekers and H. A. M. Neumann, *Arch. Dermatol. Res.*, 2003, **295**, 117-123.

30. J. A. Shabbits, Y. Hu and L. Mayer, *Mol. Cancer Ther*., 2003, **2**, 805-813.

31. V. M. Dirsch, A. L. Gerbes and A. M. Volmar, *Mol. Pharmacol*., 1998, **53**, 402-407.

University of Cape Town

32. D. S. M. Antlsperger, V. M. Dirsch, D. Ferreira, J.-L. Su, M.-L. Kuo and A.M. Vollmar, *Oncogene*, 2003, **22**, 582-589.

33. M. Li, J. M. Minm, J. R. Cui, L. H. Zhang, K. Wang, A. Valette, C. Davrinche, M. Wight and J. Leung-Track, *Nutr. Cancer*., 2002, **47**, 241-247.

34. U. Munchberg, A. Anwar, S. Mecklenburg and C. Jacob, *Org. Biomol. Chem*., 2007, **5**, 1505-1518.

35. C. H. Kaschula, R. Hunter, N. Stellenboom, M. R. Caira, S. Winks, T. Ogunleye, P. Richards, J. Cotton, K. Zilbeyaz, Y. Wang, V. Siyo, E. Ngarande and M. I. Parker, *Eur. J. Med. Chem*., 2012, **50**, 236-254.

36. H. Gallwitz, S. Bonse, A. Martinez-Cruz, I. Schlichting, K. Schumacher and R.L. Krauth-Siegel, *J. Med. Chem*., 1999, **42**, 364-372.

37. L. D. Lawson and Z. J. Wang, *Planta Med*., 1993, **59S**, A688-A689.

38. T. Hosono, T. Fukao, J. Ogihara, Y. Ito, H. Shiba, T. Seki and T. Ariga, *J. Biol. Chem*., 2005, **80**, 41487-41493.

39. K. Torssell and K. Wahlberg, *Acta Chem. Scand*., 1967, **21**, 53-62.

40. A. P. Krysin, T. G. Egorova and V. G. Vasil'ev, *Russ. J. Gen. Chem.*, 2010, **18**, 275-283.

41. E. Block, S. Ahmad, J. L. Catalfamo, M. K. Jain and R. Apitz-Castro, *J. Am. Chem. Soc*., 1986, **108**, 7045-7055.

42. R. Hunter, C. H. Kaschula, I. M. Parker, M. R. Caira, P. Richards, S. Travis, F. Taute and T. Qwebani, *Bioorg. Med. Chem. Lett*., 2008, **18***,* 5277-5279.

43. C. Cerella, C. Scherer, S. Cristofanon, E. Henry, A. Anwar, C. Busch, M. Montenarh, M. Dicato, C. Jacob and M. Diederich, *Apoptosis*, 2009, **14**, 641-654.

44. C. Y. Han, S. H. Ki, Y. W. Kim, K. Noh, D. Y. Lee, B. Kang, J.-H. Ryu, R. Jeon, E. H. Kim, S. J. Hwang and S. G. Kim, *Antioxid. Redox Signal.*, 2011, **14**, 187-202.

45. Y. Maki, K. Kikuchi, H. Sugiyama and S. Seto, *Tetrahedron Lett*., 1975, **38**, 3295-3296.

46. M. M. Toveta, M. Moran, T. L. Amyes and J. P. Richards, *J. Am. Chem. Soc*., 2002, **125**, 8814-8819.

47. J. Cotton, Master Thesis, University of Cape Town, 2010.

University of Cape Town

48. R. Grice and L. N. Owen, *J. Chem. Soc*., 1963, 1947-1954.

49. A. bugaut, K. Jantos, J.-L. Wietor, R. Rodriguez, J. K. M. Sanders and S. Balasubramanian., *Angew. Chem. Int. Ed*., 2008, **47**, 2677-2680.

50. T. Mosmann. *J. Immunol. Methods.*, 1983, **65**, 55–63.

51. D. Xiao, A. Herman-Antosiewicz, J. Antosiewicz, H. Xiao, M. Brisson, J. S. Lazo and S. V. Singh, *Oncogene*, 2005, **24**, 6256–6268.

52. A. F. Stepan, D. P. Walker, J. Bauman, D. A. Price, T. A. Baillie, A. S. Kalgutkar and M. D. Aleo, *Chem. Res. Toxicol.*, 2011, **24**, 1345–1410.

53. M. Jensen, J. Jorgensen, T. Binderup and A. Kjaer, *BMC. Med. Imaging*., 2008, **8** (1), 16-21.

54. C. De Kok, C. H. Kaschula and L. Wiesner, Unpublished Data. 2012.

55. R. Aptiz-Castro, M. K. Jain, F. Bartoli, E. Ledezma, M. Ruiz and R. Salas, *Biochem. Biophys. Acta.*, 1991, **1094**, 269-280

56. E. H. Kerns and L. Di, *J. Assoc. Lab. Autom.,* 2005, **10** (2), 114-123.

57. L. Pan, Q. Ho, K. Tsutsui and L. Takahashi, *J. Pharm. Sci.*, 2001, **90**, 521-529.

58. R. Hunter, Unpublished Data. 2012.

59. *Light Scattering by Small Particles*, H. C. van de Hulst, Ed. Dover Publications, New York, 1981, pp. 114-130.

University of Cape Town